

1 **Lahar events in the last 2,000 years from Vesuvius eruptions. Part 1: Distribution and impact**
2 **on densely-inhabited territory estimated from field data analysis**

3 Mauro A. Di Vito (1,*), Ilaria Rucco (2), Sandro de Vita (1), Domenico M. Doronzo (1), Marina Bisson (3), Mattia de'
4 Michieli Vitturi (3), Mauro Rosi (4), Laura Sandri (5), Giovanni Zanchetta (4), Elena Zanella (6), Antonio Costa (5)

5 (1) Istituto Nazionale di Geofisica e Vulcanologia - Sezione di Napoli Osservatorio Vesuviano, Napoli, Italy

6 (2) Heriot-Watt University, School of Engineering and Physical Sciences, Edinburgh, United Kingdom

7 (3) Istituto Nazionale di Geofisica e Vulcanologia - Sezione di Pisa, Pisa Italy

8 (4) Università di Pisa, Dipartimento di Scienze della Terra, Pisa, Italy

9 (5) Istituto Nazionale di Geofisica e Vulcanologia - Sezione di Bologna, Bologna, Italy

10 (6) Università di Torino, Dipartimento di Scienze della Terra, Torino, Italy

11 *Corresponding author: Mauro A. Di Vito (mauro.divito@ingv.it)

12

13 **Abstract**

14 Lahars represent some of the most dangerous phenomena in volcanic areas for their destructive
15 power, causing dramatic changes in the landscape with no premonitory signs and impacting on
16 population and infrastructures. In this regard, the Campanian Plain turns out to be very prone to the
17 development of these phenomena, since the slopes of the Somma-Vesuvius and Campi Flegrei
18 volcanoes, along with the Apennine reliefs are mantled by pyroclastic deposits that can be easily
19 ~~remobilised~~remobilized, especially after intense and/or prolonged rainfall.

20 This study focuses on the analysis of the pyroclastic fall and flow deposits and of the syn- and post-
21 eruptive lahar deposits related to two sub-Plinian eruptions of Vesuvius, 472 AD-CE (Pollena) and
22 1631. To begin with, historical and field data from the existing literature and from hundreds of
23 outcrops were collected and organized into a database, which was integrated with several new pieces

24 of data. In particular, stratigraphic, sedimentological (facies analysis and laboratory) and
25 archaeological analyses were carried out, in addition to rock magnetic investigations and impact
26 parameter calculations. The new data are mainly also referred to the finding of ash beds in more distal
27 areas, which was-were included into new isopach maps for the two sub-Plinian eruptions.

28 The results show that for both the eruptions the distribution of the primary deposits is wider than the
29 one previously known. A consequence of these results is that a wider areal impact should be expected
30 in terms of civil protection, as the sub-Plinian scenario is the reference one for a future large eruption
31 of Vesuvius. Such distribution of the pyroclastic deposits directly affects the one of the lahar deposits,
32 also because a significant remobilization took place during and after the studied eruptions, which
33 involved the distal phreatomagmatic ash. From these integrated analyses, it was possible to constrain
34 the timing of the deposition and the kind of deposits remobilized (pyroclastic fall vs. flow), as well
35 as was possible to calculate the velocities and dynamic pressures of the lahars, and ultimately infer
36 the lahar transport and emplacement mechanisms.

37 The multidisciplinary approach adopted in this work shows how it is crucial to assess the impact of
38 lahars in densely populated areas even at distances of several to tens of km from active volcanoes.
39 This especially applies to large parts of the densely populated areas around Somma-Vesuvius up to
40 the nearby Apennine valleys.

41 **Keywords:** Somma-Vesuvius; Apennine valleys; pyroclastic deposits; lahars; areal distribution; local
42 impact.

43

44 **1. Introduction**

45 The emplacement-movement of volcaniclastic mass flows, and the consequent damage along the
46 flanks of active volcanoes and perivolcanic plains, represent a constant threat to inhabited areas and
47 populations (e.g., Waitt et al., 1983; Lowe et al., 1986; Pierson, 1985; Newhall and Punongbayan,

48 1996). ~~These phenomena~~Such systems are variably-fluidized, gravity-driven flows that consist of a
49 ~~mixture of pyroclastic sediment and water.~~ ~~They can be~~ triggered by various mechanisms, among
50 which the most common are intense or prolonged atmospheric precipitations (Arguden and Rodolfo,
51 1990; Rodolfo and Arguden, 1991; Pareschi et al., 2000; Rodolfo, 2000; Scott et al., 2001; Vallance
52 and Iverson, 2015). Such precipitations ~~or water runoff~~, especially during and/or ~~immediately~~ after
53 the eruptions, ~~can~~ cause the ~~detachment of landslides that can evolve into lahars~~ ~~remobilization of~~
54 ~~pyroclastic deposits evolving into water-saturated multiphase systems called lahars~~ (e.g., White et al.,
55 1997; Sheridan et al., 1999; Scott et al., 2001; [Baumann et al., 2020](#)). The last century was affected
56 by a significant number of highly-impacting lahar events associated to well-studied explosive
57 volcanic eruptions worldwide, such as for example at Colima (Mexico) in 1913 (Rodriguez-Sedano
58 et al., 2022), Nevado del Ruiz (Colombia) in 1985 (Voight, 1990), Ruapehu (New Zealand) in 2007
59 (Lube et al., 2012), and Merapi (Indonesia) in 2011 (Jenkins et al., 2015).

60 According to Rodolfo (2000), Sulpizio et al. (2006), and Vallance and Iverson (2015), volcaniclastic
61 mass flows can be generated at variably ~~long~~ time ~~intervals~~, spanning from eruptive ~~veon~~ to post-
62 eruptive phases of tens to hundreds of years. In case ~~thesey flows~~ are directly related to volcanic
63 eruptions (*i.e.*, ~~that is occurring~~ during or shortly after the eruptive event), lahars are defined as syn-
64 eruptive, and can represent an important ~~multi~~hazard factor in the short ~~to~~ middle term for
65 perivolcanic areas (Rodolfo, 2000; Sulpizio et al., 2006). ~~On the other hand~~ ~~Instead~~, in case they are
66 unrelated to any eruption dynamics, ~~so that is~~ occurring during ~~long periods of~~ volcanic quiescence,
67 they are defined as post ~~or inter~~ eruptive (Vallance and Iverson, 2015), and can represent a long-
68 term hazard factor (e.g., Siebe et al., 1999; Pareschi et al., 2002; Zanchetta et al., 2004a, 2004b;
69 Sulpizio et al., 2006). Usually, ~~these latter~~ ~~post-eruptive lahars~~ are not accounted for ~~in the~~
70 ~~assess~~menting of volcanic hazard, although their study is important for hydrogeological hazard
71 assessment and long-term territorial planning.

72 In this sense, *i.e.*that is from the hazard assessment point of view, one of the priorities concerns the
73 assessment of those areas potentially exposed to such a threat, taking into account the temporal

74 recurrences of the phenomena (~~during over~~ days to months after an eruption, or years to decades after)
75 and ~~the~~ physical features of the volcaniclastic mass flows (volume, thickness, velocity, dynamic
76 pressure, concentration, and invasion areas). We stress the fact that the definition of syn-eruptive
77 lahars (Sulpizio et al., 2006; Vallance and Iverson, 2015) adopted in the present work is important
78 when accounting for the multihazard of explosive eruptions, which in areas like Vesuvius and
79 surroundings should not be neglected for its assessment and mapping purposes (de' Michieli Vitturi
80 et al., this issue; Sandri et al., this issue). The methodology used in this work is geological (see Section
81 3.2), and the syn-eruptive definition of lahars is necessary to avoid underestimations of the volcanic
82 hazard from sub-Plinian eruptions at Vesuvius.

83 A lot of the existing literature analyzed the hazard related with volcaniclastic mass flows on the flanks
84 of active volcanoes, through the reconstruction of historical and prehistoric events (e.g., Scott, 1989;
85 Scott et al., 1995; Vallance and Scott, 1997; Zaragoza et al., 2020), by using empirical relationships
86 or physical models (e.g., Macedonio and Pareschi, 1992; Costa, 1997; Iverson et al., 2000; Walsh et
87 al., 2020). However, the areas affected by these phenomena can be extended well beyond the
88 boundaries of the volcanic complex, also including the surrounding plains and the downwind-lying
89 mountainous areas, which are subjected to tephra fallout sometimes even at great distances from the
90 volcano (e.g., Siebe et al., 1999; Pareschi et al., 2000, 2002; Zanchetta et al., 2004a, 2004b; Di
91 Crescenzo and Santo, 2005). In these areas, volcaniclastic mass flows may cause victims and
92 damages, even where considered safe or scarcely affected by other volcanic hazards.

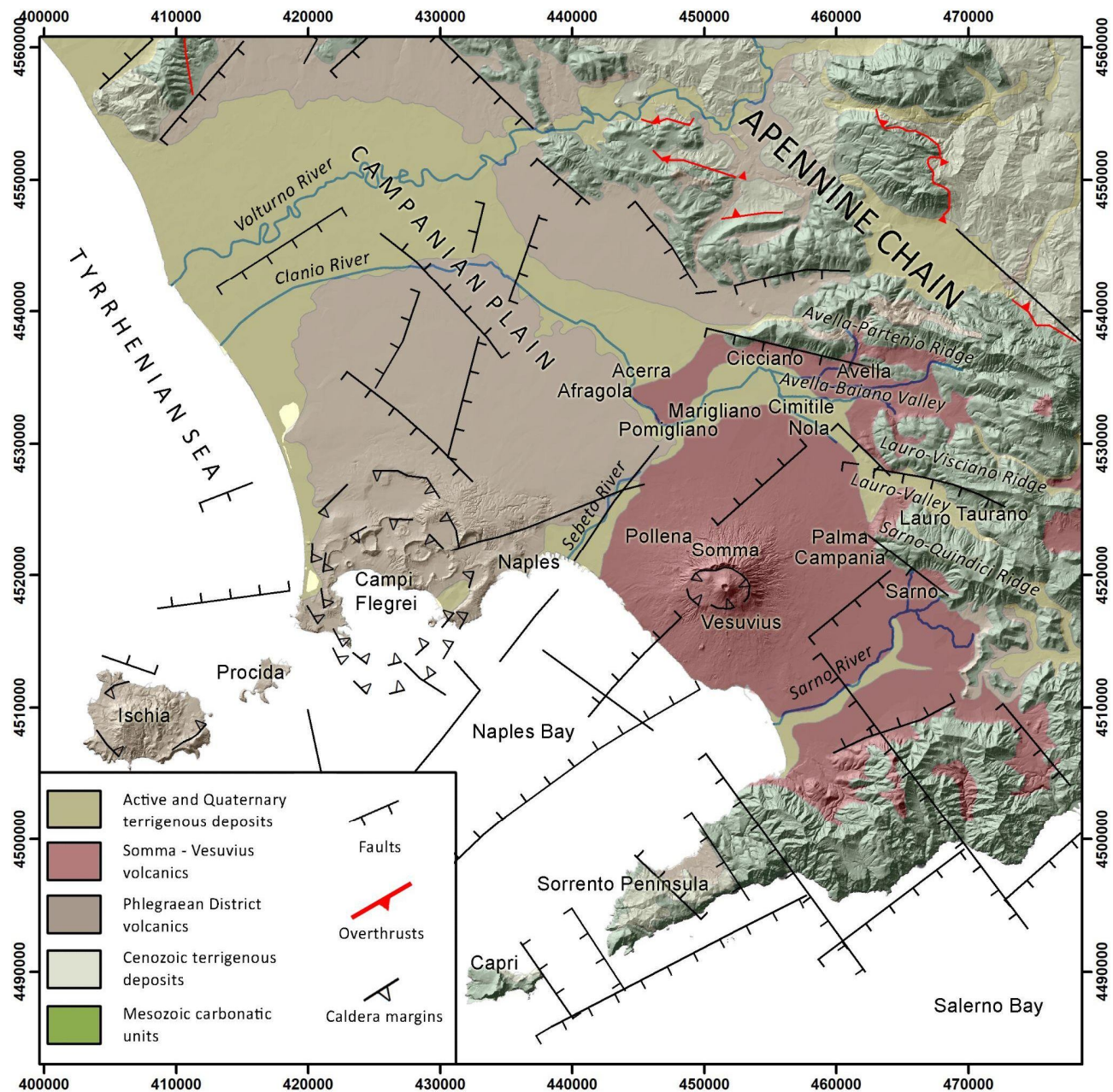
93 In this paper, we present the results of a multidisciplinary study, including geomorphological,
94 stratigraphic, sedimentological and rock magnetic investigations, as well as impact parameter
95 calculations by reverse engineering from the deposits. These investigations followed several
96 surveying campaigns carried out in natural exposures, archaeological excavations, and trenches dug
97 specifically for this purpose in the plain surrounding the Vesuvius edifice and along the Apennine
98 valleys (Fig. 1). One of the goals of the this study is to show the presence of lahar deposits even in
99 areas several km very far from both the source areas of the Apennine hills and the valleys of Somma-

100 Vesuvius edifice, demonstrating the high mobility of these flows. Indeed, These two areas acted as
101 source areas because they ~~been~~were largely affected by deposition of primary pyroclastic deposits
102 offrom Plinian and sub-Plinian Somma-Vesuvius eruptions. Technically, the ones descending on the
103 Apennine flanks should be termed as volcaniclastic debris flows; here we merge into an only one
104 term, lahar, to indicate secondary mass flows strictly related to specific eruptions. The study of the
105 past lahar deposits has been useful for the understanding of the feeding drainage basins for different
106 types of volcaniclastic mass flows, their extent and facies variations with distance from the source
107 area, and the ir associated environmental impact on landscape. As already pointed out by Di Vito et
108 al. (2013, 2019), in the past 4.5 ka repeated lahar and flooding episodes related to the main eruptions
109 of Somma-Vesuvius and Campi Flegrei volcanoes strongly stroke the Campanian Plain and its human
110 settlements, influencing their partial or total abandonment or evidencing attempts of resettlement. In
111 particular, for the areas around Vesuvius, these phenomena included: i) large volume and high energy
112 lahars, originated from the volcanic edifice, which affected the volcanic apron; ii) large flooding
113 phenomena, i.e. overflowing of water affecting the Campanian plain; iii) lahars originated from the
114 perivolcanic mountains that affected the Apennine valleys, and invaded the areas of the plain at their
115 mouths. All of these phenomena differed to each other in terms of amount and grain-size of the
116 involved sediment. The data and pieces of information described here were the basis for validating a
117 new model for lahar transport (de' Michieli Vitturi et al., submittedthis issue), which was applied for
118 assessing the related hazard at Vesuvius and Campanian Plain (Sandri et al., submittedthis issue).
119 The structure of the work consists of an integrated geological, geomorphological, stratigraphic and
120 sedimentological integrated study, a paleomagnetic and sediment-mechanic impact assessment
121 calculation, and a comprehensive discussion on the lahar problem in the Campanian Plain.

122

123 **2. Geological setting**

124 The study area is part of the Campanian Plain, which includes the lowlands surrounding Mount
125 Vesuvius volcano and the nearby Apennine ridges and valleys (Fig. 1). The orography of the area is
126 characterized by three WNW-ESE trending mountain ridges that border eastward the plain, with an
127 elevation ranging from 500 to 1600 m a.s.l., and slope angles from 30 to 60°. From north to south,
128 the Avella-Partenio, Lauro-Visciano and Sarno-Quindici mountain ridges are separated by two
129 depressions: the Avella-Baiano ~~V~~valley, in which the alluvial plain of the Clanio river occurs, and
130 the Lauro valley. Both are narrow valleys that widen toward north-west, among the cities of Cicciano,
131 Nola and Palma Campania (Fig. 1). The reliefs are characterized by a high drainage density,
132 associated with a poorly developed and torrential hydrographic network, which over time has favored
133 the incision and dismantling of the pyroclastic cover on the ridges, and the development of numerous
134 detrital conoids that connect with the main valley floor (Di Vito et al., 1998).



136 Fig. 1. Geological and structural sketch of the Campania Region on a Shaded Relief derived from TINITALY DEM. The
 137 coordinates are expressed in WGS 84 UTM N33 (modified after Orsi- et al., 1996).

138
 139 Vesuvius, or more properly Mt. Somma-Vesuvius, is a composite central volcano less than 39,000
 140 years old, composed of the remnant of the oldest Mt. Somma edifice, dismantled by repeated episodes
 141 of caldera collapse, and the more recent Mt. Vesuvius, grown inside it. Its volcanic history is
 142 characterized by an initial phase, dominated by low-energy effusive and explosive eruptions, which
 143 ended at around 22,000 years ago. Since then, the volcano generated four Plinian eruptions with VEI

144 5-6, each preceded by long periods of quiescence and all accompanied by a summit caldera collapse
145 (Somma caldera; Cioni et al., 1999). The last Plinian eruption occurred in 79 CE and once again
146 modified the Somma caldera, inside which the recent cone has subsequently grown due to an
147 alternation of periods of open conduit, persistent Strombolian and effusive activity, and long periods
148 of quiescence with obstructed conduit, interrupted by high-energy sub-Plinian eruptions. In historical
149 times, the other more energetic events were the sub-Plinian 'Pollena' (472 CE) and 1631 eruptions
150 (Santacroce et al., 2008). The last eruption occurred in 1944 and caused the return to obstructed
151 conduit conditions, which characterize the current quiescent phase of the volcano. The rocks
152 composition varies from slightly silica-undersaturated (K-basalt to K-trachyte) to highly silica-
153 undersaturated (K-tephrite to K-phonolite). The Somma-Vesuvius complex is characterized by
154 ~~Mount Vesuvius is a composite central volcano with~~ a well-developed radial drainage network, which
155 feeds an extensive volcaniclastic apron that morphologically connects the edifice with the
156 surrounding plain (Santacroce et al., 2003). It represents the active southern termination of the Plio-
157 Quaternary volcanic chain that borders the eastern Tyrrhenian margin (Peccerillo, 2003). Volcanism
158 in this margin is related to the extensional tectonic phases that accompanied the anticlockwise rotation
159 of the Italian peninsula, during the complex interaction between the Africa and Eurasian plates, which
160 generated the Apennine thrust-and-fold belt (Ippolito et al., 1973; D'Argenio et al., 1973; Finetti and
161 Morelli, 1974; Bartole, 1984; Piochi et al., 2004; Patacca and Scandone, 2007; Vitale and Ciarcia,
162 2018). The extension along the Tyrrhenian margin of the Apennine chain was accommodated by the
163 activation of NW-SE normal faults and NE-SW normal to strike-slip transfer fault systems, which
164 dismembered the chain in horst and graben structures, and allowed magmas to reach the surface and
165 feed the volcanism (Mariani and Prato, 1988; Faccenna et al., 1994; Acocella and Funiciello, 2006).
166 The Campanian Plain is one of these grabens that hosts the Neapolitan volcanic area. It is a NW-SE
167 elongated structural depression, filled by a thick sequence of marine and continental sedimentary
168 deposits, and volcanic-volcaniclastic successions that compensated its subsidence, leading to a
169 complete emersion at around 39 ka (Brocchini et al., 2001; De Vivo et al., 2001; Santangelo et al.,

170 2017). This graben is bordered toward NW, NE and SE by the Meso-Cenozoic carbonate and
171 terrigenous successions of the Apennine chain, and is subdivided in minor NE-SW oriented horst-
172 and-graben structures (Carrara et al., 1973; Finetti and Morelli, 1974; Fedi and Rapolla, 1987;
173 Brancaccio et al., 1991). Neapolitan volcanoes lie on these second-order structural highs (Marotta et
174 al., 2022 and reference therein), and the products of their most powerful eruptions blanketed the
175 Apennine reliefs and filled their valleys with several meter-thick covers of loose pyroclastic fall
176 deposits, composed of byof pumice lapilli and ash layers separated by paleosoils (Pareschi et al.,
177 2002; Bisson et al., 2007; Cinque and Robustelli, 2009; [Gurioli et al., 2010](#)).

178 In terms of water drainage ~~of the water~~, the pyroclastic cover has peculiar geotechnical characteristics,
179 such as a positive correlation between grain-size and permeability, which enabled the development
180 of lahars in the area. In particular, coarser pumice layers are characterized by ~~interconnected~~
181 ~~inner~~inter-clast void spaces that control water accumulation, instead ash layers, soils and paleosoils
182 by a high water retention capacity (Andosol-like soils), so that the differential behavior can regulate
183 equilibrium among deposits stability vs. remobilization (Fiorillo and Wilson, 2004).

184 Regarding the volcanic activity of Vesuvius in the last 2,000 years, the largest eruptions after the 79
185 CE Plinian one were two sub-Plinian eruptions, the 472 CE Pollena and 1631 ones, but several other
186 effusive and explosive events ~~frequently~~ occurred in historical times. In the Campanian Plain, lahar
187 deposits related to these two eruptions are quite abundant due to past heavy rains ([Fiorillo and Wilson,](#)
188 [2004; Zanchetta et al., 2004b; Stanzione et al., 2023](#)), also the sub-Plinian scenario is of interest for
189 civil protection purposes, which is why in the present work we focus on the ~~se reference explosive~~
190 CE Pollena and 1631 eruptions. ~~Throughout the work, a~~ A particular attention is put given on to the
191 distribution of the primary pyroclastic deposits and ~~the~~ related syn-eruptive lahars, which are mass
192 flow events ~~strictly directly~~ related to specific eruptions, even if the condition is not necessarily that
193 of an event contemporaneous to the eruption. ~~Those~~ Those deposits are mainly composed by of >90%
194 fragments from the parental eruption, while the remaining fragments pertain to other eruptions mixed
195 by volcaniclastic colluvium (Sulpizio et al., 2006). The syn-eruptive feature is thus related to the

196 involvement remobilization of pyroclastic deposits more than to the exact timing of lahar
197 emplacement, the latter being of the order of max a few years (before significant humification
198 processes or significant human activities can occur). Such a feature distinction is important because
199 directly related to volcanic hazard.

200

201 **3. Materials and methods**

202 **3.1. Evidence from historical sources**

203 We collected data from historical sources, maps, documents, and newspapers to supplement the
204 geological data, gathered directly or indirectly, for the definition of the areal distribution of the syn-
205 eruptive and post-eruptive lahar deposits at Vesuvius and in the surrounding region. Such collection
206 concerned the phenomena that took place starting from the sixteenth century CE to 2005. This time
207 span has been chosen depending on data availability, and to show the high recurrence of events over
208 time in the area. The data were collected and grouped not only by years but also by the municipal
209 areas existing at those times. It should be noted that the distribution of the data can be affected by the
210 different urbanization over time, and by the presence of damage to people, thingsinfrastructures and
211 goods, economic activities and settlements. In the absence of local instrumental
212 meteorologicalweather data series, corresponding to over the analyzed period, we assumed that the
213 phenomena of remobilization of the pyroclastic deposits, and the consequent generation of large
214 alluvialflooding events and volcaniclastic mass flows, coincided with extreme weather events often
215 described and reported in the analyzed sources. The reports reach a quite significant number,
216 approximately 500, and concern 97 municipalitiesWe identified about 500 individual reports,
217 covering events between the sixteenth century CE and 2005 that took place in 97 different
218 municipalities— The data were organized in a geospatial database, so that it was possible to define
219 different areas affected by frequent syn-eruptive floods and lahars, concomitant/related with the sub-
220 Plinian eruption of 1631, to be used as benchmark for the main geological analyses. With reference

221 ~~to~~We could not add the Pollena eruption to this historical data set, as there are no historical available
222 sources for similar occurrences other than documents deriving from archaeological excavations
223 ~~activities~~(see next sections).

224 The municipalities with the highest number of reports are: Sarno (43), Salerno (32), Siano (26), Vietri
225 sul Mare (22), Bracigliano (21), Nocera Inferiore (20), Maiori (19), Quindici (17) (Fig. 1). The events
226 of greatest intensity, which affected more than five municipal territories at the same time, are 19;~~they~~
227 ~~likely were multiple soil slip debris flows~~. Some of these occurrences result closely connected with
228 the volcanic events of Vesuvius, such as those that occurred in 1631, 1823, 1910, 1949 and 1954,
229 simultaneously or within months to a few years after the Vesuvius eruptions of 1631, 1822, 1906 and
230 1944.

<u>Eruption</u>	<u>Lahar/Intense Alluvial Event</u>	<u>Municipalities affected</u>
<u>December 1631</u>	<u>16/12/1631</u>	<u>Sant'Anastasia, San Giorgio a Cremano, Massa di Somma, Somma, Ottaviano, San Sebastiano, Trocchia, Torre del Greco, Portici, Pugliano, Madonna dell'Arco, Palma, Nola Arpaia, Arienzo, Cicciano, Marigliano, Benevento, Avellino</u>
<u>October 1822</u>	<u>24/01/1823</u>	<u>Amalfi, Bracigliano, Cava de' Tirreni, Cetara, Minori, Nocera Inferiore, Pagani, Salerno, Sant'Egidio del Monte Albino, Tramonti, Vietri sul Mare</u>
	<u>12/02/1823</u>	<u>Maiori</u>
	<u>12/04/1823</u>	<u>Sarno</u>
	<u>18/10/1823</u>	<u>Corbara, Praiano, Sant'Egidio del Monte Albino, Sarno, Siano</u>
	<u>15/11/1823</u>	<u>Salerno</u>
<u>April 1906</u>	<u>24/10/1910</u>	<u>Amalfi, Boscorese, Cetara, Ercolano, Giffoni Valle Piana, Maiori, Marano di Napoli, Minori, Napoli, Pollena Trocchia, Torre del Greco, Vico Equense, Vietri sul Mare, Sant'Anastasia, San Giorgio a Cremano, Sarno, Scala, Pomigliano d'Arco, Portici, Ravello, Salerno</u>
<u>March 1944</u>	<u>02/10/1949</u>	<u>Lauro, Maiori, Minori Nocera Inferiore, Sarno, Vietri sul Mare</u>
	<u>25/10/1954</u>	<u>Cava de' Tirreni, Maiori, Minori, Nocera Inferiore, Salerno, Tramonti, Vietri sul Mare</u>

231 [Tab. 1. Historical archive of lahar and alluvial events related to the four most significant Vesuvius eruption in the last](#)
232 [four centuries, and municipalities affected by such events.](#)

233 The absence of information in the Lauro and Avella-Baiano ~~y~~Valleys is likely due to the absence of
234 detailed descriptions of alluvial events, or most likely to the position of the inhabited areas generally
235 located on the hills thus far from the lower part of the valleys. [The investigated area has been](#)~~was~~
236 [affected many times by post-eruptive lahars](#) events due to the presence of thick variable~~ley~~-weathered
237 [pyroclastic deposits mantling the steep slopes of Somma-Vesuvius and Apennines. One of the most](#)
238 [recent event occurred on May 5th 1998, when a 16-hours prolonged heavy rainfall triggered a huge](#)
239 [number of Apennine slope failures towards the towns of Quindici, Bracigliano, Siano, Sarno and San](#)
240 [Felice a Cencello, all located near the Apennine ridges east-northeast of Somma-Vesuvius \(Fig. 1\).](#)
241 [This catastrophic events](#) involved an extension area of around 60 km², and a volume of more than
242 [2,000,000 2x10⁶ m³ \(40% derived from the materials eroded along the channels\), leading to causing](#)
243 [160 victims and huge severe damages to the quoted towns \(Di Vito et al., 2019 and references therein\).](#)

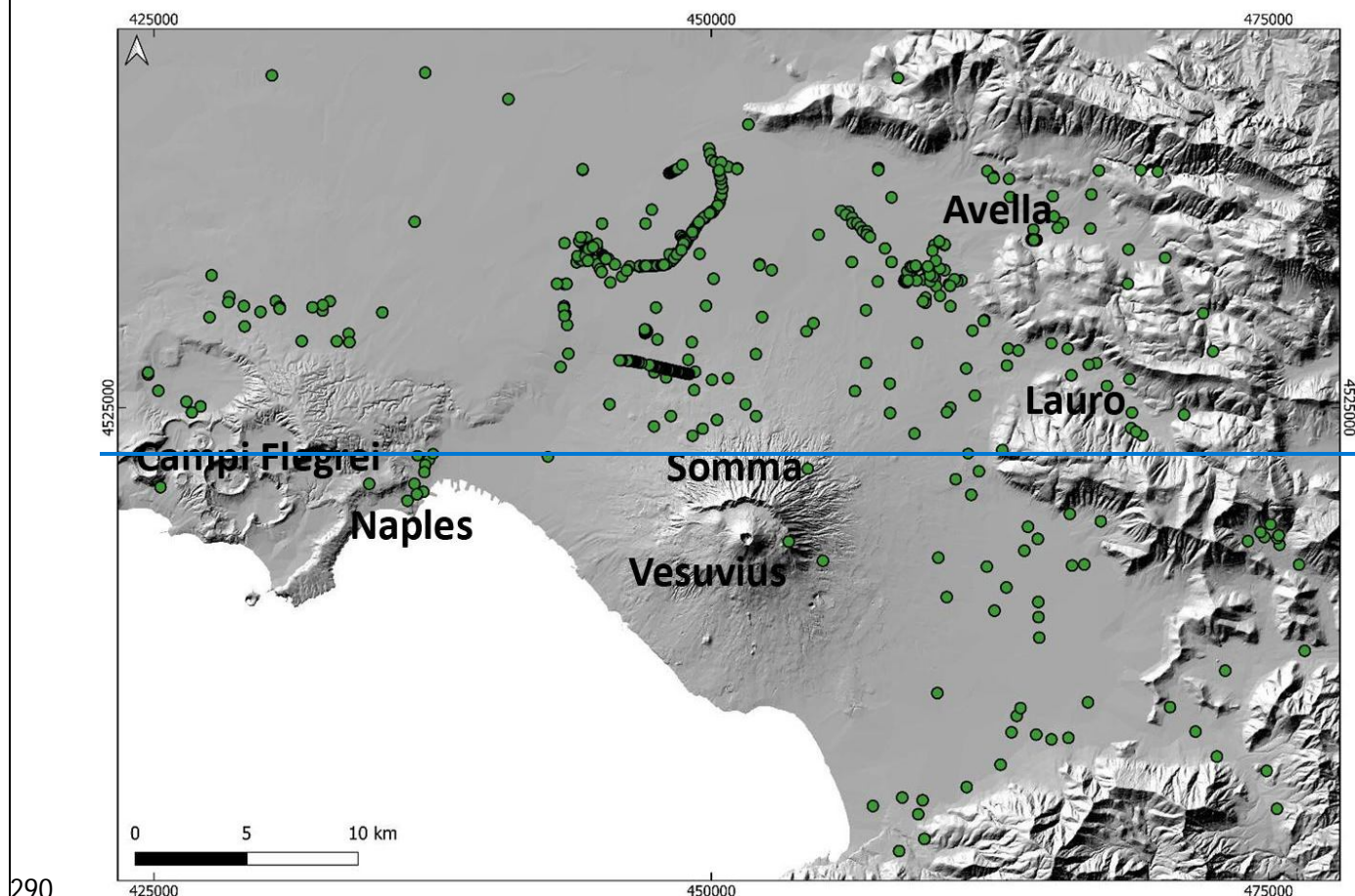
244

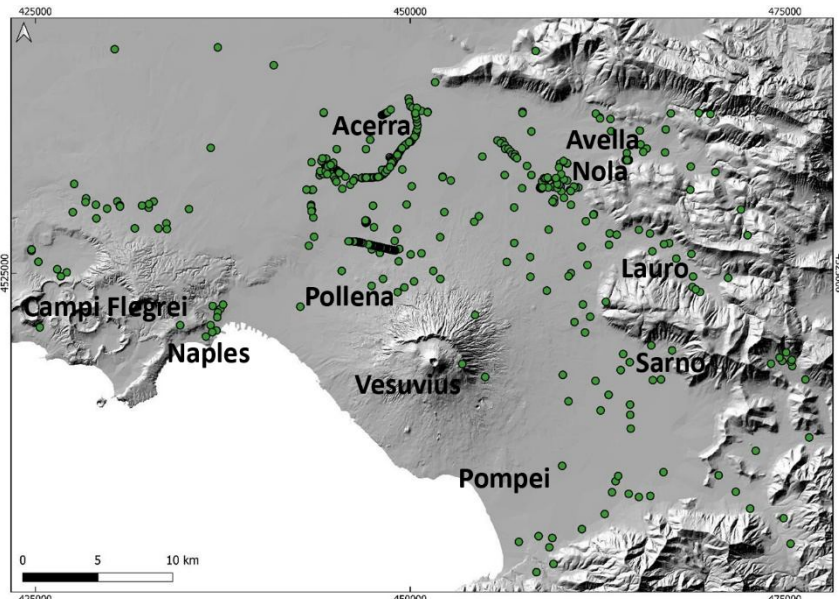
245 **3.2. Field and archaeological investigations**

246 We used a set of geological, stratigraphical, sedimentological, archaeological, and pedological
247 information for the reconstruction of the type of events, their emplacement mechanisms, timing, and
248 impact on pre-existing structures/environment. Such an approach enabled us to cross-check
249 geological and archaeological evidence allowing us to accurately fix the age of events. Conversely,
250 the presence of well-dated primary pyroclastic deposits can define the age of human traces otherwise
251 not easily datable. Furthermore, the identification of the “primary” (fallout and pyroclastic current,
252 along with the archeological findings) can give the absolute age (*ante* or *post quem*) of a given deposit.
253 The definition of isochronic paleosurfaces can also contribute to the reconstruction of the paleo-
254 environments affected by the deposition, and of the variations that occurred during depositional
255 processes. For this purpose, particular attention was paid to the basal contacts between the deposits.

256 In some areas like Nola (10-15 km from Apennine source valleys), the lahar deposits directly overlie
257 the primary pyroclastic deposits (of both for the 472 CE Pollena or and 1631 eruption), while in
258 other ~~eases-areas~~ some pyroclastic units or the whole primary deposits are missing (eroded) or
259 lacking. Only the correlation with the nearby areas ~~P~~permitted to define whether the emplacement of
260 the ~~secondary deposits~~lahars eroded partly or ~~entirely~~significantly the underlain primary deposits,
261 vice versa the complete absence in the emplacement areas ~~was~~could also be “simply” due to the
262 distribution of these latter. The analysis of the internal structure marked by sharp changes in grain
263 sizes, color, presence of erosive erosional unconformities, or interposition of lenses of coarser
264 material also permitted the identification of one or more flow units within the same individual deposit
265 package. The macroscopic characteristics of the sequences permitted some inferences on the transport
266 and depositional mechanisms, while the grain-size and componentry ~~analysis~~analyses provided
267 information ~~of on~~ the source deposits that were remobilized. This brings to another important
268 definition, that is syn-eruptive vs. post-eruptive lahars, according to the definition of Sulpizio et al.
269 (2006) and Iverson and Vallance (2015), which applies during or ~~respectively~~ soon after the eruption
270 vs. several years to centuries after the eruption ended, respectively. The macroscopic analysis allowed
271 us to distinguish between the syn-eruptive and post-eruptive deposits, ~~which~~. The first ones are
272 defined by the occurrence of pyroclastic components with ~~homogeneous a~~ lithology, similar to the
273 one of the primary deposits, ~~and the post (or inter) eruptive deposits~~. The second ones are
274 characterized by some evidence of depositional stasis, ~~such as like~~ humified paleosurfaces, ~~evidence~~
275 below the lahar deposits or of ~~anthropic anthropogenic~~ activities, or ~~also through~~ deposits that
276 ~~contain~~ by the presence of humified material and/or fragments of older eruptions in the
277 deposits ~~following the progressive erosion within the feeding slopes and valleys~~. All these
278 characteristics allowed the correlation between the various volcaniclastic units for the whole set of
279 the studied sequences, marking the differences needed to hypothesize on the source and invasion
280 areas.

281 We reviewed all the volcanological and archaeological data collected during the last 20 years from
282 drill cores, outcrops, archaeological excavations, and from the existing literature, in collaboration
283 with colleagues of the Archaeological Superintendence of Campania region. The preliminary
284 collection and analysis of the existing data permitted to plan a hundred of new stratigraphic trenches
285 (Fig. 2), with the aim of collecting stratigraphic, ~~stratimetric~~, sedimentological, lithological and
286 chronological data on the ~~sequences both of~~ primary pyroclastic and secondary (lahar) deposits.
287 Particular attention was also paid to the ~~primary pyroclastic deposits and to syn- and post-eruptive~~
288 ~~lahars, and to their~~ geometric relations of these deposits with the paleotopography and ~~the~~ preexisting
289 ~~anthropic~~ anthropogenic structures.





291 Fig. 2. Shaded relief of the studied area and location of all the sites where stratigraphic analyses were carried out.

292

293

294 The collected data were organized into a geospatial database (QGIS Platform), in which each point
 295 represents an investigated site linked to a series of information, such as the precise location, the
 296 kindtype of volcanic sequence, and the stratimetricstratigraphic features (primary and secondary
 297 units, thickness, type of deposit, etc...). The data were visualized using a Digital Elevation Model
 298 (DEM) of the Campanian Plain as reference topography and the UTM WGS 84 – Zone 33N reference
 299 projection.

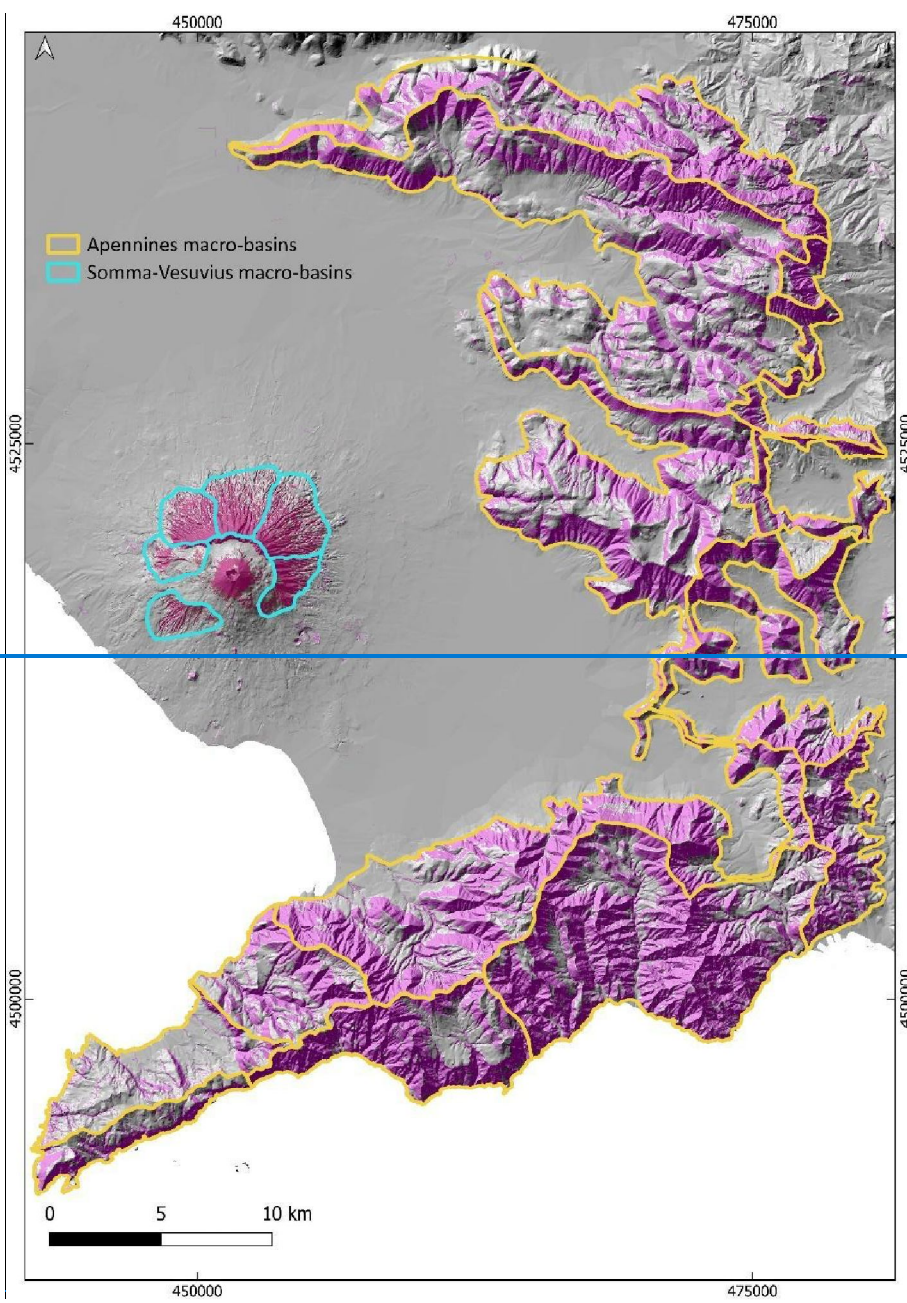
300

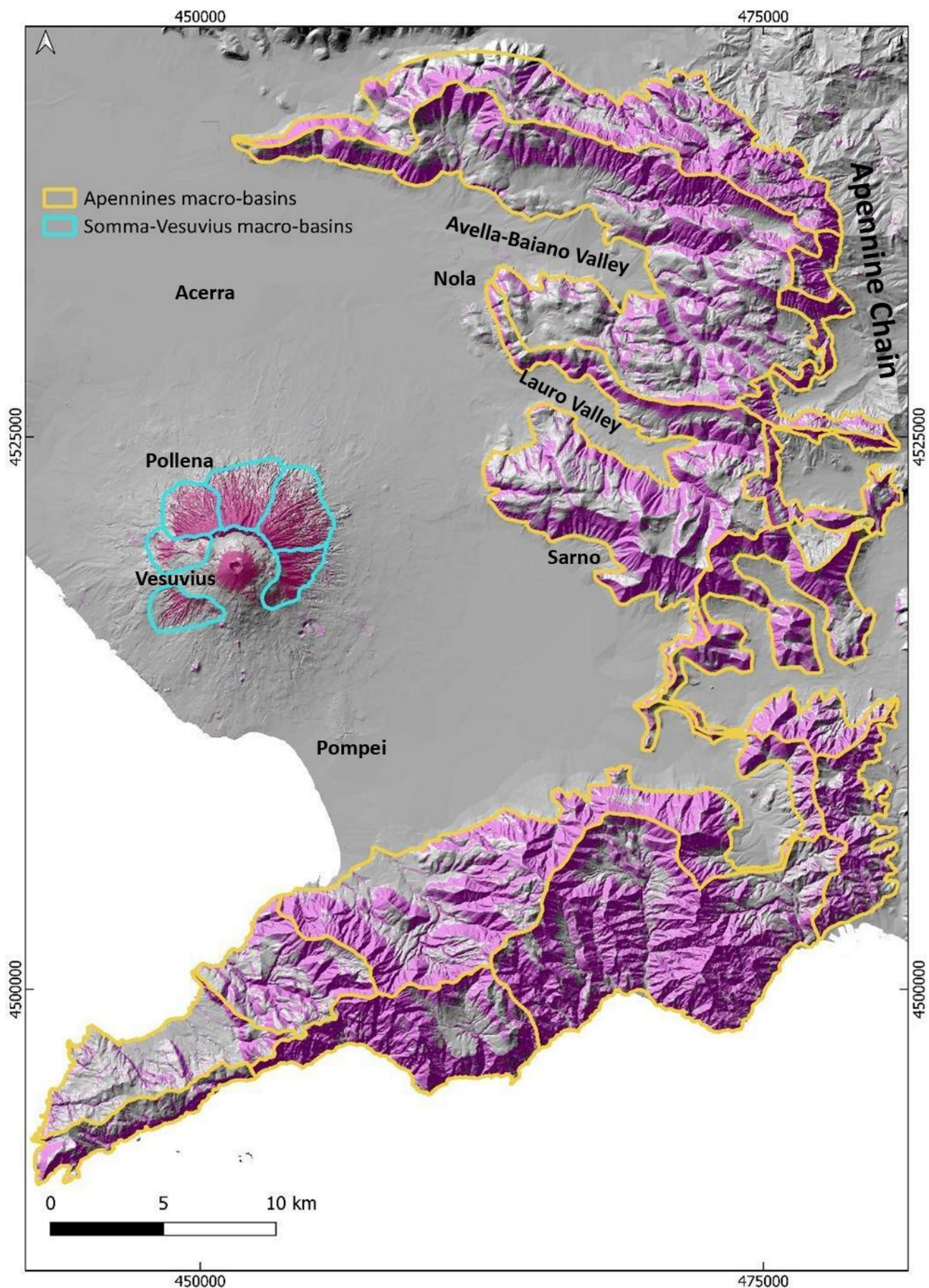
301 **3.3. Geomorphological analysis**

302 This analysis is aimed at identifying the macro-basins that fed the lahars in the study area after the
 303 two sub-Plinian eruptions (Pollena and 1631). The analysis was carried out on the basis of the slopes
 304 distribution and the watersheds extracted from a Digital Elevation Model (DEM). The DEM was
 305 derived from a LiDAR flight of 2012 and stored with (cell size of 10 m). In particular, six macro-
 306 basins characterized by slopes $> 20^\circ$ were identified in the Somma-Vesuvius area, whereas fifteen
 307 macro-basins with slopes $> 25^\circ$ were identified in the Apennines to the East of the volcano (Fig. 3).

308 The different slopes thresholds are defined starting from previous studies (Pareschi et al., 2000, 2002;

309 see also Bisson et al., 2013, 2014), and on the basis of a better analysis of the physical characteristics
310 of the remobilized material, in turns related to the various types of deposits. In fact, ~~along the slopes~~
311 ~~of on the steep slopes and in the valleys of~~ Somma-Vesuvius, ~~they~~ ~~deposits~~ are ~~mainly mainly~~ ash-
312 rich pyroclastic current ~~deposits and subordinately lapilli fallout~~ deposits, while ~~for on~~ the
313 ~~Apennines~~Apennines they are ash and lapilli fallout deposits ~~emplaced along the variably deep~~
314 ~~slopes~~. Each basin was considered as a single feeding unit for the lahars generation, and this is an
315 input for the modeling of possible future lahars in the companion papers (de' Michieli Vitturi et al.,
316 ~~submitted this issue~~; Sandri et al., ~~submitted this issue~~).





319 Fig. 3. The macro-basins defined on the basis of their geomorphological features to study the areas of possible
320 accumulation and mobilization of deposits, which are used in modeling lahar generation of future events.

321

322 **3.4. Laboratory and analytical work**

323 **3.4.1. Grain-size**

324 In ~~several the selected studied sites among all the studied ones reported in~~ (Fig. 4), macroscopic
325 ~~analysis analyses~~ of the stratigraphic sequences ~~was were~~ ~~first~~ carried out in the field to ~~first~~ identify
326 any homogeneities or similarities between the juvenile fraction of the primary and secondary deposits,
327 and ~~then~~ recognize the various volcaniclastic units. This was followed by sampling the deposits and
328 carrying out the laboratory analyses.

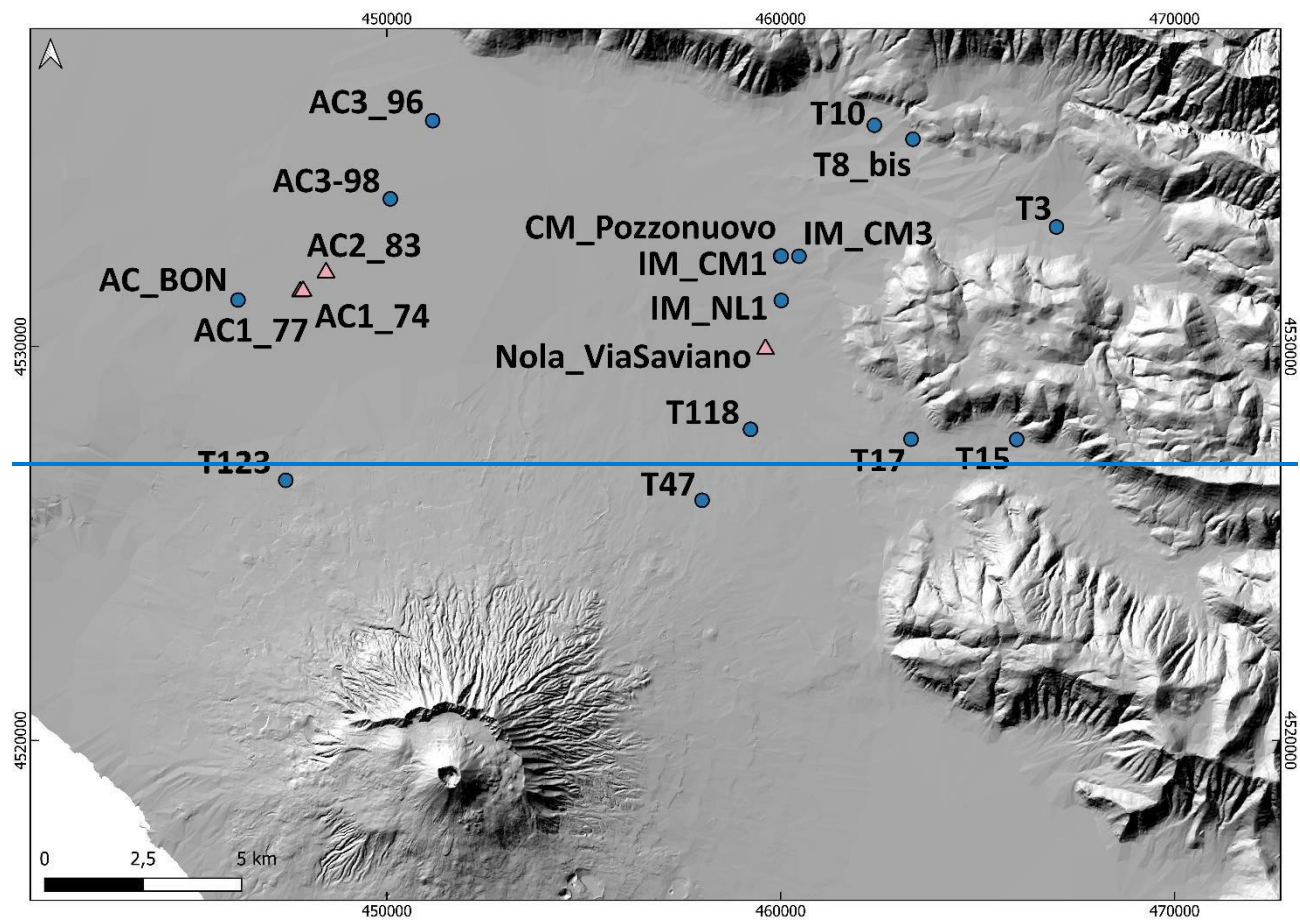
329 In particular, the sampling was mostly made on the syn-eruptive lahar deposits, but also on the post-
330 eruptive and, in a few cases, on the primary pyroclastic deposits. All lab analyses were performed in
331 the laboratories of sedimentology and optical microscopy at the Istituto Nazionale di Geofisica e
332 Vulcanologia, Sezione di Napoli Osservatorio Vesuviano (INGV – OV). The material samples were
333 pre-heated at a temperature of 60-70 °C to eliminate any fraction of humidity, then were quartered
334 and sieved. To avoid any breaking of fragile clasts like pumices, the dry sieving of the grain-size
335 classes between -4 (a coarse limit variable depending on the sample) and 0 phi was made manually,
336 while for the classes between 0.5 and 5 phi a mechanical sieving apparatus was used.

337 In particular, ~~Tthe the~~ fine ash-rich deposit samples with ~~a~~ high degree of cohesion ~~(with a significant~~
338 ~~amount >0 phi)~~ were ~~first combined with~~ ~~diluted in~~ distilled water ~~and thus, then~~ boiled to remove all
339 ~~the~~ ash aggregates, before being analyzed for ~~granulometry grain-sizes~~ following a wet procedure,
340 ~~and finally dried and weighted by classes. The cumulative class >5 phi was further separated by~~
341 ~~interpolation modelling (de' Michieli Vitturi et al., this issue).~~ In the post-processing of the data, the
342 GRADISTAT excel package by Blott and Pye (2001) was used to determine the main statistical
343 parameters. On selected samples, a microscopic component analysis was performed, consisting of

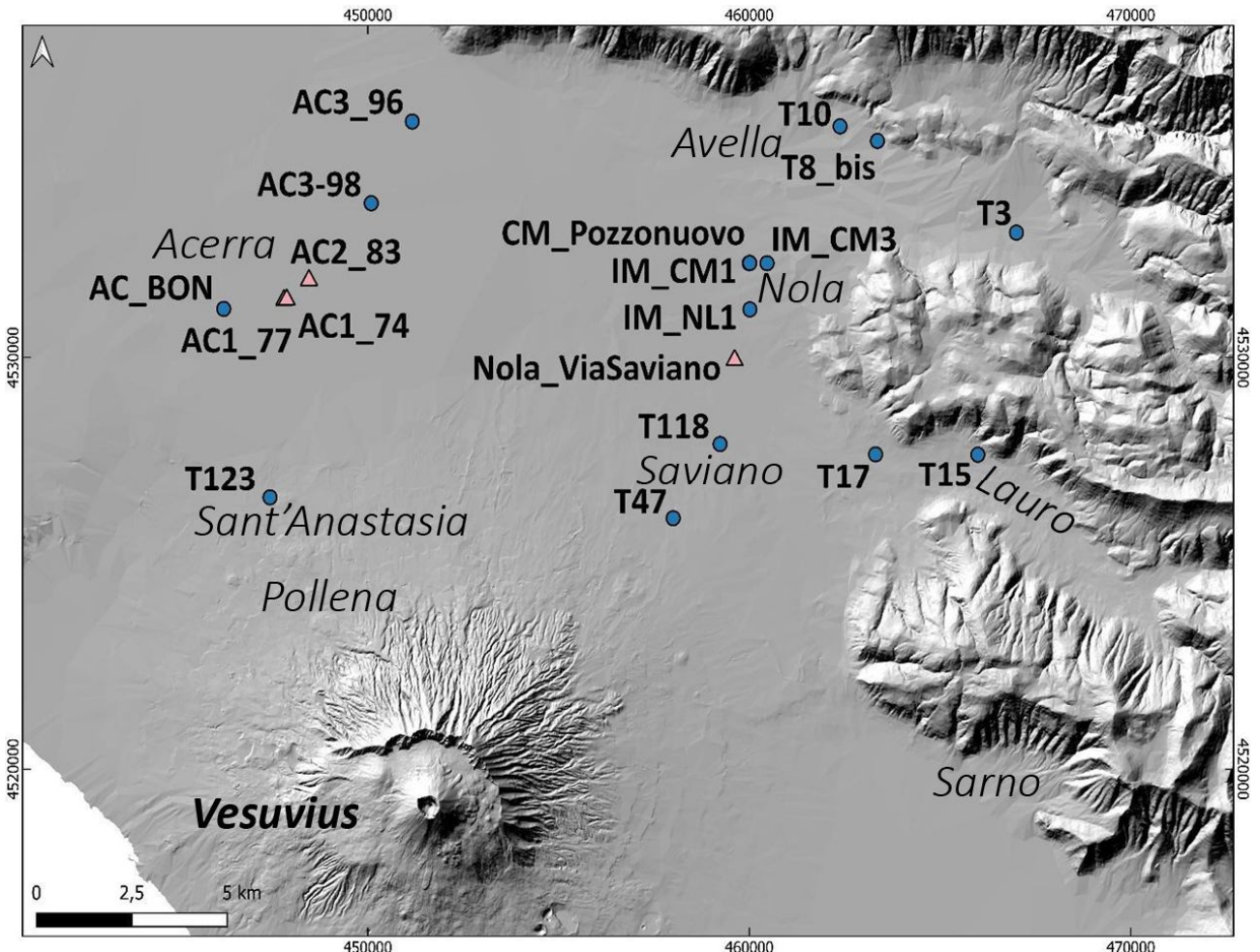
344 recognizing and separating the various lithotypes that compose the volcaniclastic deposits, that is
345 juvenile, lithic and crystal clasts. The clasts recognition was made manually for the coarser fractions,
346 while for the finest fractions it was necessary the use of a reflected-light binocular microscope.

347

348



349



351 Fig. 4. Location of sites in which the sampling was carried out for sedimentological and paleomagnetic analyses. The
 352 pink triangles represent the sites for which a paleomagnetic study was carried out (AC1_74, AC1_77, AC2_83, and
 353 Nola_Via Saviano). In several sites, multiple samples were taken at different stratigraphic heights; samples labeled with
 354 US were taken at CM_Pozzonuovo site (see results).

355

356 **3.4.2. Input for impact parameters**

357 A significant number of large clasts and boulders was also found embedded in the ~~ash matrix of the~~
 358 lahar deposits at different locations. These clasts have dimensions from several centimeters to several
 359 tens of centimeters in diameter, and their nature is variable, that is limestone, ceramic, brick, tephra,
 360 lava, sandstone, iron (in order of abundance). Most of the clasts are fragments of artifacts from
 361 buildings, structures, and other archaeological finds of the Roman period, and their shape can be

362 approximated in the field to ellipsoid. All these features suggest that they were entrained from
363 substrate into the lahars to ultimately be deposited together with the ashmain finer solid load of the
364 lahars. In the dynamics of volcaniclastic mass flows like lahars and pyroclastic currents, the
365 occurrence of boulder entrainment by flow dynamic pressure is recognized as a ~~it is~~ quite common
366 feature (e.g., Zanchetta et al., 2004a; Pittari et al., 2007; Duller et al., 2008; Toyos et al., 2008; Cas
367 et al., 2011; Carling, 2013; Doronzo, 2013; Jenkins et al., 2015; Roche, 2015; Martí et al., 2019;
368 Guzman et al., 2020). The capability of a flow to entrain a clast is a function of flow properties
369 (velocity, density) and clast properties (dimension, density, shape), and dynamic pressure well
370 syntheses and quantifies such capability also in terms of flow hazard (Toyos et al., 2008; Zuccaro and
371 De Gregorio, 2013; Jenkins et al., 2015). In Appendix ~~4A~~, a theoretical scheme is presented to invert
372 these field features for calculation of the impact parameters at local scale.

373

374 **3.4.3. Rock magnetism**

375 The lahar deposits related to the Pollena eruption were analyzed by rock magnetism ~~at two~~
376 ~~localities, in the municipalities of~~ Acerra (12 km from Somma-Vesuvius) and Nola (10-15 km from
377 10-15 km from Apennine source valleys) ~~at four localities (Fig. 4), where the lahars interacted with~~
378 ~~anthropogenic structures. At each locality, we collected oriented samples, then measured about 200~~
379 ~~specimens.~~ We sampled both the deposit matrix and some potsherds embedded along three trenches
380 (74, 77 and 83) and in the “Nola-Via Saviano” excavation (~~Fig. 4~~). The purpose of the magnetic
381 measurements was threefold: i) evaluating the magnetic fabric of the deposits to infer the local to
382 regional flow directions of the lahars and possibly their origin, whether from the Apennines ~~or from~~
383 Vesuvius. The magnetic fabric in this type of deposits records the main flow direction (local/regional)
384 followed during the emplacement processes; ii) estimating the deposition temperature (T_{dep}) of the
385 deposits, to understand whether the lahar was triggered soon after the eruption or at later times. The
386 hypothesis is that the temperature is higher in case of syn-eruptive lahars deriving from hot

387 (pyroclastic current) deposits, and lower in all other cases of post-eruptive ones; iii) testing the
388 relative sequence (contemporaneity) of the lahars emplacement with respect to the Pollena eruption.
389 All hand-samples were oriented *in-situ* with magnetic and solar compasses and reduced to standard
390 sizes at the CIMaN-ALP laboratory (Peveragno, Italy), where all the magnetic measurements were
391 made. In Appendix 2B, the adopted paleomagnetic techniques and nomenclature are described.
392

393 **4. Results**

394 **4.1. Field stratigraphy and sedimentological features**

395 In this study, data of about 500 sites were collected, covering an area of >1000 km² from the plain
396 around the volcanic edifice to the Apennine valleys to the north and east (Fig. 2).

397

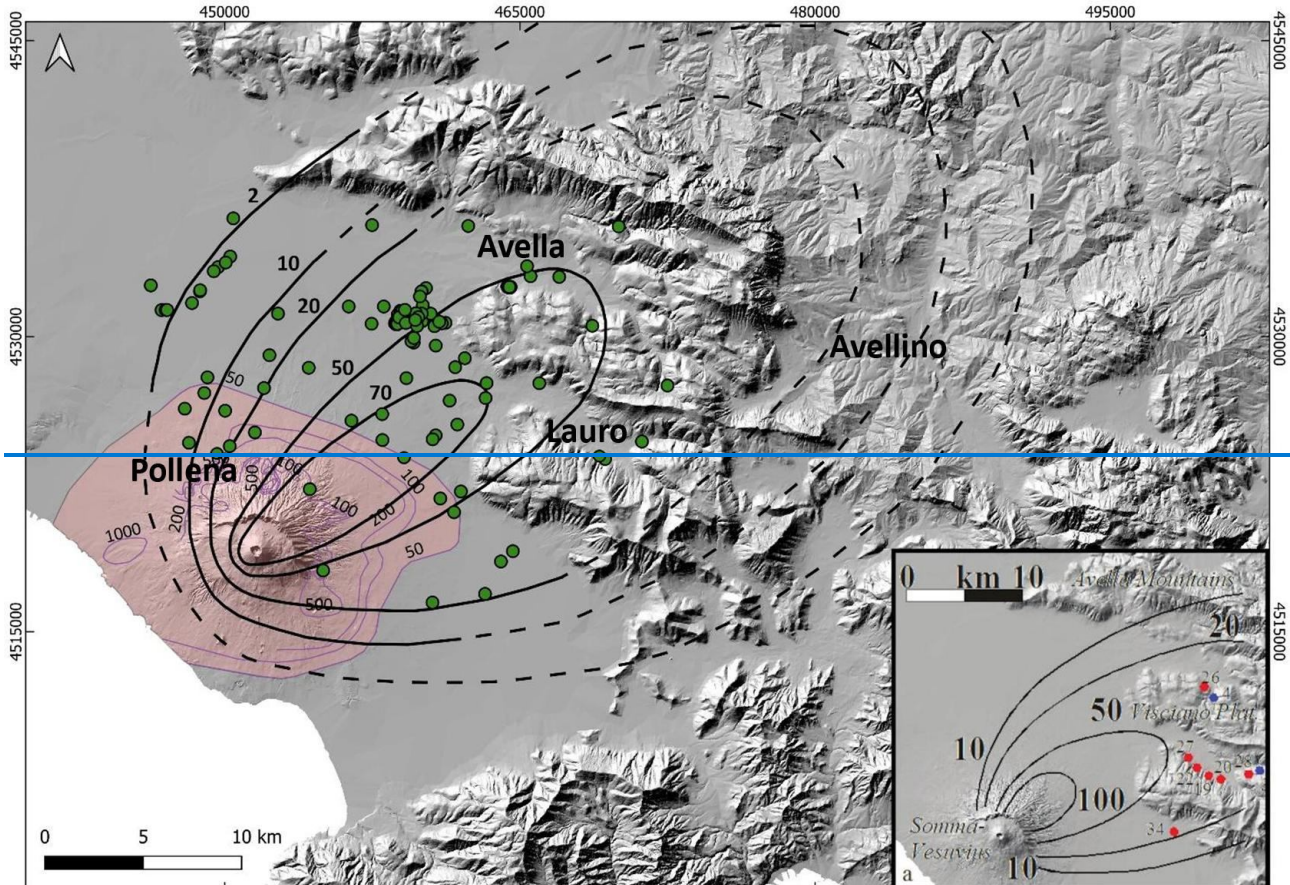
398 **4.1.1. Pyroclastic deposits: eruptions of Pollena and 1631 eruptions**

399 The integration of the collected data with the existing ones (Rosi and Santacroce, 1983; Rosi et al.,
400 1993; Rolandi et al., 2004; Sulpizio et al., 2005; Perrotta et al., 2006; Bisson et al., 2007; Santacroce
401 et al., 2008; Gurioli et al., 2010; De Simone et al., 2011) allowed the reconstruction of the distribution
402 maps for both the fallout and pyroclastic current deposits. In particular, the spatial distribution
403 highlights that for both the Pollena and 1631 primary deposits, thick fine ash deposits are widely
404 distributed and cover the coarse fallout sequence or directly the ground, modifying the isopachs
405 reconstructed by previous authors (Sulpizio et al., 2006 and references therein; Figs. 5 and 6). This
406 enlargement of the area affected can have important implications on the hazard evaluation in terms
407 of possible damages on a densely inhabited territory.

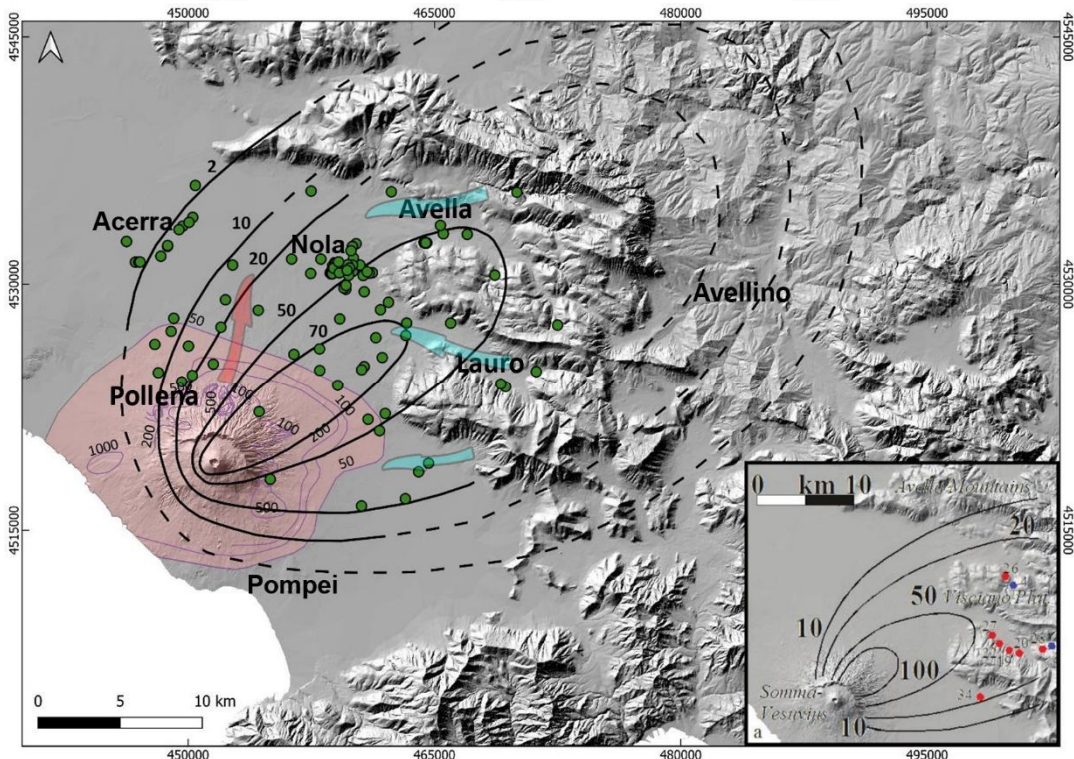
408 The area covered by the comprehensive isopach maps (including both ~~the~~-lapilli ~~fallout~~ and ash
409 fallout) turns out to be wider than ~~the one~~-previously known, above all because we ~~also~~-took into
410 account for the ash ~~deposited by~~ fallout occurred during the final phreatomagmatic stages of the
411 eruptions, ~~mostly dominated by phreatomagmatic explosions~~ (Rosi and Santacroce, 1983; Sulpizio et

412 al. 2005). The great ~~distribution and~~ availability ~~and distribution~~ of these ash deposits could explain
413 the wide generation and distribution of the syn-eruptive lahars in the area. This has important
414 implications ~~in-on~~ the evaluation of the source area and ~~of the~~ material available for ~~the~~ lahars
415 accompanying and following ~~this these~~ eruptions. ~~In particular~~ Interestingly, there is an increase of
416 the areas covered by pyroclastic deposits ~~and the calculated volume of the emitted products. For~~
417 ~~example, the area covered by the pyroclastic current deposits thus results in is of about~~ 200 km² for
418 the Pollena eruption, and 120 km² for the 1631 eruption, while. More significantly, ~~t~~he QGIS
419 ~~recalculated 10-cm isopach area for covered by~~ the fallout deposits ~~it is of~~ 433-837.35 km² (Pollena
420 eruption) and 427-5287.51 km² (1631 eruption), respectively which compared to the lower values of
421 569 km² (Pollena eruption) and 158 km² (1631 eruption) after Sulpizio et al. (2006) give an extra
422 surface of about 47% and 230%, respectively. Geotechnically, ~~A~~nother implication is that the wide
423 presence of fine and cohesive ash, ~~not only~~ on top of the coarse fallout sequences ~~and, in general but~~
424 ~~also~~ on the ground, ~~reduces the permeability of the substrate~~, preventing ~~the~~ water infiltration ~~of the~~
425 ~~water and~~, favoring ~~the stream formation~~ surficial runoff and creating sliding surfaces (Baumann et
426 al., 2020). They can also enhance the mobility of the flows by creating sliding surfaces.

427



428



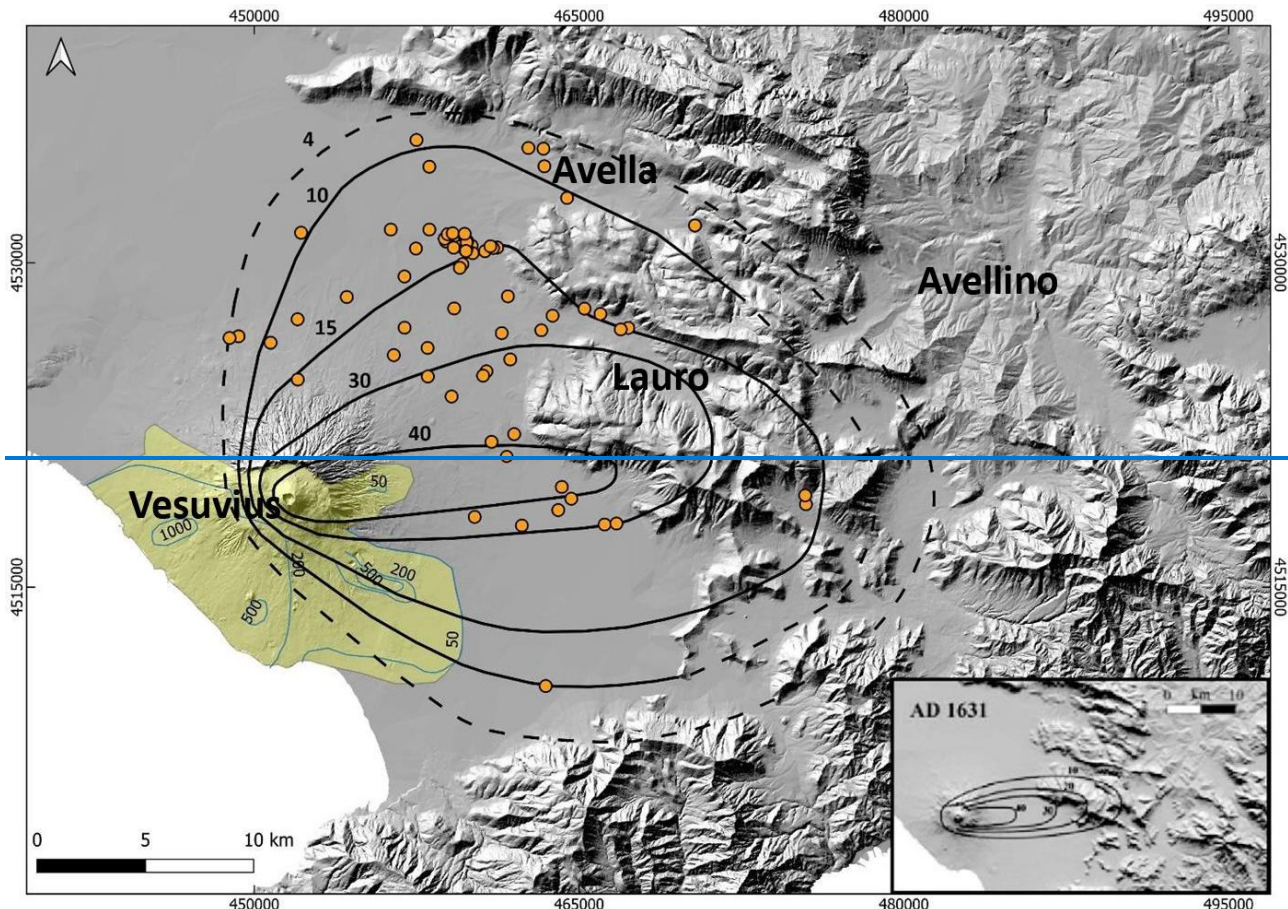
429

430 Fig. 5. Pollena eruption: the black lines represent the isopachs (in cm) of the fallout deposits modified after Sulpizio et
 431 al. (2006) (in the insert) on the basis of the new collected data (green dots), while in pink is colored the area affected by
 432 PDC—the pyroclastic current deposits (isopachs in cm, purple lines); modified after Gurioli et al. (2010) (purple lines).

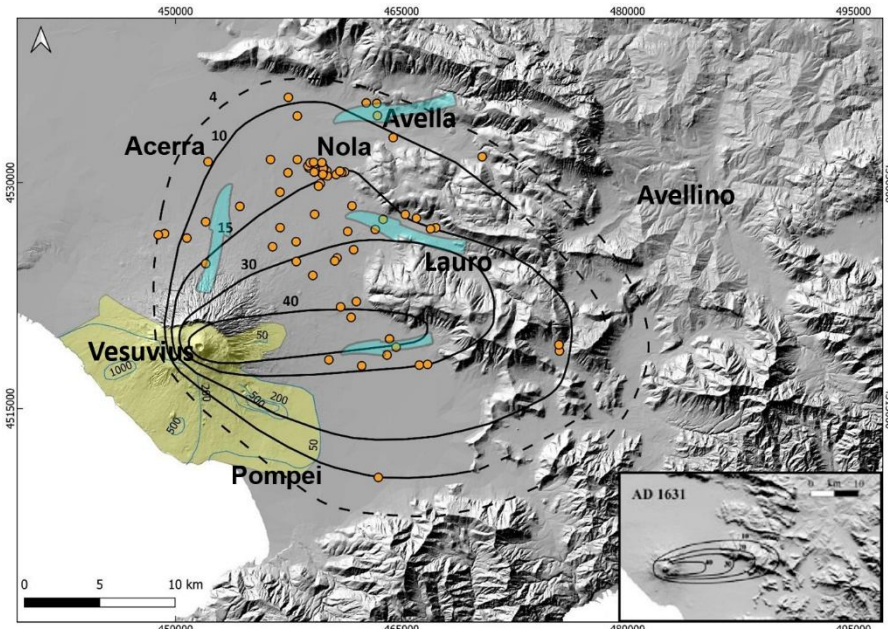
433 The dotted parts of the isopachs represent some uncertainty related to the absence of new further data are extrapolated.
434 The light blue arrows represent the general remobilization of the pyroclastic fallout deposits and lahar propagation from
435 the Apennine slopes, while the pink one represents the combined remobilization of the pyroclastic current and fallout
436 deposits and lahar propagation from Somma-Vesuvius.

437

438



439



441 Fig. 6. 1631 eruption: the black lines represent the isopachs (in cm) of the fallout deposits, modified after Santacroce et
 442 al. (2008) (in the inset) on the basis of the new collected data (orange dots), while in yellow is colored the area affected
 443 by PDC-pyroclastic current deposits (isopachs in cm, light blue lines). The light blue lines represent the inferred
 444 distribution on the basis of an integration between field data and fonschronicles, modified after Gurioli et al. (2010). The
 445 dotted parts of the isopachs represent some uncertainty related to the absence of new further data are extrapolated. The
 446 light blue arrows represent the general remobilization of the pyroclastic fallout deposits and lahar propagation from the
 447 Apennine slopes and Somma-Vesuvius.

448

449 The significant widening of the area affected by accumulation of the 1631 eruption tephra-fallout
 450 deposits is wider than previously known, particularly towards the north for the 1631 eruption, which
 451 follows the inclusion of the final ash deposits into the new isopachs. Interestingly, such widening of
 452 the area agrees with the wide occurrence of lahars in the plain north of Vesuvius, as documented in
 453 the echronicles and historical sources (Rolandi et al., 1993; Rosi et al., 1993, and references therein),
 454 and as follows.

455

456 4.1.2. Lahar deposits

457 The lithological and sedimentological analyses carried out in the field allowed the macroscopic
458 definition of the primary pyroclastic deposits involved in affected by the remobilization, and of the
459 lahar deposits. In many cases, the archaeological findings permitted to define the local
460 paleoenvironment and the related land use, and also to then permitted to constrain the age and timing
461 of the deposition.

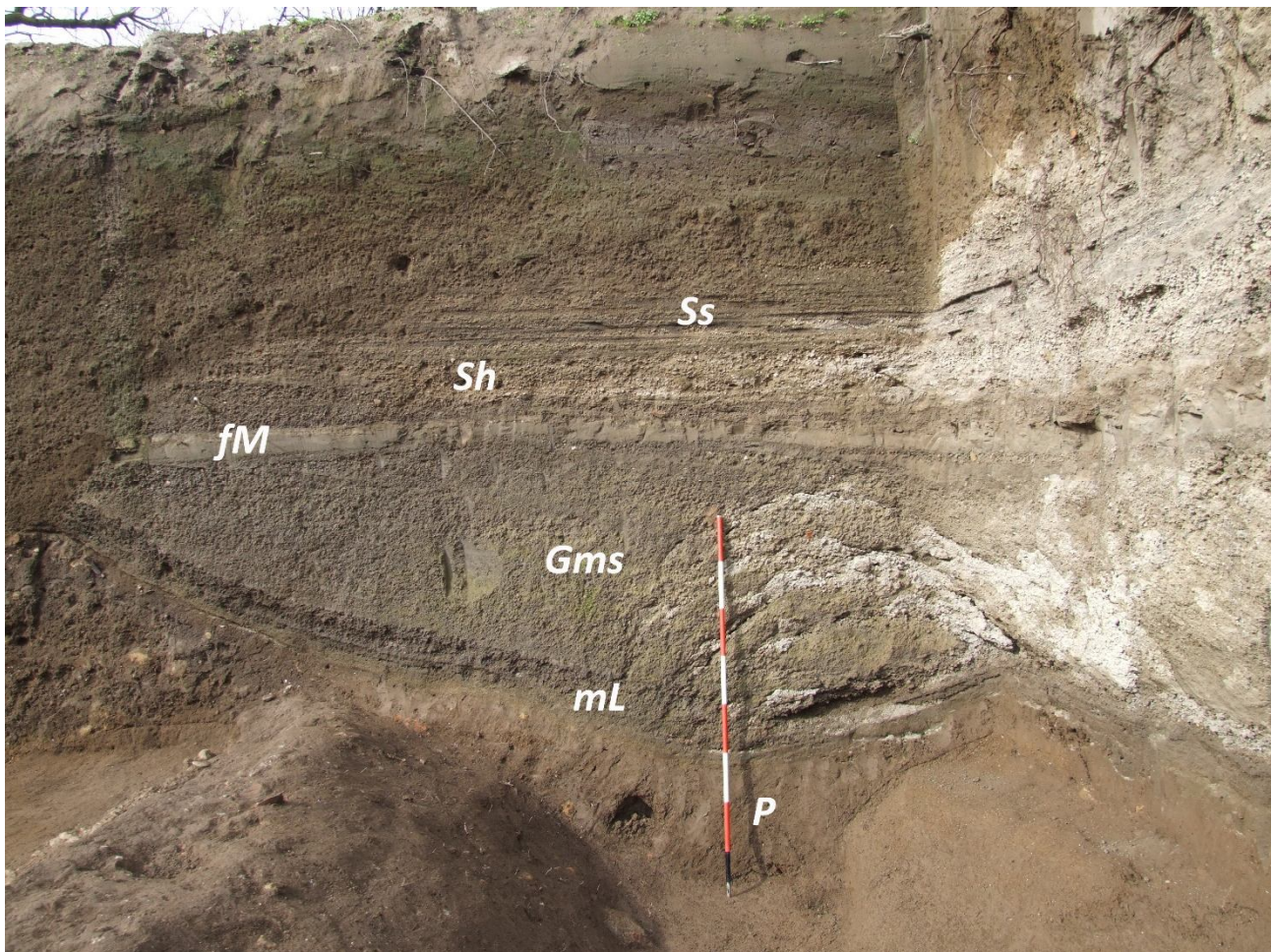
462 We grouped all deposit descriptions into representative lithofacies to more directly characterize both
463 the primary pyroclastic and lahar deposits (Tab. 2 and Fig. 7). Given the amount of data and
464 description of the studied areas, we used these lithofacies to characterize a number of macro-areas
465 between the Somma-Vesuvius sector and the nearby Apennine valleys (Appendix C). The lithofacies
466 mostly recognized are P to indicate paleosol and humified surface, mL and mA (massive lapilli and
467 massive ash, respectively) to indicate the primary deposits, while the lahar deposits usually belong to
468 the facies Gms and mM, which indicate massive, matrix-supported gravel deposits and massive lahar
469 deposits, respectively. Other recognized lithofacies are Sh, Ss and fM. Sh indicates hyper-
470 concentrated flow deposits, and consists of an alternation of coarse and fine beds. Ss includes scour
471 and fill structures, and consists of an erosive, concave upwards basal surface and a planar/convex
472 top. fM is fine mud, and indicates the decantation deposit formed when the flow loses its energy.

<u>Symbol</u>	<u>Lithofacies</u>
P	<u>Paleosol</u> and humified surface, massive and composed of fine sand and silt from brown to dark brown, with several percentages of clay and organic matter. It indicates a stasis in the depositional processes.
ml	<u>Alternation of massive lapilli layers. Pyroclastic fall deposit, massive and composed of pumices and scoria lapilli with sparse accidental lithics.</u>
mA	<u>Massive ash. Pyroclastic fall deposit, massive and composed of fine to coarse ash with sparse pumice fragments, scoriae and accidental lithics.</u>
Gms	<u>Massive gravel and sand deposit, matrix-supported and poorly-sorted. The matrix is composed of fine to coarse sand, while the gravel clasts comprise scoriae and pumice clasts from the pyroclastic fall deposits. The massive feature of the single layers suggests a rapid emplacement from a highly-concentrated lahar.</u>
mM	<u>Massive mud deposit composed of fine sand, silt and clay, sometimes with sparse pumice and lithic clasts. It is generated from a mud-dominated lahar.</u>

Sh	Horizontal lamination and bedding features in sands. The deposit is composed of an alternation of fine to coarse sand and gravel, which can be gradual or <u>netsharp</u> . It comes from an hyper-concentrated lahar (less dense than the Gms one).
Ss	Scour and fill structures composed of fine to coarse sand, generally with a normal grading. A single structure consists of an erosive, concave upwards basal surface and a planar/convex top.
fM	Fine mud deposit composed of fine sand, silt and clay. It is generated when the lahar loses its energy and the fine grains settle gently.

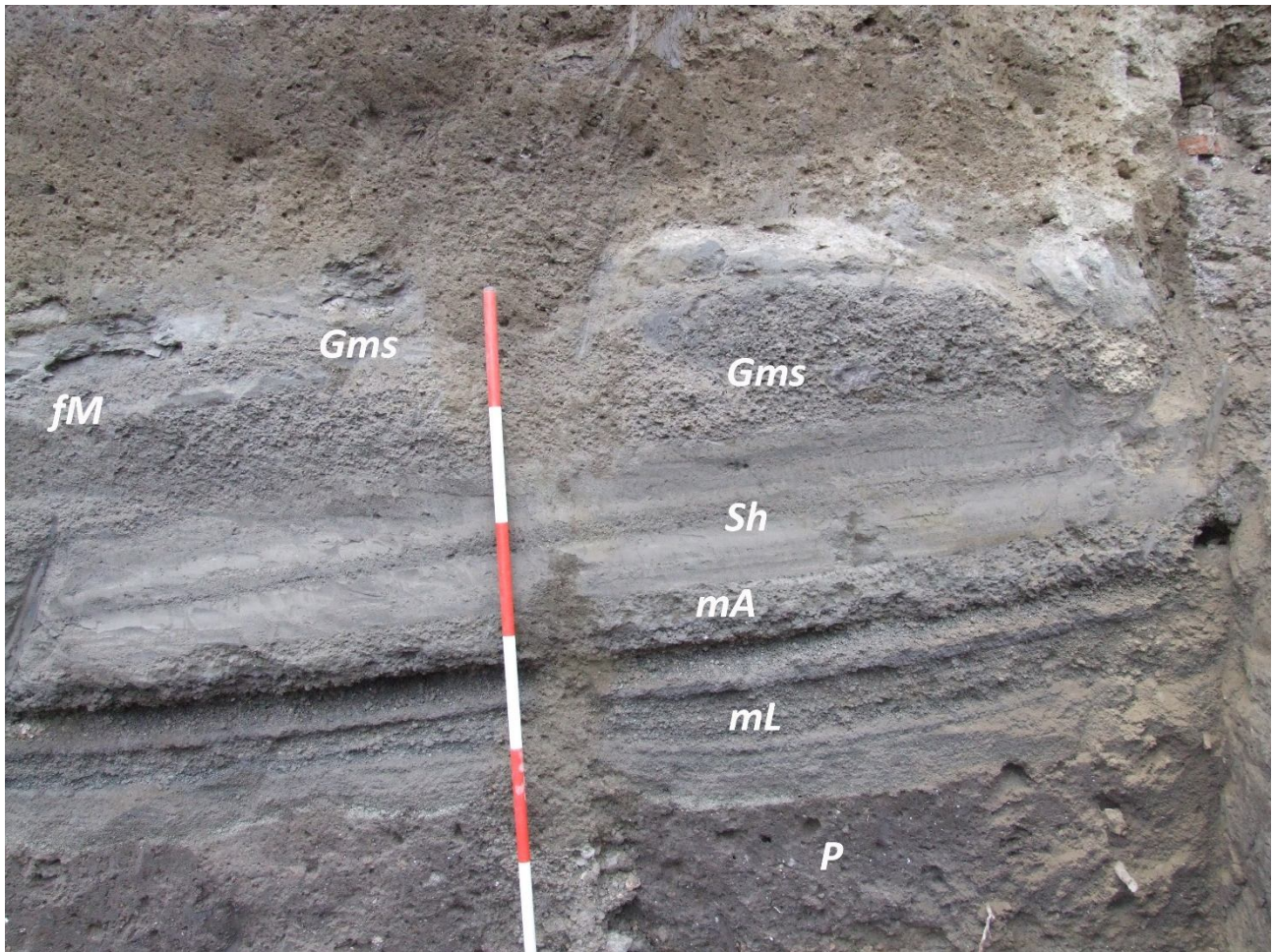
473 [Tab. 2. Symbol and description of the recognized lithofacies, and photos representative of each of them.](#)

474

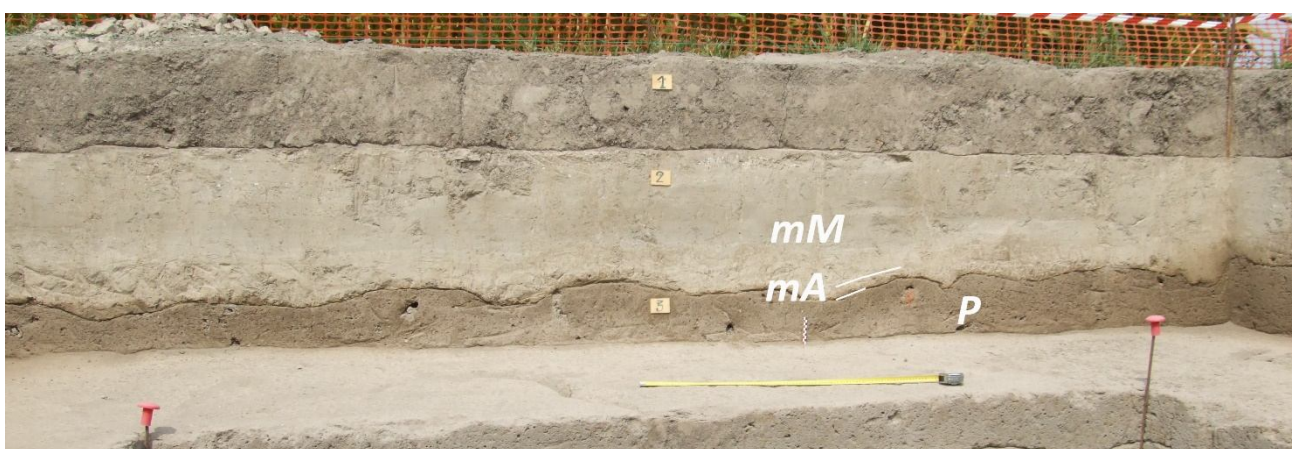


475

476 a)



478 b)



480 c)

481 Fig. 7. In these three photos of archaeological excavations (a-b, Nola at 10-15 km from Apennine source valleys; c, Acerra
482 at 12 km from Somma-Vesuvius), the main lithofacies recognized in the field are shown, including paleosols, pyroclastic
483 deposits, and lahar deposits; the corresponding lithofacies descriptions are reported in Tab. 2.

484

485 Usually, the syn-eruptive lahar deposits directly overlie the primary pyroclastic deposits, sometimes
486 eroding them. They have a matrix-supported texture and are composed of fine to very fine cohesive
487 ~~cohesive~~ ash, and contain ~~scattered and~~ more or less abundant ~~mm to cm-sized~~ pumices and lithic
488 fragments. ~~In general, The~~~~se~~~~y~~ deposits are generally composed of ~~consist of~~ multiple depositional
489 flow units, each one resulting from single ~~pulse~~ “en masse” ~~transport~~~~emplacement~~, the piling of
490 ~~which~~ resulting from rapid progressive aggradation through multiple flow pulses, in analogy with
491 ~~dense~~ pyroclastic currents (Sulpizio et al., 2006; Doronzo, 2012; Roche, 2012, 2015; Breard and
492 Lube, 2017; Smith et al., 2018; Guzman et al., 2020; see Sulpizio et al., 2014, p. 56) ~~and similarly to~~
493 ~~lahar~~ events occurred for example at Ischia (Italy) in 2022 (De Falco et al., 2023). ~~For~~
494 ~~this~~Consequently, the studied lahars were modelled using a shallow layer approach (de' Michieli
495 Vitturi et al., this issue). The different depositional flow units ~~in the same deposit~~ are distinguishable
496 (still in continuity) from each other based on vertical granulometric changes, sparse pumice
497 alignments, ~~internal lamination~~ deposit layering and/or unconformities. ~~Compared,~~ ~~f~~For example,
498 compared ~~with~~ to ~~channeled~~ channelized pyroclastic currents, dense water flows and floods, such
499 depositional units (layers) could have been repeatedly emplaced, from bottom to top, under
500 accumulation rates ~~of several~~ of a few tens to ~~a few~~ hundreds kg/m²s (Lowe, 1988; Russell and
501 Knudsen, 1999; Whipple et al., 2000; Girolami et al., 2010; Roche, 2015; Marti et al., 2019; Guzman
502 et al., 2020). In various areas, ~~the “en masse” transports~~such rapid sequential emplacement is
503 suggested by the presence of water escape structures through the whole deposit ~~and~~by crossing the
504 sequence of several units. These are vertical structures consisting of small vertical “pipes” filled ~~by~~
505 with fine mud, transported by the escaping water, and formed soon after the emplacement of the lahar
506 units. The ~~lithological~~ textural characteristics are variable even within the same site, but in general
507 the deposits are ~~generally~~ massive, and contain vesicles, from circular to flattened ~~and~~, coated by fine
508 ash ~~that adhered into the voids after water evaporation loss~~. For the syn-eruptive lahar deposits, the
509 pumice fragments are those of the primary deposits, ~~while~~, On the other hand, in the upper parts of
510 the sequences it is not uncommon to find units that contain pumices ~~s~~ fragments related to previous

511 eruptions, ~~in particular the~~ (9.0 ka B.P. "Mercato" and ~~the~~ 3.9 ka B.P. "Avellino" Plinian eruptions),
512 recognizable based on pumice texture and crystal content (Santacroce et al., 2008). In this second
513 case, these lahar deposits are considered as post-eruptive, meaning that the pyroclastic deposits older
514 than the two studied sub-Plinian eruptions were progressively involved in an advanced erosion of the
515 slopes and valleys exposed to weathering for some time, and then were deeply remobilized. Also,
516 ~~t~~The presence in the sequences of slightly humified surfaces below the lahar deposits or the evidence
517 trace of human artifacts, such as for example excavations, plowingploughing, etc., are considered
518 as constraints evidence for of a long period non-without deposition, and; also in this case, the lahars
519 generation is are considered as post-eruptive. In other words, the similar componentry of the
520 secondary lahar deposits vs. and primary pyroclastic deposits for related to the two sub-Plinian
521 eruptions, as well as, and the evidence of short-term exposure between these two ~~vertical continuity~~
522 ~~between the fallout and lahar deposits directly lying on the fallout deposits~~, are strong indicators of
523 the syn-eruptive occurrence of the lahar events. Instead, the absence of such features is more
524 indicative of a post-eruptive origin, ~~with i.e.~~ lahar events ~~also~~ more spaced in time from the
525 corresponding eruption.

526 In Appendix 3C, a description is reported for some of the most representative sequences, which were
527 sampled in different areas throughout the plain (Figs. 2 and 4).

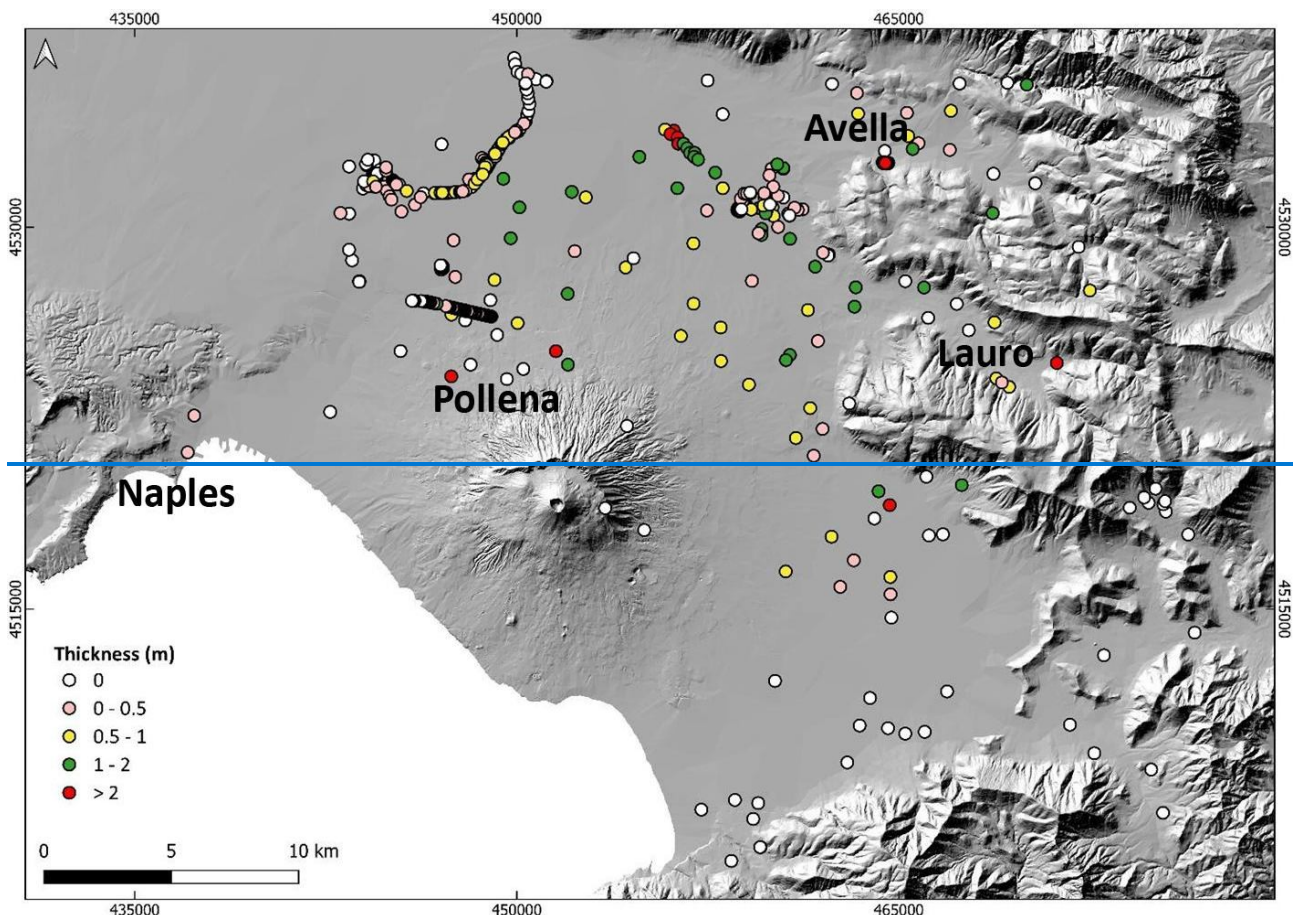
528

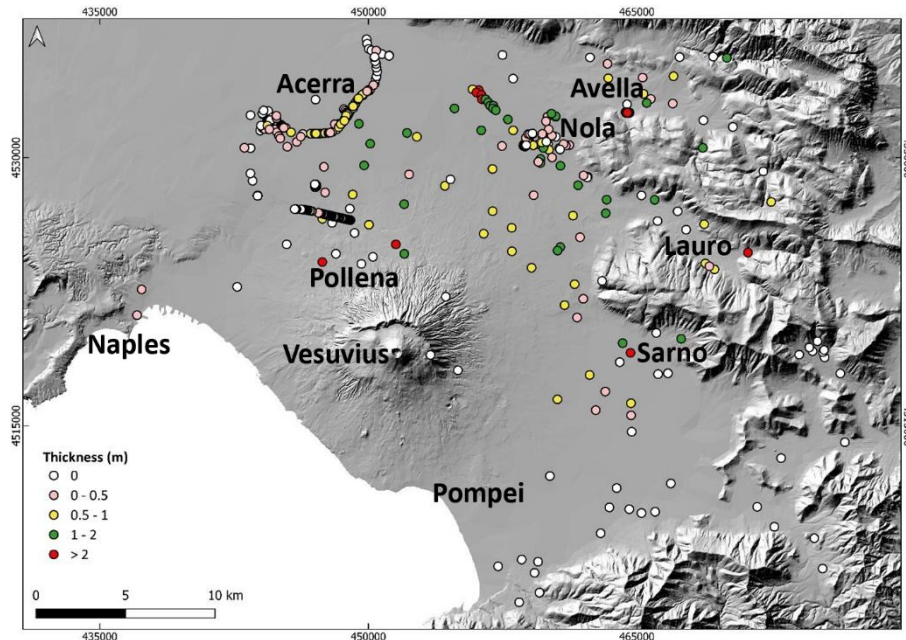
529 **4.1.3. Distribution maps of the lahar deposits**

530 Here we present ~~the~~ distribution maps for the lahar deposits of the ~~eruption of~~ Pollena and 1631
531 eruptions (Figs. 87-110). The maps show the distribution of all thicknesses detected in the studied
532 sites. In particular, the syn-eruptive Pollena lahar deposits are distributed in the NW quadrants of the
533 volcano and in the Avella, Lauro and Sarno valleys (see Fig. 1), with a thickness exceeding 1 m in
534 the Vesuvius apron and in the plain between Nola and Cimite at about 10-15 km from Apennine
535 source valleys (see Figs. 1 and 87). A volume estimation of the remobilized deposits is of the order

536 of 7.3×10^{67} m³ for the northern Vesuvius area, and 4.2×10^{67} m³ for the Lauro Valley. Such volumes
 537 are referred to the depositional areas, and not to the detachment ones; for the latter see de' Michieli
 538 Vitturi et al. (this issue) and Sandri et al. (this issue). The provenance of the material in each site was
 539 inferred by sedimentological recognition and magnetic reconstruction. Then, the covered areas were
 540 subdivided into polygons in the geospatial database, in order to weight the local deposit thicknesses
 541 and estimate the volumes with a lower approximation.

542





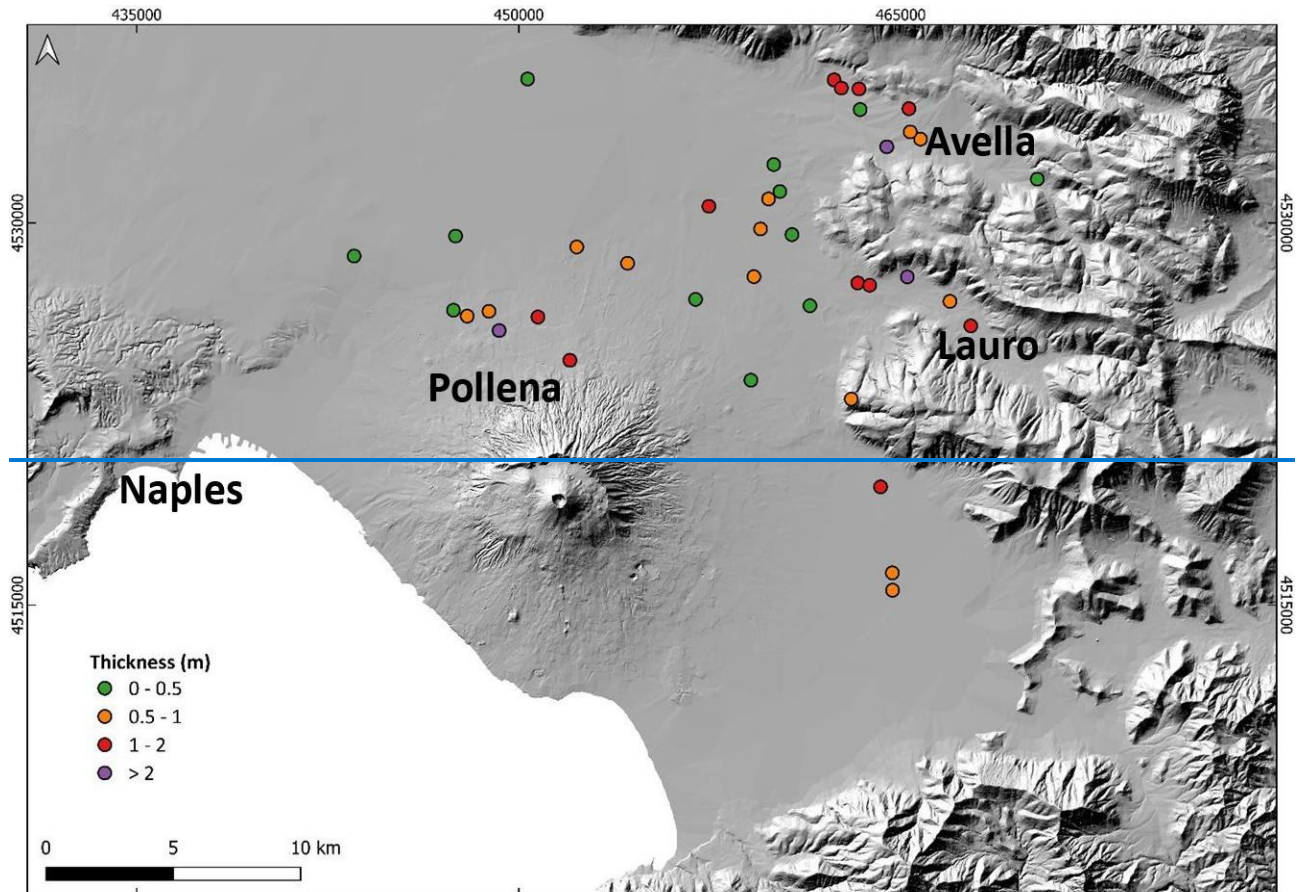
544

545 Fig. 87. Distribution of the syn-eruptive lahar deposits related to the Pollena eruption. The 0 m points represent the studied
 546 sites where the lahar deposits were absent, and in some cases even the primary pyroclastic deposits below were absent;
 547 they are reported anyway, as their absence might have not necessarily occurred by no deposition (local erosion).

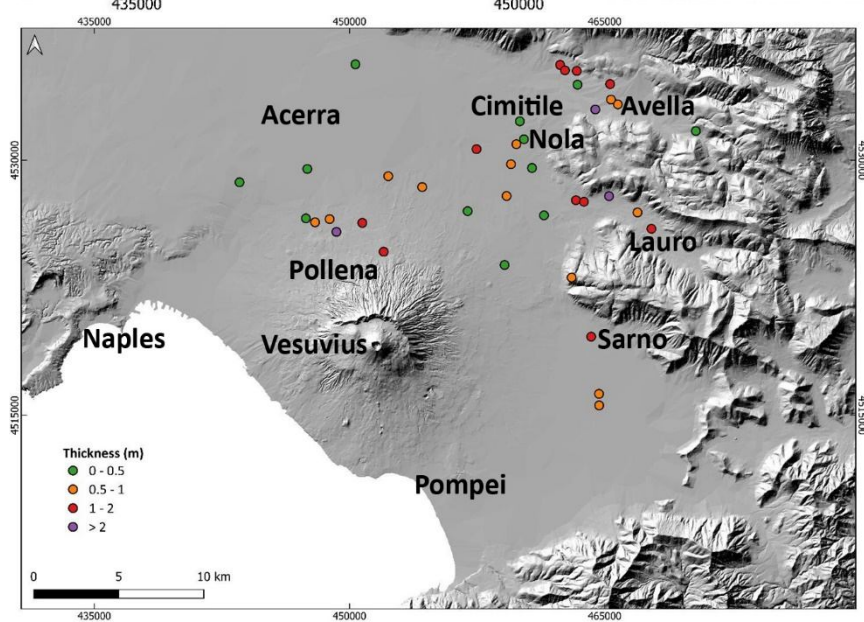
548

549 The post-eruptive lahar deposits of the Pollena eruption are more concentrated-distributed in the
 550 Avella and Lauro valleys, and in the plain north of the volcano close to the apron area (low-angle
 551 edifice outer slopes) (Figs. 1 and 98). Their deposits contain both fragments from the Pollena eruption
 552 and from preceding eruptions, suggesting that pyroclastic deposits of the older sequences were
 553 progressively eroded and involved in remobilization processes over time. As an example, in-on Figs.
 554 A3a-d C1-4 it is possible to recognize to remark that whitish pumice fragments from the Pomici di
 555 Avellino and Mercato eruptions were identified on top of the Pollena lahar deposits.

556



557



558

559

Fig. 98. Distribution of the post-eruptive lahar deposits related to the Pollena eruption.

560

561

The distribution of the syn- and post-eruptive Pollena lahar deposits is related to the primary

562

pyroclasts deposition: the dense distribution of the lahar deposits north of Somma-Vesuvius depends

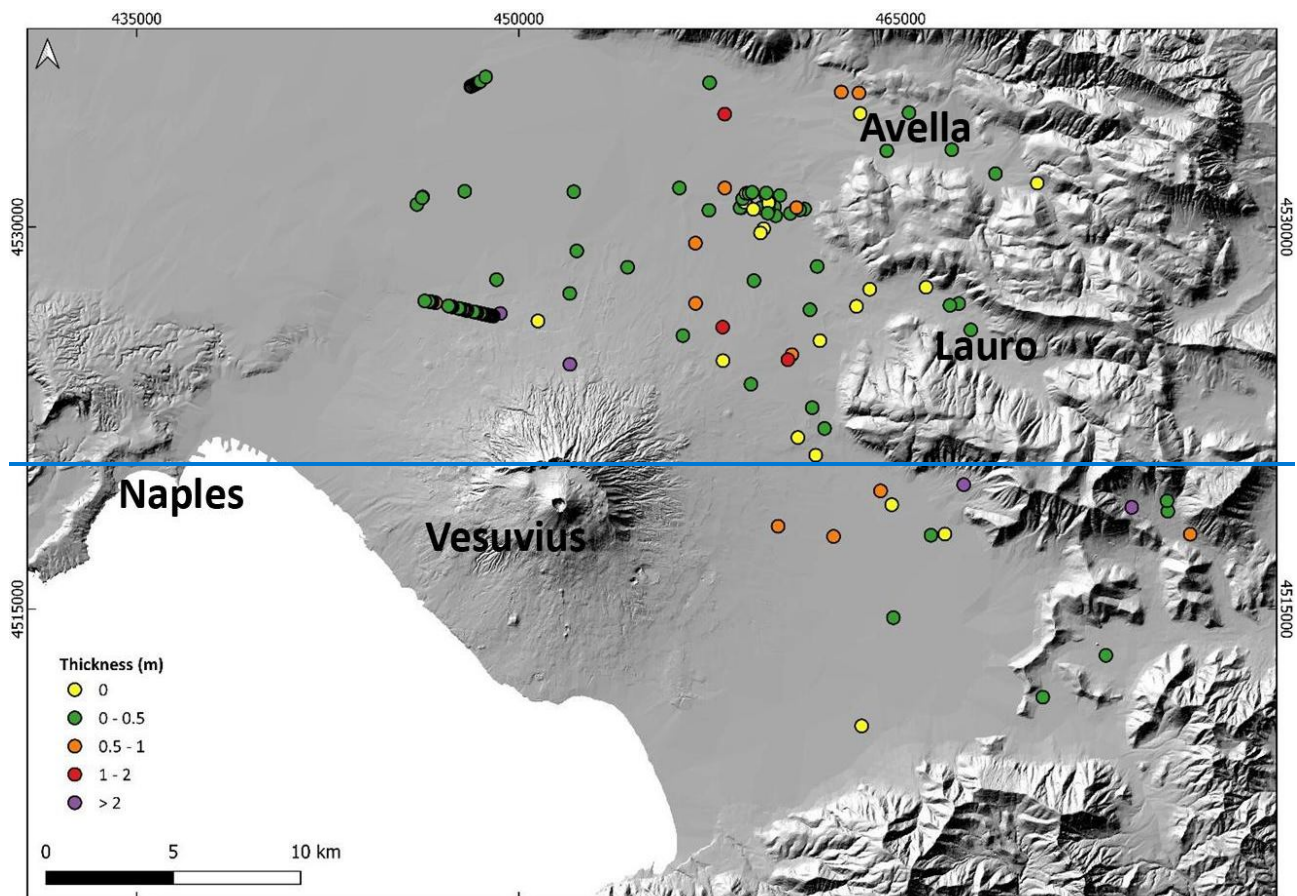
563

on the presence of thick pyroclastic current deposits that were remobilized from the northern slopes

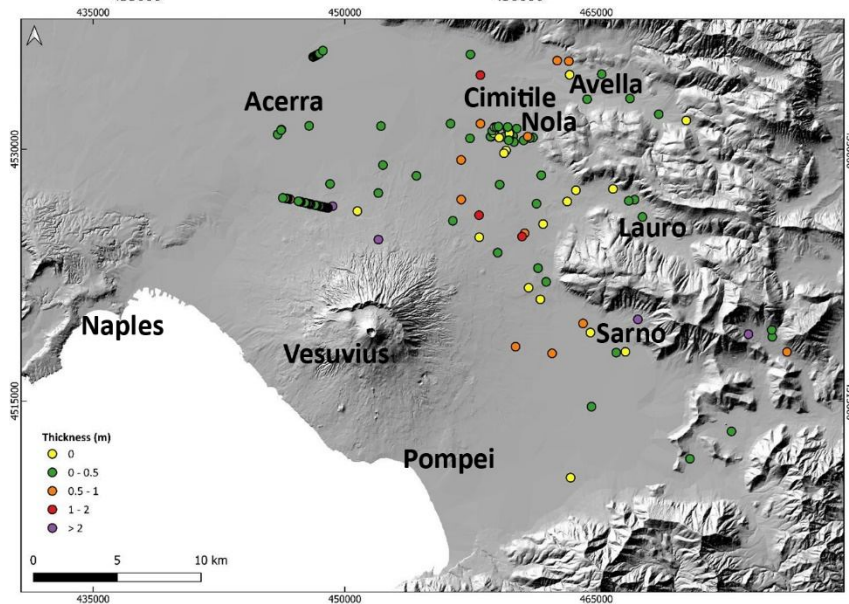
564 of the volcano, while the distribution in the Apennine valleys is related to the fallout deposits that are
565 thicker along the major Pollena dispersal axis (Fig. 5).

566 Above the Pollena ~~primary and secondary~~pyroclastic and lahar deposits ~~(meaning after the~~
567 ~~emplacement of the Pollena lahars)~~ (both syn- and post-eruptive), the studied sequences in almost all
568 the sites show the presence of a well-developed soil bed with many traces of cultivation, as well as
569 of ~~the presence of~~ inhabited areas and buildings (Figs. A3a-d C1-4). These traces and the presence of
570 ~~a well developed~~the soil bed are evidence of a progressive geomorphological stabilization of the
571 territory. The occurrence of the 1631 sub-Plinian event determined a new phase of marked
572 geomorphological instability for a large territory surrounding the volcano. In Fig. 109, it is shown the
573 distribution of the syn-eruptive lahar deposits for the 1631 eruption in all the studied areas ~~with~~,
574 having a variable thickness, generally <50 cm. They Such distribution affected mostly the areas of
575 Acerra-Nola, Sarno, the Vesuvius apron and the Apennine valleys (Figs. 1 and 109). Rosi et al. (1993)
576 and Sulpizio et al. (2006) reported that floods and lahars heavily impacted (also with injuries and
577 victims) the N and NE quadrants of Somma-Vesuvius soon after the eruption with a timescale of days
578 (Rosi et al., 1993; see also the historical chronicles of Braccini, 1632), corroborating the syn-eruptive
579 behavior of such lahars. Furthermore ~~s~~Some lahar deposits are ~~also~~ intercalated within the primary
580 pyroclastic deposits, ~~while but in~~ generally they directly stand ~~in continuity~~ on top of the ~~primary~~
581 pyroclastic deposits (Rosi et al., 1993); both cases unequivocally constrain the syn-eruptive behavior
582 of the 1631 eruption lahars.

583



584



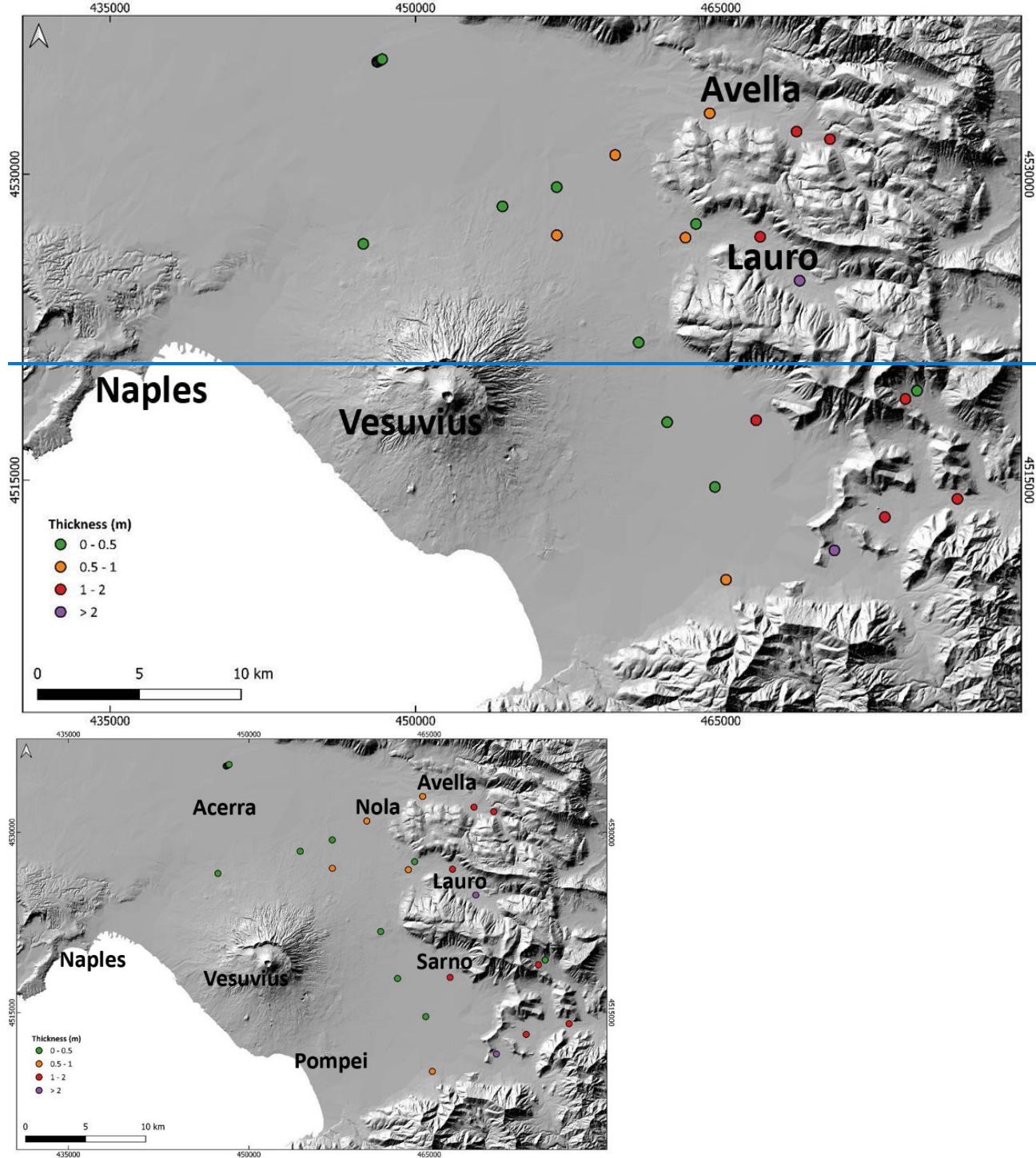
585

586 Fig. 109. Distribution of the syn-eruptive lahar deposits related to the 1631 eruption. The 0 m points represent the studied
 587 sites where the lahar deposits were absent, and in some cases even the primary pyroclastic deposits below were absent;
 588 they are reported anyway, as their absence might have not necessarily occurred by no deposition (local erosion).

589

590 In Fig. 110, ~~M~~inor post-eruptive lahar deposits of the 1631 eruption are reported in Fig. 10, with a
591 preferential distribution to the E quadrants of the volcano from N to S, both in the plain and the
592 valleys. These deposits are still significant, with a thickness of around half a meter to a meter or more
593 in a few points.

594



597 Fig. 110. Distribution of the post-eruptive lahar deposits related to the 1631 eruption.

598

599 The distribution of the syn- and post-eruptive 1631 lahar deposits mainly reflects the major dispersal
600 axis affecting the fallout deposits distribution, while the pyroclastic current deposits were minorly
601 remobilized as exposed on the gentler slopes of southwestern Vesuvius (Fig. 6).

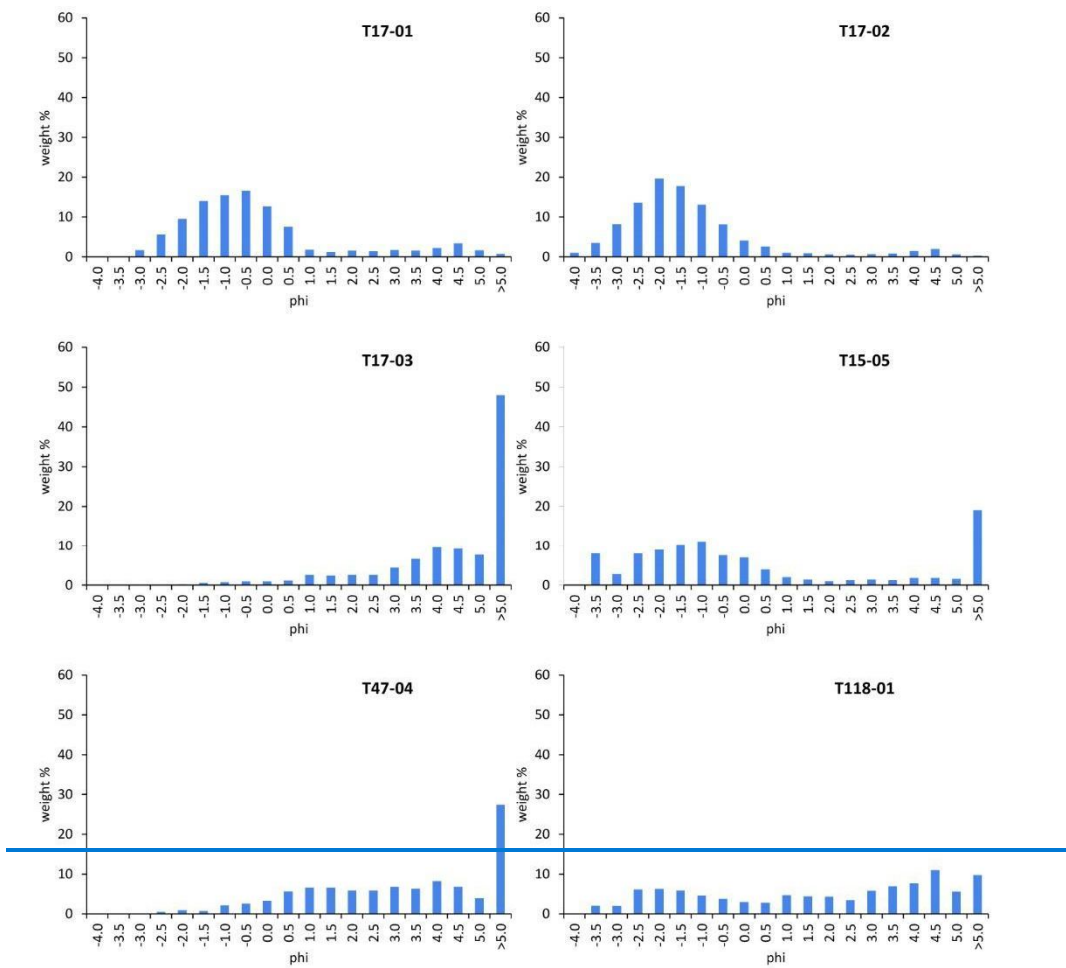
602

603 **4.1.4. Sedimentological characteristics of the Pollena lahar deposits**

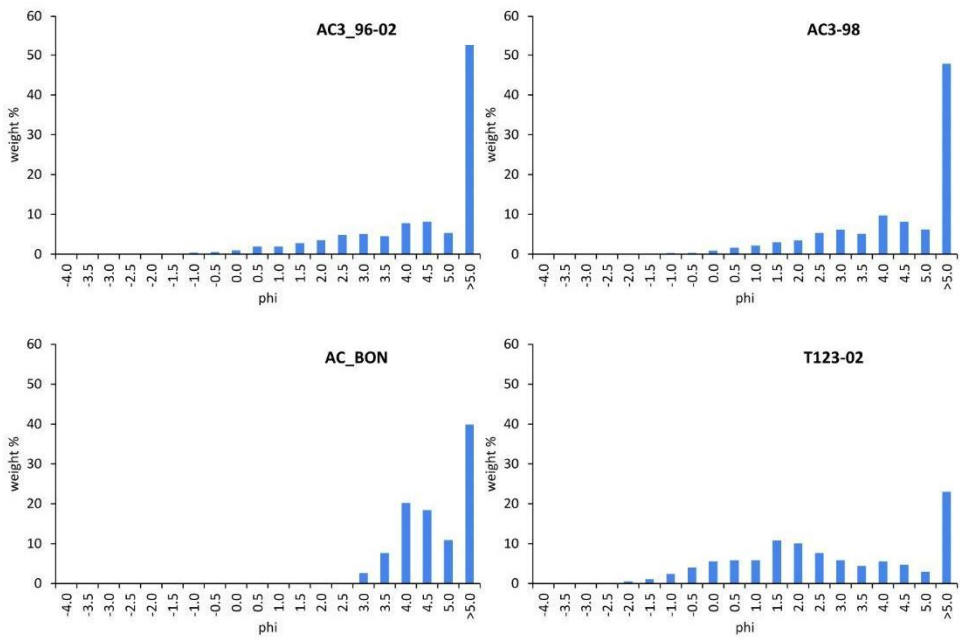
604 The field analysis was carried out ~~on-in~~ about 500 ~~studied-different~~ sites ~~for the construction of the~~
605 ~~database and maps, and-while~~ the laboratory analysis ~~carried out~~ was carried out on 30 ~~selected~~
606 ~~representative~~ samples representative of the different areas ~~contribute~~; ~~both analyses contributed to~~
607 ~~the distinction between syn- and post-eruptive lahars in the area~~. The results of the grain-size analyses
608 ~~in the form of (histograms cumulative curves)~~ and statistical parameters) are presented in Fig. 124 and
609 Tab. 1.

610 Petrological analysis on the syn-eruptive lahar deposits have not been performed because the
611 lithology (colour, texture, mineral content) of the components is the same as the juvenile material of
612 the primary deposits (more details can be found described in Sulpizio et al., (2005). The loose crystals
613 consist of sanidine, leucite, biotite and pyroxene fragments. Based on the results of the grain-size
614 analyses distributions of the samples, the coarser classes are defined from -4 to -1 phi, the medium
615 ones are from -0.5 to 2.5 phi, and the finest one are from 3 phi. The juvenile pumice clasts are an
616 ubiquitous component of the lahar deposits (both syn- and post-eruptive), but they decrease with
617 distance toward for the finer grain-size classes, while the crystal content increases in with the same
618 progression. The lithic clasts are abundant in for the coarser classes, they decrease with distance in
619 for the middle-medium grain size classes, and increase again in for the finer classes.

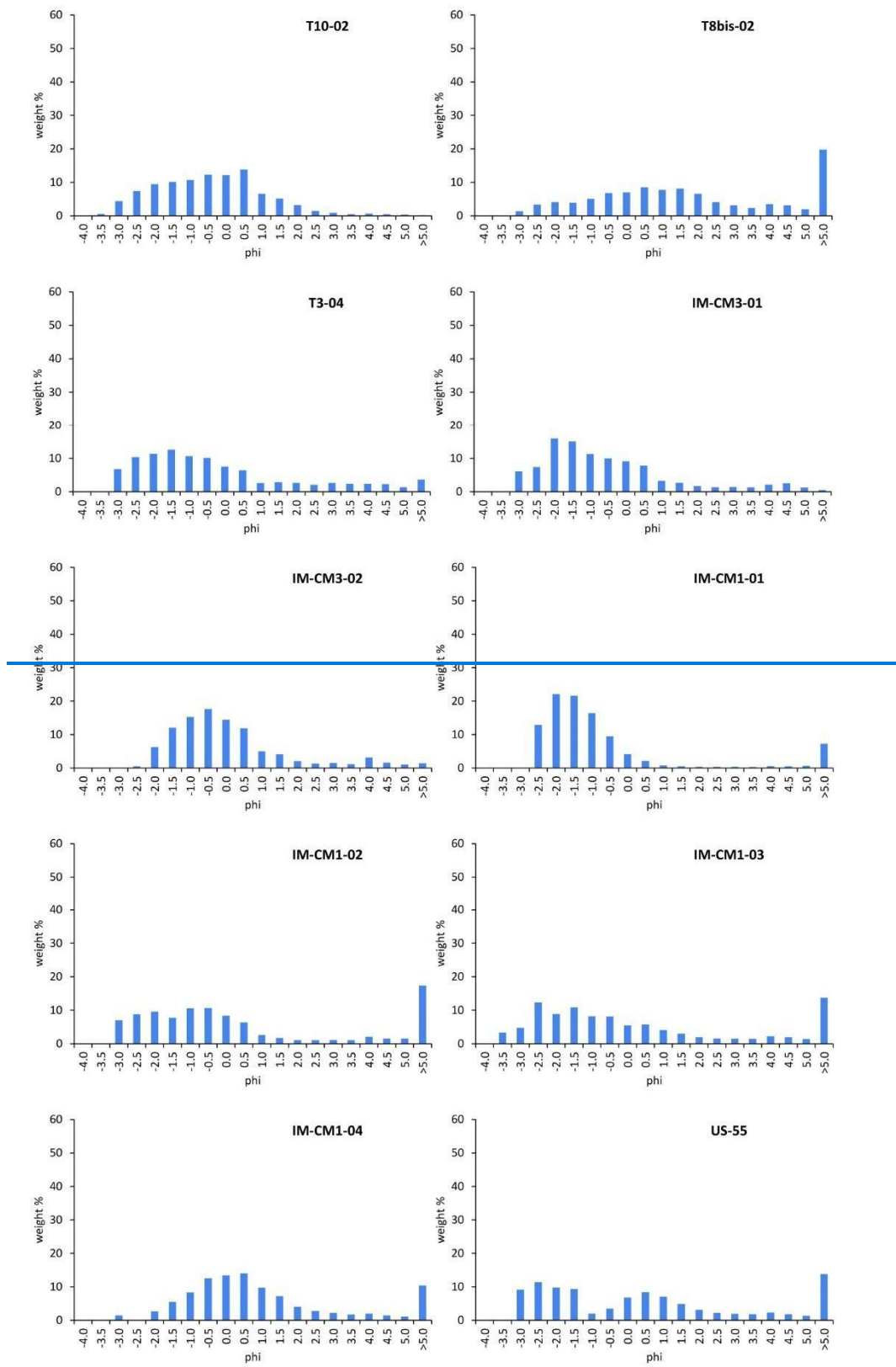
Vallo di Lauro



Somma-Vesuvius



Valle di Avella



621

622

623

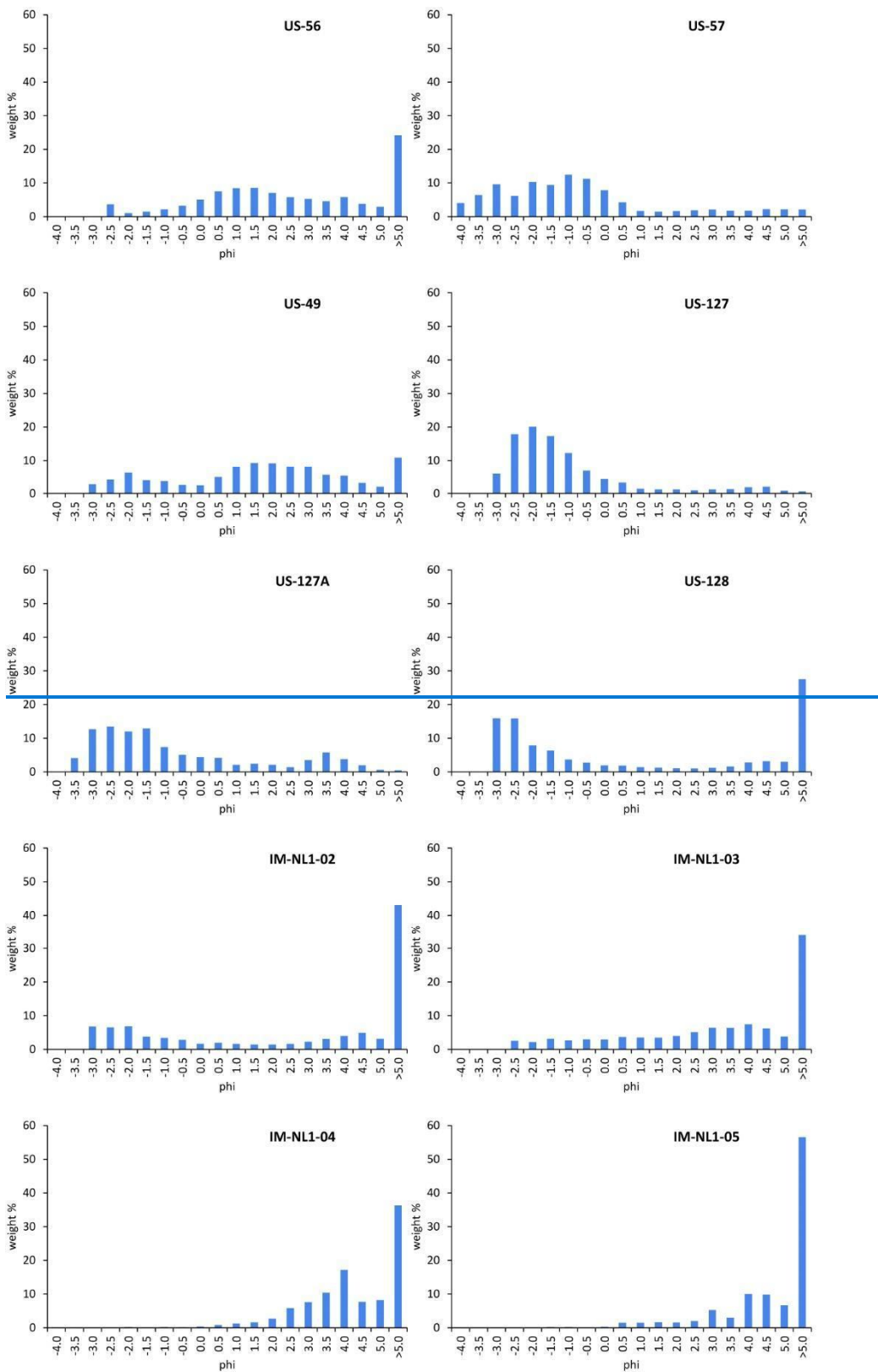
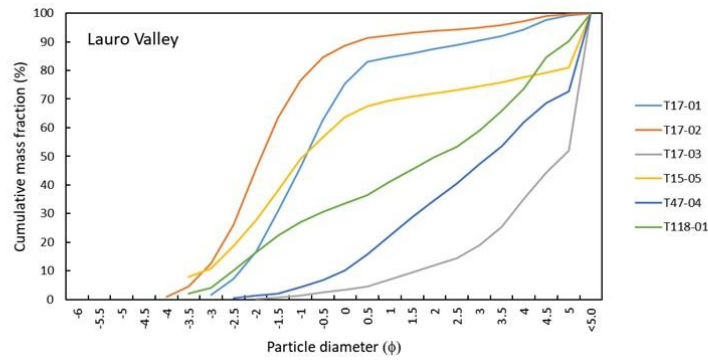
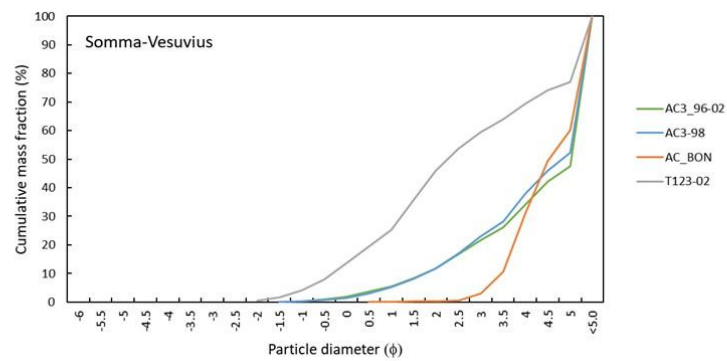


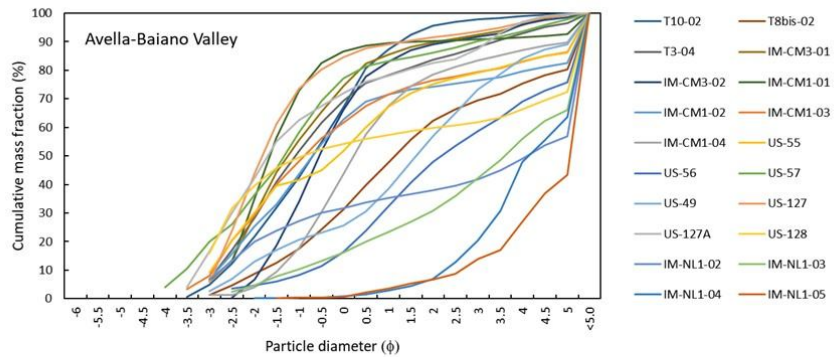
Fig. 11. Histograms of the grain-size analysis on selected samples for the locations reported in Fig. 4.

626



627





628

629 Fig. 12. Cumulative curves of the grain-size analysis on the samples taken at the locations reported in Fig. 4, and
630 subdivided in three sectors: Lauro Valley (top), Somma-Vesuvius (middle), and Avella-Baiano Valley (bottom).

631

<u>Site</u>	<u>Distance from Mt. Somma-rim</u>
<u>T17</u>	<u>12.8 km</u>
<u>T15</u>	<u>15 km</u>
<u>T47</u>	<u>7.6 km</u>
<u>T118</u>	<u>9.9 km</u>
<u>AC3-96</u>	<u>15 km</u>
<u>AC3-98</u>	<u>13 km</u>
<u>AC-BON</u>	<u>11.5 km</u>
<u>T123</u>	<u>6.5 km</u>
<u>T10</u>	<u>18 km</u>
<u>T8bis</u>	<u>18.4 km</u>
<u>T3</u>	<u>19.1 km</u>

<u>IM-CM3</u>	<u>14.3 km</u>
<u>IM-CM1</u>	<u>14 km</u>
<u>US-55</u>	<u>13.6 km</u>
<u>US-128</u>	<u>13.6 km</u>
<u>IM-NL1</u>	<u>13 km</u>

SAMPLE	MODE 1	MODE 2	MODE 3	SKEWNESS	SORTING	FACIES
Lauro Valley						
T17-01	-0.743			1.179	1.464	Gms
T17-02	-2.243			1.532	1.404	Gms
T17-03	0.747	3.731		-1.054	1.481	Sh
T15-05	-3.743	-1.243	3.731	0.890	1.752	Gms
T47-04	1.247	3.731		-0.447	1.579	Mm
T118-01	-2.243	0.747	3.731	-0.049	2.352	Gms
Avella-Baiano Valley						
T10-02	0.247			0.274	1.457	Sh
T8bis-02	-2.243	0.247	1.247	-0.009	1.742	Sh
T3-04	-1.743	1.247	3.237	0.881	1.789	Gms
IM-CM3-01	-2.243			1.015	1.587	Gms
IM-CM3-02	-0.743	3.731		1.134	1.379	Gms
IM-CM1-01	-2.243			1.954	1.010	Gms
IM-CM1-02	-2.243	-1.243	3.731	0.932	1.633	Gms
IM-CM1-03	-2.743	-1.743	0.247	0.810	1.809	Gms
IM-CM1-04	0.247			0.406	1.394	Fm
US-55	-2.743	0.247	3.731	0.495	1.941	Gms
US-56	-2.743	1.247	3.731	-0.402	1.700	Sh
US-57	-3.243	-2.243	-1.243	0.756	1.860	Gms
US-49	-2.243	1.247		-0.460	2.012	Gms
US-127	-2.243			1.686	1.507	Gms
US-127A	-2.743	-1.743	3.237	0.914	2.167	Gms
US-128	-3.243	3.731		1.434	1.990	Gms
IM-NL1-02	-3.243	-2.243	3.731	0.609	2.378	Gms
IM-NL1-03	-1.743	0.247	3.731	-0.458	1.996	Gms
IM-NL1-04	3.731			-1.698	0.995	Mm
IM-NL1-05	1.247	2.737	3.731	-1.137	1.224	Mm
Somma-Vesuvius						
AC3_96-02	0.247	2.237	3.731	-0.734	1.245	Mm
AC3-98	2.737	3.731		-0.838	1.197	Mm
AC_BON	3.731			-3.026	0.425	Mm
T123-02	0.247	1.247	3.731	-0.228	1.420	Mm

Sample	Mean (ϕ)	Sorting (ϕ)	Lithofacies
Lauro Valley			
T17-01	-0.93	1.41	Gms
T17-02	-1.83	1.23	Gms
T17-03	2.42	1.46	Sh

<u>T15-05</u>	<u>-1.39</u>	<u>1.74</u>	<u>Gms</u>
<u>T47-04</u>	<u>1.67</u>	<u>1.61</u>	<u>Mm</u>
<u>T118-01</u>	<u>1.13</u>	<u>2.7</u>	<u>Gms</u>
Avella-Baiano Valley			
<u>T10-02</u>	<u>-0.78</u>	<u>1.47</u>	<u>Sh</u>
<u>T8bis-02</u>	<u>0.31</u>	<u>1.83</u>	<u>Sh</u>
<u>T3-04</u>	<u>-0.95</u>	<u>1.83</u>	<u>Gms</u>
<u>IM-CM3-01</u>	<u>-1.13</u>	<u>1.54</u>	<u>Gms</u>
<u>IM-CM3-02</u>	<u>-0.48</u>	<u>1.35</u>	<u>Gms</u>
<u>IM-CM1-01</u>	<u>-1.66</u>	<u>0.86</u>	<u>Gms</u>
<u>IM-CM1-02</u>	<u>-1.17</u>	<u>1.62</u>	<u>Gms</u>
<u>IM-CM1-03</u>	<u>-1.13</u>	<u>1.83</u>	<u>Gms</u>
<u>IM-CM1-04</u>	<u>0.06</u>	<u>1.39</u>	<u>Fm</u>
<u>US-55</u>	<u>-0.84</u>	<u>1.97</u>	<u>Gms</u>
<u>US-56</u>	<u>1.17</u>	<u>1.8</u>	<u>Sh</u>
<u>US-57</u>	<u>-1.51</u>	<u>1.86</u>	<u>Gms</u>
<u>US-49</u>	<u>0.69</u>	<u>2.16</u>	<u>Gms</u>
<u>US-127</u>	<u>-1.66</u>	<u>1.39</u>	<u>Gms</u>
<u>US-127A</u>	<u>-1.02</u>	<u>2.23</u>	<u>Gms</u>
<u>US-128</u>	<u>-1.72</u>	<u>1.91</u>	<u>Gms</u>
<u>IM-NL1-02</u>	<u>-0.5</u>	<u>2.49</u>	<u>Gms</u>
<u>IM-NL1-03</u>	<u>1.25</u>	<u>2.1</u>	<u>Gms</u>
<u>IM-NL1-04</u>	<u>2.99</u>	<u>0.89</u>	<u>fM</u>
<u>IM-NL1-05</u>	<u>2.64</u>	<u>1.20</u>	<u>fM</u>
Somma-Vesuvius			
<u>AC3_96-02</u>	<u>2.37</u>	<u>1.26</u>	<u>mM</u>
<u>AC3-98</u>	<u>2.48</u>	<u>1.2</u>	<u>mM</u>
<u>AC_BON</u>	<u>3.52</u>	<u>0.38</u>	<u>mM</u>
<u>T123-02</u>	<u>1.37</u>	<u>1.5</u>	<u>mM</u>

634

635 Tab. 34. Statistical parameters ([mean and sorting](#)) extracted from the grain-size analyses, and reference lithofacies (see
 636 [Tab. 2 for descriptions](#)). ~~Mode 1, 2 and 3 indicate the coarsest, medium and fine modes, respectively. Mode 1, 2 and 3~~
 637 ~~represent the most frequently occurring grain size classes.~~

638

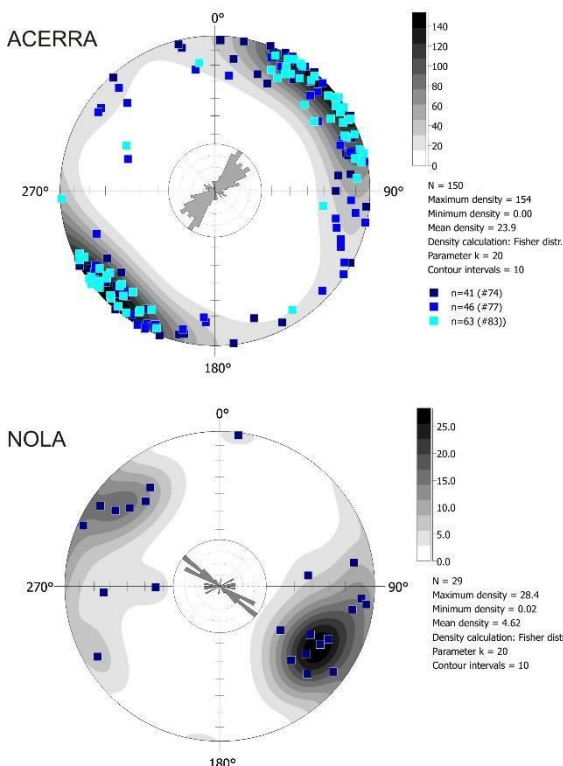
639 Field observations and [statistical granulometric grain-size parameters analyses](#) (modes, skewness,
 640 [sorting](#)), highlight significant differences between the sectors of Lauro Valley, Avella-Baiano Valley,
 641 and Somma-Vesuvius. A common feature between the three sectors is that the lahar deposit samples
 642 are mostly massive, poorly-sorted and [polimodal](#)[polymodal](#); only a few samples are moderately-
 643 sorted and unimodal ([more than one grain size are present but one prevail](#)[sorting <1.5 phi](#)). On the

644 other hand, the grain-size modes ~~extracted~~found show some interesting differences (in Fig. 12 the
645 cumulative curves are shown). The coarse modes for Lauro Valley and Avella-Baiano Valley span
646 from fine/medium lapilli to coarse ash, while for Somma-Vesuvius span from coarse to fine ash. The
647 medium modes for Lauro Valley and Avella-Baiano Valley span from coarse to medium ash, while
648 for Somma-Vesuvius span from medium to fine ash. The fine modes for Lauro Valley and Avella-
649 Baiano Valley, and for Somma-Vesuvius span from medium to fine ash. Also, the skewness values
650 ~~for Lauro Valley and Avella-Baiano Valley show a fine to coarse mode while for Somma-Vesuvius~~
651 ~~show a coarse mode.~~ All these differences basically depend on the origin of the primary pyroclastic
652 deposits, fallout vs. pyroclastic currents, which were remobilized from different sectors, Apennines
653 and Somma-Vesuvius. The grain-size analysis ~~of the above-described granulometry~~ is used to
654 ~~informas~~ an input information for the ~~model of~~ lahar transport model (de' Michieli Vitturi et al.,
655 ~~submitted~~this issue) aimed at assessing the related hazard (Sandri et al., ~~submitted~~this issue).
656

657 4.2. Magnetic results

658 Both Acerra (12 km from Somma-Vesuvius) and Nola (10-15 km from Apennine source valleys)
659 localities show a well-defined magnetic fabric ~~for the (Pollena syn-eruptive lahar deposits-~~
660 ~~irrespective of being syn- or post-eruptive)~~. Principal susceptibility axes (K₁>K₂>K₃) are clustered,
661 Magnetic lineation (K₁) and magnetic foliation (K₃, pole of the plane) are mostly sub-horizontal or
662 gently embriicated, and the magnetic ~~The~~ anisotropy degree P_j (K₁/K₃) is mostly lower than 1.060,
663 but can reach high values ~~(P=~~ like 1.200). At Acerra, the magnetic foliation is always dominant, and
664 the fabric is oblate. The P_j is linearly correlated to the mean susceptibility (k_m). In Appendix B, the
665 full nomenclature is defined for completeness. The magnetic fabric has a horizontal magnetic
666 foliation and a clustered magnetic lineation, whose mean direction is NE-SW. Considering the chaotic
667 nature of the lahar deposits, the high P_j and the clustered susceptibility axes can highlight a
668 channelized flow (Fig. 132). At Nola, instead, the fabric is both prolate/oblate, and P_j is lower than

669 1.040. The susceptibility axes are more dispersed than at Acerra, but mean magnetic lineation clearly
670 shows a NW-SE direction. If one considers the oblate specimens only, the magnetic foliation is sub-
671 horizontal, on the contrary, the magnetic foliation of the prolate specimens is steeply dipping (65°)
672 toward SE. At Nola, the flow direction inferred by AMS is consistent and parallel to the invasion
673 basin.



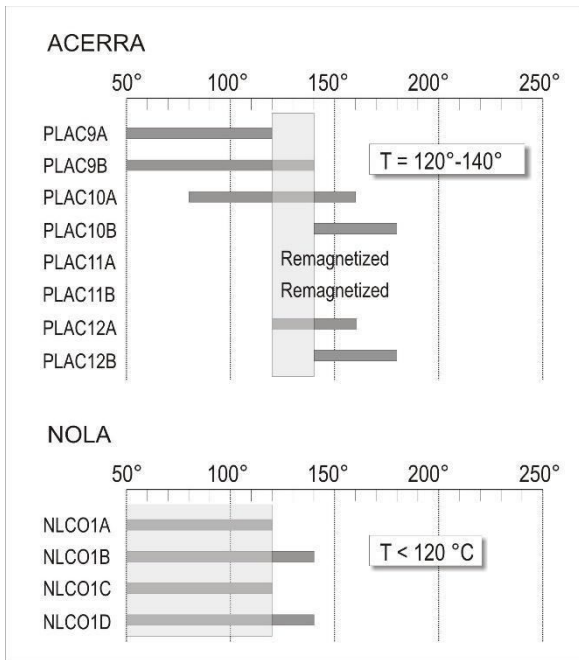
674

675 Fig. 132. Equal area projection and Rose diagram of the K_1 directions at Acerra (12 km from Somma-Vesuvius) and Nola
676 (10-15 km from Apennine source valleys).

677

678 ~~The deposition temperature is low at both deposits.~~ At Acerra, the T_{dep} interval is 120-140 °C, while
679 for Nola T_{dep} is lower than 120 °C (Fig. 143). In the Nola case, a low temperature magnetization
680 component lower than 120 °C cannot be directly considered as a TRM. In fact, the low T_b Earth's
681 field component of magnetization can also be produced by a viscous remanent magnetization (VRM),
682 acquired during exposure to weak fields (Bardot and McClelland, 2000). The acquisition of the VRM
683 depends on the duration of the exposure. For age around that of the Pollena eruption, the minimum

684 T_{dep} which can be distinguished is ca. 120 °C. For this reason, we considered the Nola lahar to be
685 emplaced at low temperature.



686

687 Fig. 143. Deposition temperature at Acerra and Nola. The site T_{dep} is estimated from the overlapping reheating
688 temperature ranges for all lithic clasts sampled.

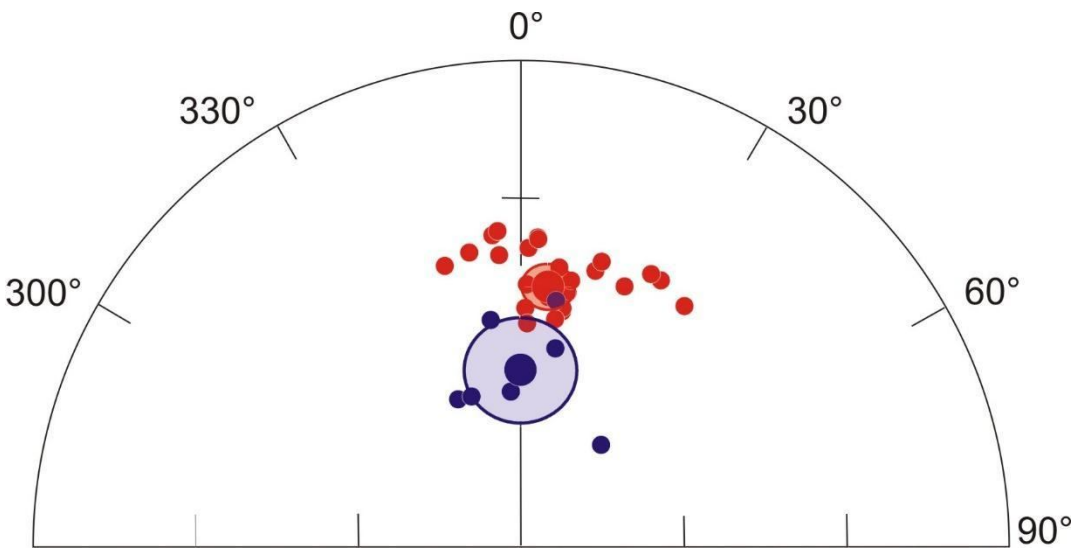
689

690 The mean paleomagnetic direction for each locality, calculated using Fisher's statistics, is well-
691 defined, and its directional value and confidence limits do not overlap (Fig. 154). Thus, the two
692 directions and is are statistically distinguishable at the 95% confidence limits (Fig. 14). Since a
693 paleomagnetic direction is a record of the Earth's magnetic field acting during the emplacement, it
694 follows that Therefore, the lahar deposits of at these two localities are not synchronous.

695 Overall, all magnetic measurements just discussed show distinctly different characters between
696 Acerra and Nola, clearly indicating two distinct events of emplacement.

697

698



699

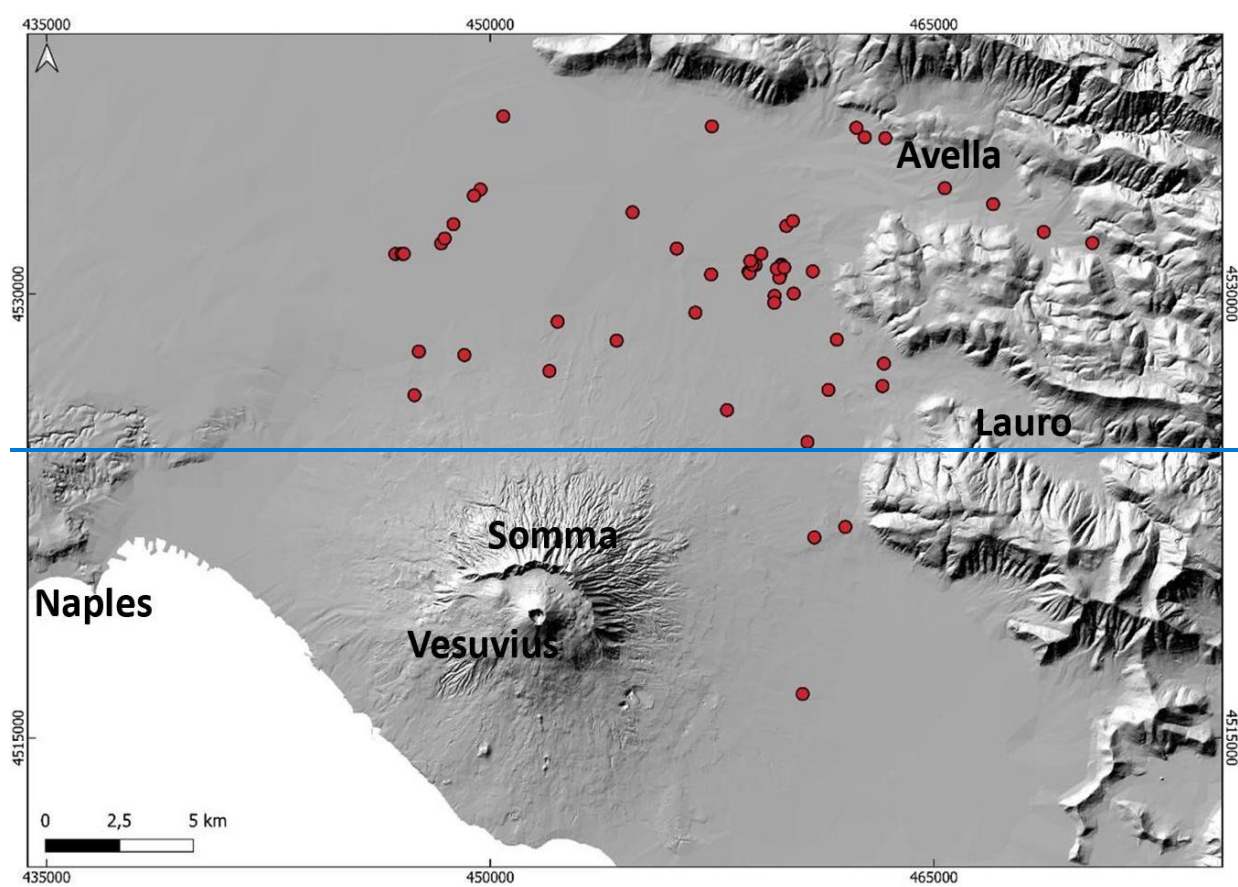
700 Fig. 154. Equal-area projection of the characteristic remanent magnetization directions, and their mean value with
 701 associated confidence limit, from Acerra (red dots, mean value: $n=26$ $D=7.5^\circ$, $I=43.4^\circ$, $\alpha_{95}=3.5^\circ$), and Nola (blue
 702 dots, mean value: $n=7$, $D=0.8^\circ$, $I=60.2^\circ$, $\alpha_{95}=9.0^\circ$).

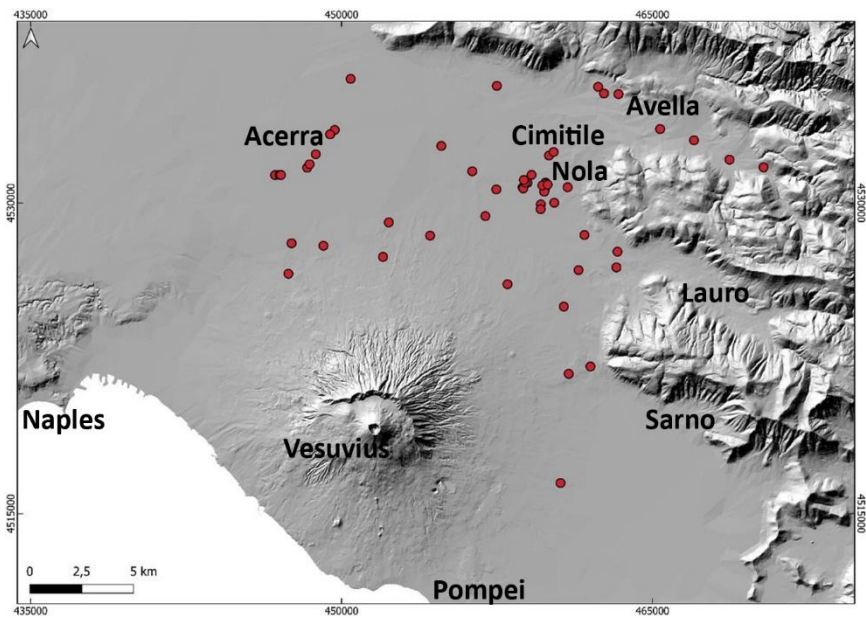
703

704 **4.3. Lahar dynamics**

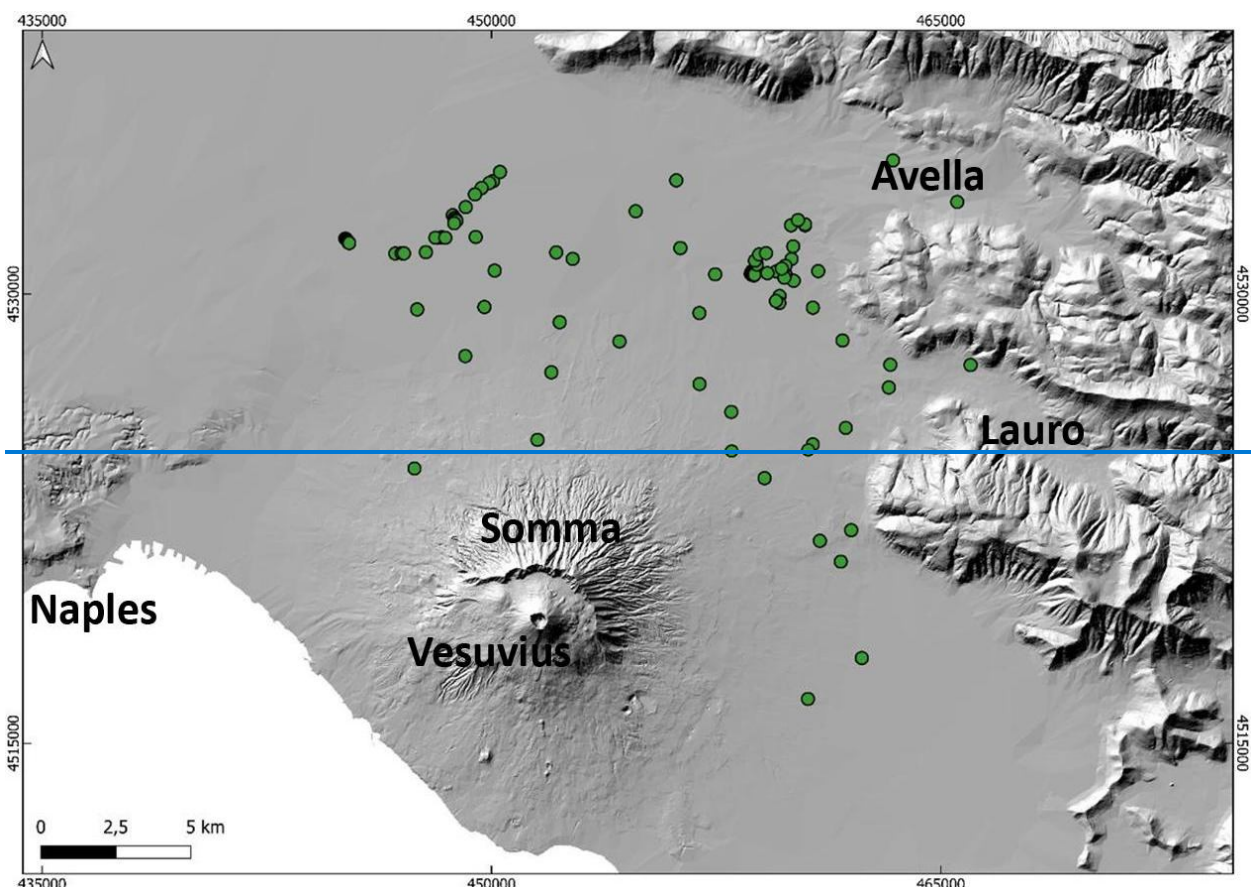
705 By inverting the field evidence and data, it is possible to reconstruct the macroscopic flow dynamics
 706 that occurred in the lahar invasion, which are particularly interesting to understand the impact that
 707 those lahars had on the Vesuvius territory. As already described, the lahar deposits show thicknesses
 708 that are variable from several centimeters to a few meters, and this can depend on multiple local
 709 factors: i) topography; ii) distance from source; iii) erosion; iv) source area and type of remobilized
 710 sediment (variably sized fallout vs. flow deposits). In particular, thicker deposits are found near the
 711 mouth of the valleys and in the flat alluvial plain, as shown in the deposit distribution maps. On the
 712 other hand, the deposits show ~~on the whole~~ a general tabular-like shape (Fig. 7), ~~and the with an~~
 713 average thickness ~~is~~ of the order of 0.5-1 m recurrent for several studied sites, which is the first
 714 evidence of the lahars impact and mass flow emplacement in the area. In terms of runout distance,
 715 the lahars travelled for 10 to 15 km from sources (Somma-Vesuvius and Apennine detachment areas),
 716 ~~measured directly on the deposit distribution maps based on the geospatial database that includes all~~
 717 studied sites. It was possible to infer the source areas based on the common sedimentological features

718 of the lahar deposits between nearby sites. On the other hand, distant sites with sedimentologically
719 different deposits were fed from different source areas. These important quantitative constraints are
720 used to validate and inform lahar numerical models (de' Michieli Vitturi et al., submitted this issue)
721 and simulations (Sandri et al., submitted this issue) using a shallow layer approach for hazard
722 assessment. We cannot rule out that lahar pulses from different source areas (Somma-Vesuvius vs.
723 Apennines) might have overlapped and further aggravated in the open plain.
724 At several locations, we found erosive erosional unconformities between (Fig. 165a) between the
725 lower and upper flow units (Fig. 165b), as well as between primary the pyroclastic deposits and lahar
726 units deposits. Erosion is an important factor for the entrainment of pre-existing materials and objects,
727 which includeing large-size clasts external to the remobilized pyroclastic material. Size and density
728 of the largest clasts embedded in the deposits can give an idea of the carrying capacity of the lahars.
729

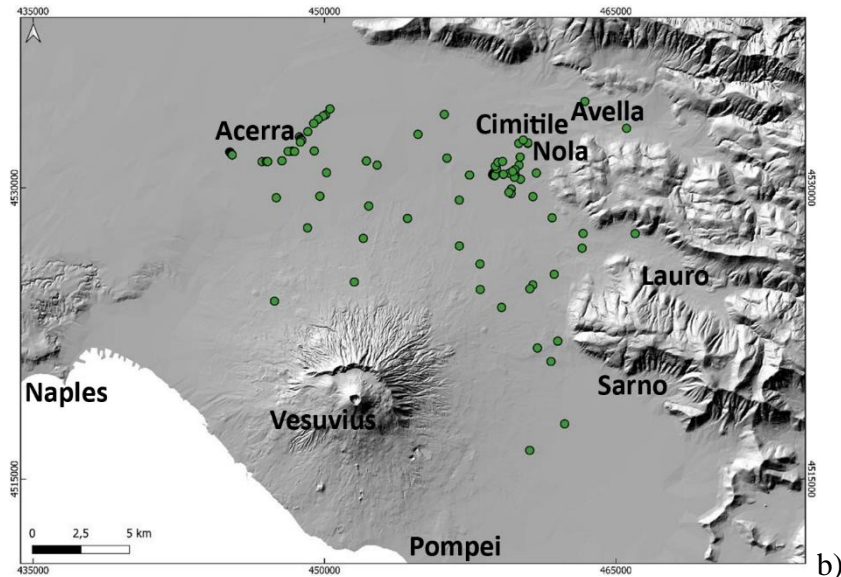




731 a)



732



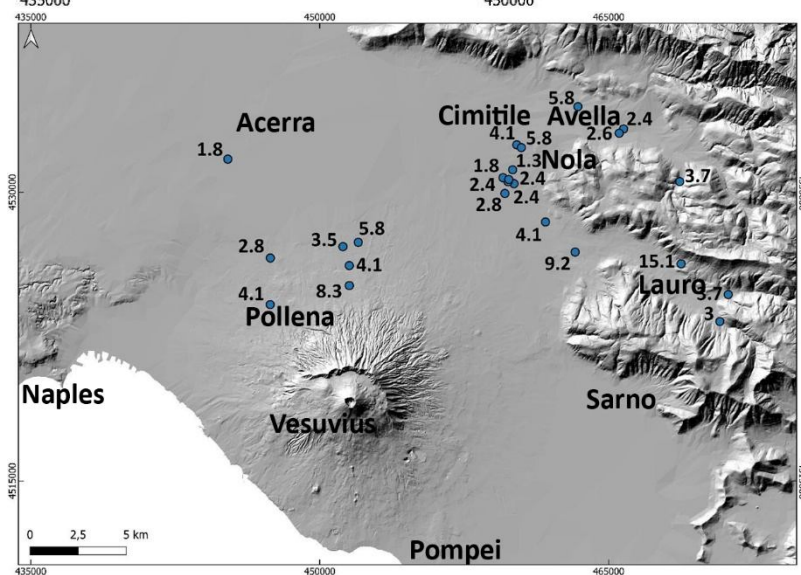
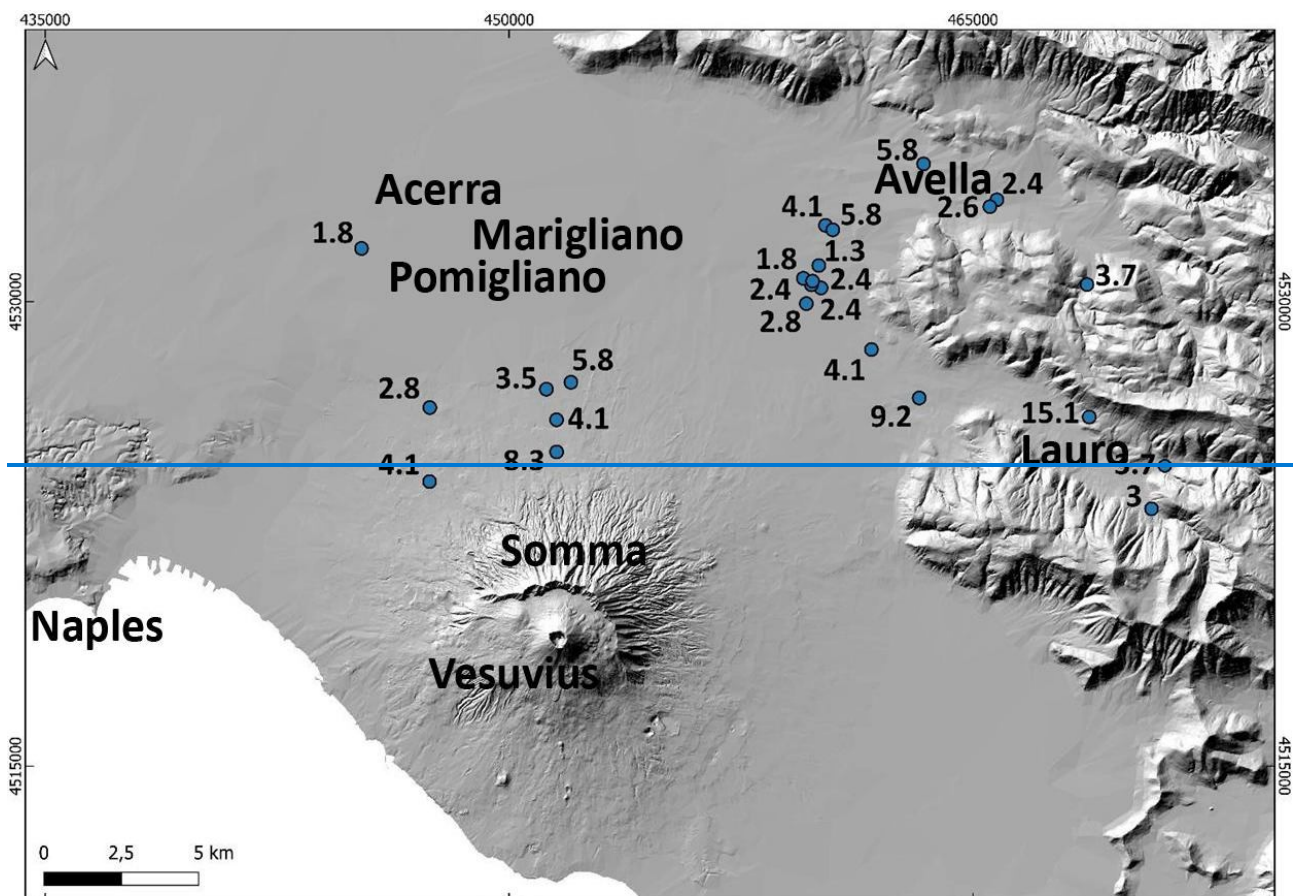
733 Fig. 165. a) Sites with evident erosion traces at the base of the lahar units; b) Sites in which multiple depositional flow
 734 units are vertically identified. Both evidences corroborate the interpretation of the depositional mechanisms, as well as
 735 constrain the choice of the shallow layer approach for the lahar models and simulations (de' Michieli Vitturi et al., this
 736 issue; Sandri et al., this issue).

738

739 Evidence Occurrences of oversize large clasts and boulders are observed reported in all the studied
 740 areas invaded both by the syn- and post-eruptive lahars, with a distribution that is similar to follows
 741 the one of the lahar deposits themselves (but with less proportions), and in particularly both are found
 742 at the mouth of the valleys, and in the alluvial plain (Fig. 15a). The presence of the erosional features
 743 (Fig. 16a), and the fact that the deposits are ubiquitously mostly composed of massive and relatively
 744 thick units (Fig. 16b), suggest that high sediment transport and deposition were not exclusive
 745 processes both occurred, i.e. they both occurred even at local scale in the same area (Doronzo and
 746 Dellino, 2013; Roche, 2015). Such occurrences of erosion and accumulation of multiple units were
 747 useful to inform the lahar modelling of de' Michieli Vitturi et al. (this issue).

748 We calculated local velocities of the syn- and post-eruptive Pollena lahars based on the biggest clasts
 749 that are found in the deposits at various stratigraphic heights, with boulder dimensions from several
 750 centimeters to a meter, and for flow density \geq water density (Appendix 4A). The faster the lahar the
 751 higher the capability of its flow to entrain bigger external clasts. This occurred at locations where

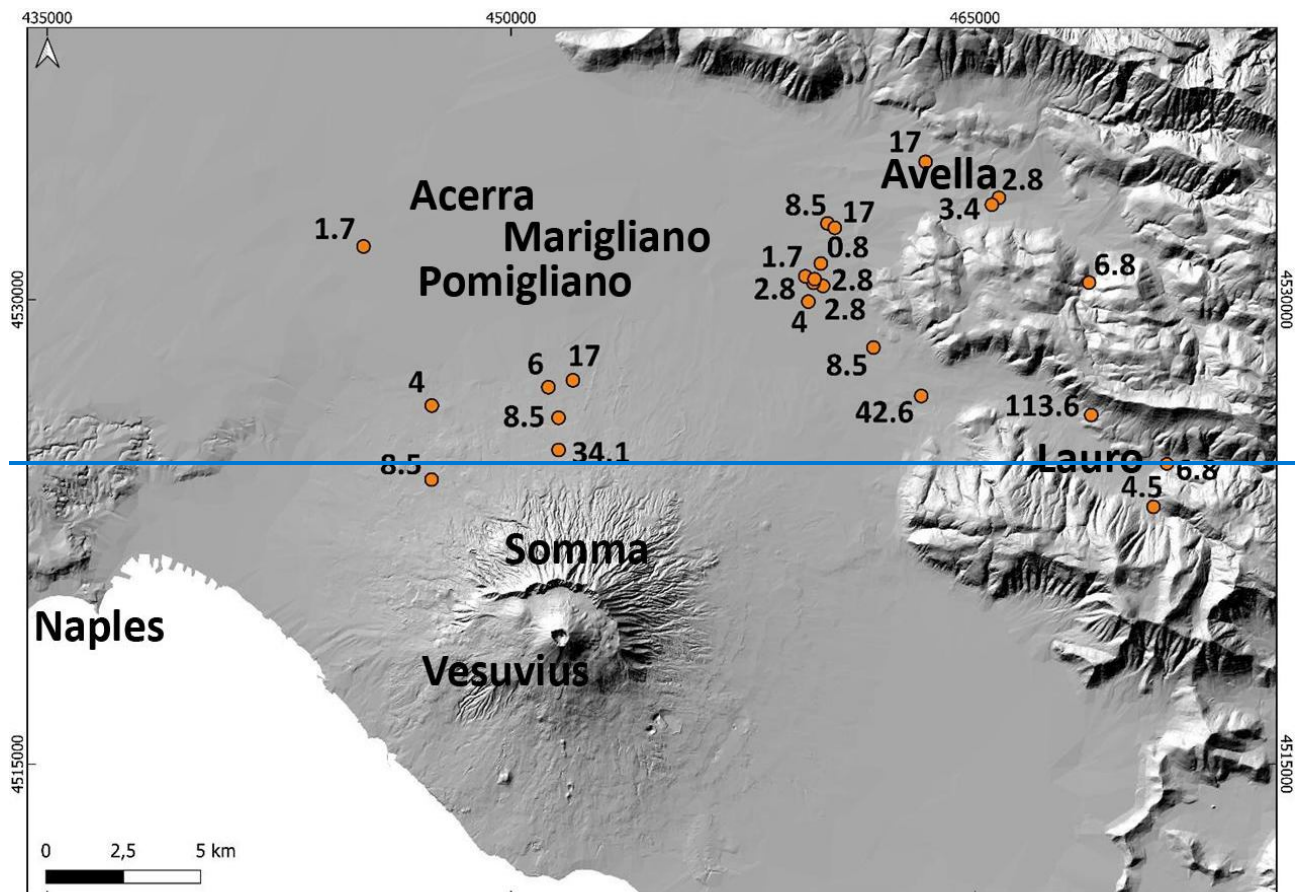
such clasts were freely available on the substrate, or where the lahars impacted and damaged anthropogenic structures.



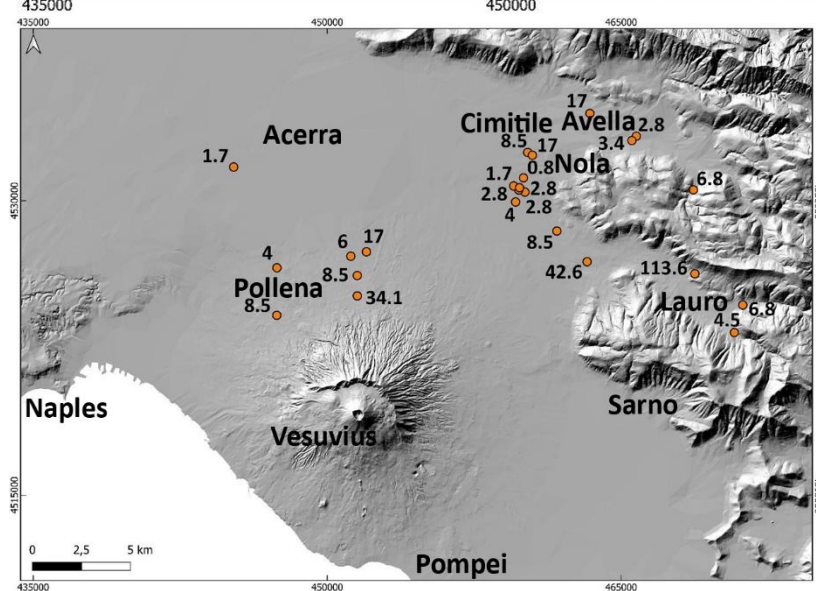
755 Fig. 176. Average lahar velocities (in m/s) estimated with a point-by-point reverse engineering approach.

760 187) as a function of the clast properties (size, density and shape). The obtained estimations are used
761 by Sandri et al. ([submitted this issue](#)) to validate the pProbabilistic hHazard aAssessment of lahars
762 from Vesuvius eruptions.

763



764



765

766 Fig. 187. Average lahar dynamic pressures (in kPa) estimated with a point-by-point reverse engineering approach.

767

768 The data presented in Figs. 1⁷⁶ and 1⁸⁷ represent ~~respectively~~ minimum local values of the flow
769 velocity and dynamic pressure, ~~respectively~~, useful to assess some minimum impact of the lahars in
770 the alluvial plain. An approximation of this point-by-point approach is that the values were calculated
771 for the finding locations of the clasts in the deposits, meaning that the values are overestimated for
772 those exact locations, while they should more properly be referred to the immediate surroundings
773 upstream. In particular, wWe did a parametric test to quantify the sensitivity for different physical
774 states of the multiphase flow, depending on initial fluidization and flow density, and considering two
775 end members, from a non-fluidized case to an initially fluidized and non-expanded case (see
776 Appendix ⁴A; Roche et al., 2013). From the performed analysis (see Appendix 1), we found that the
777 most typical values are referred to the initially fluidized and slightly expanded case (that is a few %
778 more expanded than the non-expanded case), with most of the points falling in the range of velocity
779 of 2-4 m/s, and dynamic pressure of 4-8 kPa.

780 Lastly, in eight ~~points~~locations we found the lahar deposits emplaced against meter-sized obstacles,
781 from which we estimated, by comparison, local flow heights of the order of 1-1.5 m, and particle
782 volumetric concentrations of ~30% or more, i.e. the deposit thickness is ~1/3 of the lahar thickness
783 (cf. Capra et al., 2018). ~~On the other hand, it is reasonable to argue that these are local values, and~~
784 ~~that flow height, particle concentration, and deposit thickness significantly varied over space due to~~
785 ~~the multiphase nature of the lahars (see de' Michieli Vitturi et al., submitted; Sandri et al., submitted).~~
786

787 5. Discussion

788 The historical sources used as benchmark for ~~the problem of the~~ lahars around Somma-Vesuvius and
789 in the Apennine valleys remark the frequent and broad impact that explosive eruptions of Vesuvius
790 had in historical times. Some of the eruptions ~~occurred~~ in the last four centuries (e.g., 1631, 1822,
791 1906 and 1944) ~~reached contemporaneously and repeatedly over time~~impacted on a number of
792 municipalities ~~due to the explosive character of the events~~, particularly in~~during~~ the sub-Plinian

793 eruption of 1631. Heavy rain events caused remobilization of the primary pyroclastic deposits,
794 triggering multiple lahars during or immediately after the eruption up to a few years (syn-eruptive
795 lahars; Sulpizio et al., 2006); post-eruptive lahars were triggered on the longer term.

796 On the other hand, the 472 Pollena eruption had an even wider impact, both in terms of primary
797 pyroclastic deposition and secondary (lahar) impact. For this event, the historical sources are scarce
798 or to absent.

799 The analysis of – and realization of a database with – more than 500 stratigraphic sections were done,
800 which also includes the sedimentological features both of primary (fall, flows) and secondary (the
801 lahars, alluvial events) deposits relative to the two sub-Plinian Vesuvius eruption case-studies from
802 Vesuvius, Pollena and 1631. The detailed reconstruction and mapping of these the primary deposits
803 allow an updating of the pyroclasts distribution on the territory allowed to update the area affected by
804 pyroclast sie deposits dispersal, as and it was found that both the eruptions had an impact larger than
805 previously known. In particular, the stratigraphic and sedimentological reconstruction of the deposits
806 was done not only in open spaces the countryside but also close to urban areas, and this is important
807 in terms of local impact of the lahars vs. broad impact in the environment. Specifically, such impact
808 investigation was done in urban areas including archaeological findings (e.g., villages, urban
809 structures, walls, etc...).

810 These findings include not only new data from the Somma-Vesuvius plain, but also more distal
811 deposits data from Lauro Valley and Avella-Baiano Valley (Apennines), which were subjected to
812 heavy remobilization also of the finer primary deposits as for the presence of including the widely-
813 dispersed fine ash deposits present in both proximal and distal areas formed in the late stage of the
814 eruptions. Indeed, the accumulation areas that were reconstructed reveal an enlargement and extra
815 2047% (Pollena eruption) and 230% (1631 eruption) coverage that was not previously known and,
816 considering the physical characteristics of the ash, it and this should be considered in any the hazard
817 and impact evaluation in the Campanian plain and on the nearby Apennine reliefs. The full database

818 ~~thus~~ allows a more precise reconstruction of the new isopachs, both for the Pollena and 1631
819 eruptions, which is possible given the high number of data points in the study area.
820 With particular reference to the lahar deposits, the syn-eruptive ones ~~that were emplaced~~occurred by
821 relatively short-term (during or immediately after the eruption) events, ~~stand~~and ~~were~~ directly
822 emplaced on the primary pyroclastic deposits, both for the Pollena and 1631 eruptions ~~case studies~~.
823 Also, there are not any significant erosion surfaces ~~nor humification traces in the sequences~~ due to
824 prolonged exposure of the primary deposits, testifying that the secondary emplacement was quite
825 immediate (max a few years; Sulpizio et al., 2006) after or even during the eruption. The syn-eruptive
826 features ~~of these deposits~~ are also testified by the absence of anthropie~~anthropogenic~~ traces or
827 humified surfaces at the base of or within interbedded in the deposits~~lahar deposits~~, as further
828 evidence of a very short-term time span between the eruptions and the lahar events. ~~O~~Another
829 interesting features ~~are~~is the presence of multiple depositional flow units in the lahar deposits, as
830 evidenced by granulometrie~~grain-size~~ changes, some clast alignments and concave erosion surfaces
831 inside within the lahar deposits~~lahar deposits~~. Such flow depositional units were emplacedformed by
832 en-masse ~~deposition~~ emplacement (with reference to each single flow pulse), while the whole lahar
833 deposits were formed by rapid progressive aggradation of the various flow units (Vallance and Scott,
834 1997; Doronzo, 2012; Roche, 2012; Smith et al., 2018; Martí et al., 2019; Guzman et al., 2020; see
835 also Sulpizio et al., 2014, p. 56), which does not contradict the principle of superposition. ~~and~~this
836 can be argued by the generally massive facies of each flow unit in the deposits, and by the presence
837 of water escape structures that cross vertically the entire lahar~~deposits~~ sequences. The ~~is~~ latter
838 evidence testifies a rapid ~~and contemporaneous~~ water loss through vertical escaping “pipes” during
839 or soon after the emplacementaggradation of the sequences. In other words, the various flow units
840 (layers) must decouple from the transport system, and such decoupling occurs unit-by-unit and not
841 particlebyparticle (Sulpizio et al., 2006, 2014; Roche, 2012; Doronzo and Dellino, 2013; Breard
842 and Lube, 2017; Smith et al., 2018), through a massive accumulation rate (Duller et al., 2008;
843 Doronzo et al., 2012; Martí et al., 2019).

844 The analysis of the Pollena lahar lithofacies allowed the identification of mainly two main deposit
845 categories. The first one occurs over-on an area that extends for more than 10 km north of Mount
846 Somma, and the second one occurs on an area which-that extends west of the Apennines. For the
847 latter, we can recognize two significant sub-categories of deposits, corresponding to the main valleys
848 in northwest-southeast direction, Avella-Baiano Valley and Lauro Valley. Theis difference between
849 the first and the second deposit categories seems to reflect the type of primary deposits that was-were
850 remobilized and-(just fine ash vs. ash and lapilli). In the first area Avella-Baiano Valley the area north
851 of Mount Somma, which also comprises the municipalities of Acerra and Afragola (about 12 km from
852 Somma-Vesuvius), the primary lapilli fallout deposits is-in fact not deposited are absent, while On
853 the other hand In this part of the plain, there is almost always a very the thin level-layer of
854 phreatomagmatic ash is widely present in the pPlain, while and thick, fine-grained pyroclastic current
855 deposits are present in the Mt.Mount Somma valleys feeding the lahars that fed some of the lahars.
856 The other basin comprises many In Avella-Baiano Valley and Lauro Valley, which also comprises the
857 municipalities in the area around Nola at 10-15 km from Apennine source valleys-(Fig. 1 and
858 Appendix 3C), where the lahar deposits are generally coarser, and consist of multiple depositional
859 units with different lithofacies (Tab. 3). In this case, both granulometry grain-size and componentry
860 indicate the that lahar deposits resulted from the remobilization of the fallout deposits. Such
861 considerations also derive from the full compilation of the geospatial database. A volume estimation
862 of the remobilized syn-eruptive deposits, based on a QGIS calculation, is of 73×10^{67} m³ for the
863 northern Vesuvius area, and 42×10^{67} m³ for the Lauro Valley.

864 Referring to the 1631 eruption, previous maps have shown the distribution of the 1631 lahar deposits
865 toward east, basically following the distribution of the primary pyroclastic fall deposits (Sulpizio et
866 al., 2006), while in Figs. 109 and 110 we show a significantly larger distribution area particularly
867 toward the north (Somma-Vesuvius ramps and pPlain) and east (mountainApennines valleys), and
868 less toward the SEsoutheast. In particular, this distribution is well explained by the wide distribution

869 of the ash fallout deposit toward both north and northeast (Fig. 6), remobilized during the lahar
870 generation ~~along~~ both from the Mount Somma and Apennine slopes. On the other hand, looking at
871 the average deposit thicknesses, they reach ~~on average~~ half a meter ~~to in~~ the N_north and NE_northeast,
872 while reaching ~~ing~~ a couple of meters in some points locations to in the NE_northeast (aligned with the
873 dispersion axis of the primary fallout deposits and out of the Apennine valleys).

874 The sedimentological analyses carried out on a number of samples from the different studied sectors
875 (Somma-Vesuvius, Lauro Valley, Avella-Baiano Valley) are useful for discriminating the various
876 factors that contributed to the initiation of the lahars and emplacement of their ~~lahar~~ deposits. The
877 samples ~~for from~~ Lauro Valley and Avella-Baiano Valley are coarser (but have a significant finer
878 tail) than the ones for Somma-Vesuvius, and this can depend on three factors: i) ~~depositional~~
879 ~~mechanisms~~genetic types of the primary pyroclastic deposits (fall vs. flow); ii) interaction between
880 lahars and morphology (valley vs. plain); iii) major ~~involvement~~remobilization for in Lauro Valley
881 and Avella-Baiano Valley of the distal ~~fine~~ phreatomagmatic fine ash deposits formed in the final-late
882 eruption~~s~~ stages. In other words, the primary grain sizes involved in the remobilization (finer and
883 higher-water retention for Somma-Vesuvius), as well as the general topography (gentler but longer
884 ramp for Somma-Vesuvius) likely acted as the main factors directly impacting the distribution of the
885 lahar deposits, and the decay of the flow velocities and dynamic pressures in the area.

886 Interestingly, an emplacement temperature of (~120 °C) of the lahar deposits was calculated for those
887 generated along the Somma-Vesuvius slopes, indicating a relatively hot provenance after
888 remobilization of the pyroclastic current deposits. Instead, the remobilization from the Apennines
889 sectors involved only cold fallout deposits. The companion paper of de' Michieli Vitturi et al. (this
890 issue) investigates also the nexus between water temperature, flow viscosity, and their consequential
891 impact on fluid dynamics. Specifically, when the dominance of frictional forces is attributable to the
892 yield slope term, the initial divergence between high- and low-temperature scenarios appears
893 negligible. However, discernible dissimilarity appears over time for the inundation area of the colder

894 flow case (i.e., 27 °C) with respect to the warmer counterpart (i.e., 100 °C), the latter case being close
895 to the 120 °C one reported from paleomagnetism. Remarkably, the temperature-induced variations
896 assume a pivotal role in shaping the dynamic characteristics of the hotter flow. The diminished
897 viscosity associated with elevated temperatures not only amplifies fluid mobility but also prompts a
898 notable acceleration in sediment settling velocity. This, in turn, initiates a debulking mechanism,
899 thereby intensifying overall flow mobility. Consequently, this intricate interplay contributes to a
900 reduced footprint of deposited material from the flow, altering the spatial distribution of sediments.
901 However, the overall impact on the inundation area is typically quite reduced, being typically less
902 than 10-20% even considering a thickness threshold of 1 mm (see de' Michieli Vitturi et al., this issue).
903 The sampled clasts might have been incorporated multiple times by the flows, and the heating/cooling
904 processes that we interpret as indicating T_{dep} in the diagrams are the last to have occurred and affected
905 the samples. Besides, a third heating component is clearly observed for some of them. The
906 paleomagnetic ~~data directions of flow direction are statistically distinguishable~~ also indicate,
907 supporting that the lahar emplacement at Nola (10-15 km from Apennine source valleys) and Acerra
908 (12 km from Somma-Vesuvius) was not synchronous, as ~~a~~ further evidence of the different timing
909 and ~~hence likely different~~ detachment areas involved during the pyroclasts remobilization. However,
910 the comparison with the paleosecular variation curves of the Earth's magnetic field does not allow to
911 better constrain the entity of the time span between the two lahar events. The parental lahars acted as
912 mass flows capable of entraining outsized clasts (where available) from substrate under the action of
913 shallow-layer flow ~~velocity and~~ dynamic pressure (de' Michieli Vitturi et al., this issue), then
914 emplaced massive flow units with uplifted external clasts set into the much finer matrix (see Roche,
915 2015). In ~~various~~ ~~some~~ lahar units, ~~multiple~~ ~~various~~ clasts have been found, showing some alignment
916 that depends on the mechanisms of entrainment and uplift (with respect to substrate) within the flow.

917 In terms of local impact in the Pollena case study (the largest one), while most of the calculated points
918 (44) fall in the range of lahar velocity of 2-4 m/s and dynamic pressure of 4-8 kPa, a few peak values

919 of velocity of 13-15 m/s and dynamic pressure of 90-115 kPa are also calculated, which are directly
920 related to meter-sized clasts entrained into the lahars on the steep slopes, then deposited downstream
921 of alluvial fans. Such values of the velocity and dynamic pressure are well comparable with those
922 calculated for lahars that occurred recently at Ruapehu in 2007 (Lube et al., 2012) and Merapi in 2011
923 (Jenkins et al., 2015), and in historical times at El Misti (Thouret et al., 2022). In particular, the
924 estimated velocities and pressure agree with those of Lube et al. (2012) and Jenkins et al. (2015).
925 Moreover, multiplying velocity and density gives a power per unit surface, so those most
926 representative values correspond to a flow power per unit surface of $8 \cdot 10^3$ - $3.2 \cdot 10^4$ W/m², with peak
927 values of $1.17 \cdot 10^6$ - $1.72 \cdot 10^6$ W/m², in agreement with typical values reported for floods and
928 megafloods (Russell and Knudsen, 1999; Whipple et al., 2000; Carling, 2013).

929

930 6. Conclusions

931 ~~A number of points can be highlighted after the~~ The integration of the historical, stratigraphic,
932 sedimentological, laboratory, and impact parameter analyses carried out in the Vesuvius area allow
933 us updating on the lahar invasion related to ~~for~~ the Pollena and 1631 eruptions. In general, the physical
934 characteristics of the analyzed deposits indicate that syn-eruptive lahars are related to the rapid
935 remobilization of large volumes of pyroclastic material, which is mainly fine-grained and almost
936 exclusively derived from the accumulation of products related to a single eruption. The analysis also
937 shows that tardive (post-eruptive) mass flows are common, and involve multiple and variably altered
938 deposits, and that their energy and frequency are progressively lower over time, after the last eruption
939 has occurred. In particular, a higher impact both from primary and secondary phenomena is
940 something that should be accounted in the Vesuvius area and that:¹²

941 i) The new isopach maps of the Pollena and 1631 eruptions allow us to infer a larger impact
942 than previously known for these two sub-Plinian events of the Vesuvius. Thus, it is worth
943 reconsidering the territorial impact that sub-Plinian eruptions can have in the Vesuvius

944 (but not only) area. In particular, the ash deposits can have a high impact in relation to
945 their high density and low permeability.

946 ii) The primary impact from fallout and pyroclastic current processes in the Vesuvius area
947 was - and may be in the future – followed by the secondary impact from lahars generated
948 during or immediately after the eruption events. Both impacts can have a wide distribution,
949 because they are directly controlled by the primary deposits distributions, both around
950 Somma-Vesuvius and in the Apennines valleys.

951 iii) The runouts of such lahars were significant both for the Pollena and 1631 eruptions, by
952 reaching distances of 10 to 15 km from the sources, and their deposits geometry is tabular-
953 like with average thicknesses of 0.5 to 1 m.

954 iv) The paleotemperature data highlight a relatively hot dynamics (~120 °C) for those lahar
955 flow pulses that traveled along down the Somma-Vesuvius slopes because of pyroclastic
956 current deposit remobilization. This did not occur from the Apennines sectors, where
957 pyroclastic currents did not get to, and only cold fallout deposits were remobilized.

958 v) A reverse engineering approach allowed to calculate the local lahar velocities (2-4 m/s,
959 with peaks of 13-15 m/s), dynamic pressures (4-8 kPa, with peaks of 90-115 kPa), and
960 solid volumetric concentration (~30%, implying a 1:3 ratio between deposit and flow
961 thickness), on the basis of the external clast properties entrained into the flows then
962 emplaced into the ash matrix, and on the presence of the lahar deposits in proximity of
963 obstacles and archaeological findings.

964 As a general conclusion, we have demonstrated that the areal impact of both primary deposits and
965 lahars, in case of sub-Plinian events at Somma-Vesuvius, involves a territory wider than
966 previously known and for several years, with possible decreasing damages over time.

969 A theoretical scheme is presented to quantify local velocities and dynamic pressures of the lahars, by
 970 inverting the field features at selected locations. The final goal is to map the values of velocity and
 971 dynamic pressure to assessing the hazard from lahars in the study area. Flow dynamic pressure, P_{dyn} ,
 972 results from a combination of flow density, ρ_f , and flow velocity, v , and is defined as follows

$$973 \quad P_{dyn} = 0.5 \rho_f v^2 \quad (A1)$$

974 In the study area, the original flow was a multiphase flow of water + pyroclastic sediment, which
 975 during remobilization evolved into a flow of water + pyroclastic sediment + external clasts.
 976 Generically, flow density results from a combination of particle density, ρ_p , and water density, ρ_w ,
 977 through particle volume concentration, C , and is defined as follows

$$978 \quad \rho_f = \rho_p C + \rho_w (1 - C) \quad (A2)$$

979 In order to define flow velocity, we take into account stratigraphic and sedimentological
 980 characteristics of the lahar depositsflow units: i) they are ubiquitously massive, and result from
 981 remobilization of the primary pyroclastic deposits then emplacement from mass flows; ii) they
 982 contain big external clasts entrained (by dynamic pressure) and uplifted (also by pore pressure) from
 983 substrate into the flows. With these field characteristics, flow velocity can be expressed as a
 984 combination of entrained clast properties and flow density, and is defined as follows (modified after
 985 Roche, 2015)

$$986 \quad v = \sqrt{\frac{X \psi (\rho_c - \rho_w) g}{\gamma \rho_f}} \quad (A3)$$

987 where X is clast small axis, ψ is clast shape factor, ρ_c is clast density, g is gravity acceleration and γ
 988 is an empirical constant. Eq. 3 allows quantifying the incipient motion of the big clasts, and gives
 989 minimum values of flow velocity required to entrain and uplift the clasts from substrate, possibly
 990 probably more than once, before being emplaced into the lahar deposits by flow velocity drop. Such
 991 equation has been originally derived in laboratory experiments for a multiphase flow of air +
 992 sediment, and is highly performing at $\rho_f \sim 1000 \text{ kg/m}^3$ (hindered settling) for dense pyroclastic

993 currents controlled by topography then opened to alluvial plain (Martí et al., 2019), which is a case
994 similar to the lahars in the study area. Substituting Eq. 3 into Eq. 1 and simplifying gives

$$995 \quad P_{dyn} = 0.5 \frac{X\psi(\rho_c - \rho_w)g}{\gamma} \quad (A4)$$

996 For given clast properties, flow dynamic pressure has a unique value, while flow velocity is a function
997 of flow density. Indeed, the present scheme is a spot model that basically depends on, and is limited
998 to, the finding of big clasts and boulders within the lahar deposits. An approximation is that velocity
999 and dynamic pressure are calculated for the locations where the clasts are found in the deposits,
1000 meaning that the calculated values are overestimated for those exact locations, while they are more
1001 properly referred to the immediate surroundings upstream.

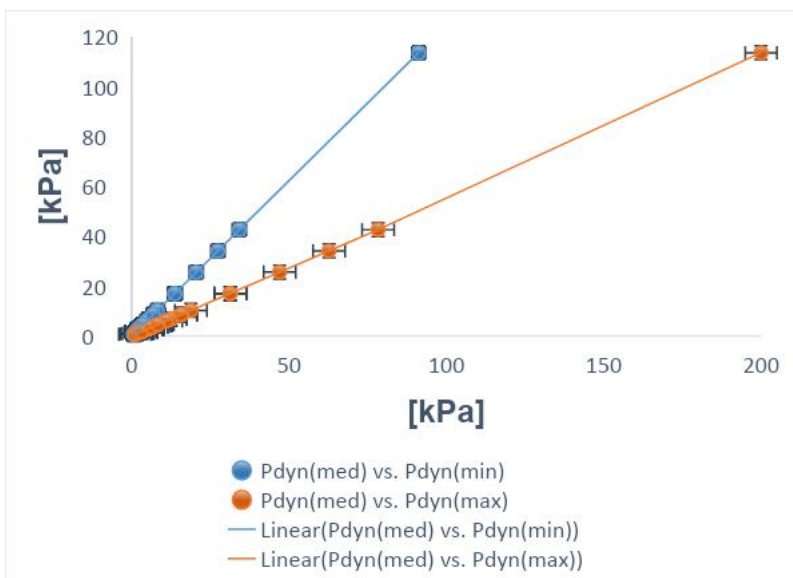
1002 At the selected locations in the study area, we collected the dimensions of the biggest clasts found in
1003 the lahar deposits, and we characterized petrographically lithologically the clasts in the field, to
1004 calculate flow dynamic pressures using Eq. 4. We used the following values for the various
1005 parameters in the calculations: ψ (ellipsoid) = 0.66; ρ_c (limestone) = 2500 kg/m³; ρ_c (ceramic) = 2000
1006 kg/m³; ρ_c (brick) = 2000 kg/m³; ρ_c (tephra) = 1500 kg/m³; ρ_c (lava) = 2500 kg/m³; ρ_c (iron) = 8000
1007 kg/m³; ρ_w = 1000 kg/m³; g = 9.81 m/s²; γ = 0.031 – 0.071. Also, we calculated flow velocities using
1008 Eq. 3, in the following range of flow density: $\rho_w \leq \rho_f \leq \rho_p$, where ρ_w = 1000 kg/m³ and ρ_p = 2000
1009 kg/m³. In this way, flow density spans from two extreme cases: i) $\rho_f = \rho_w$, negligible pyroclastic
1010 sediment and external clasts, so water flow only; ii) $\rho_f = \rho_p$, negligible water and dominant pyroclastic
1011 sediment, so ash flow only. For the empirical constant in Eq. 3, we used three different values to test
1012 the sensitivity with respect to different physical states of the multiphase flow: γ (non-fluidized) =
1013 0.031; γ (initially fluidized and slightly expanded) = 0.057; γ (initially fluidized and non-expanded)
1014 = 0.071 (see Roche et al., 2013; Fig. A1).

1015 Regarding flow velocity, after calculation we can rewrite Eq. 3 in a simpler form (to more directly
1016 relate velocity to density) as follows

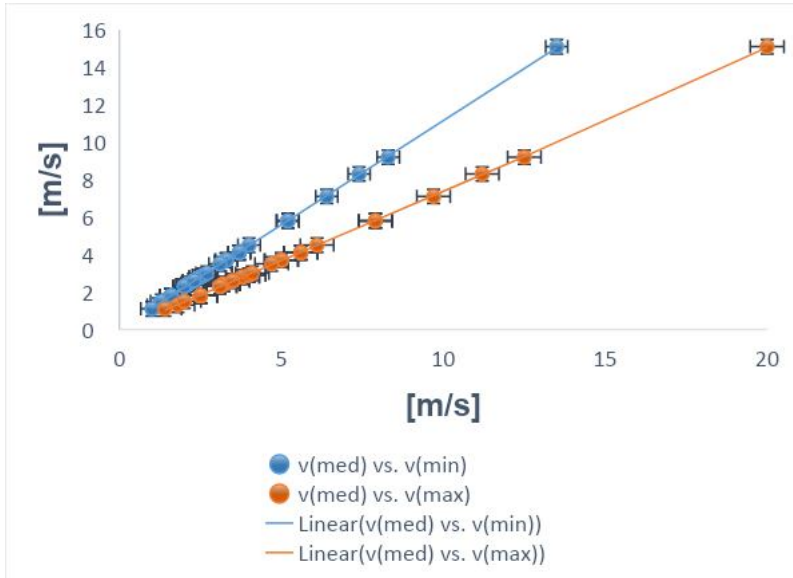
1017

$$v = \frac{a}{\sqrt{\rho_f}} \quad (A5)$$

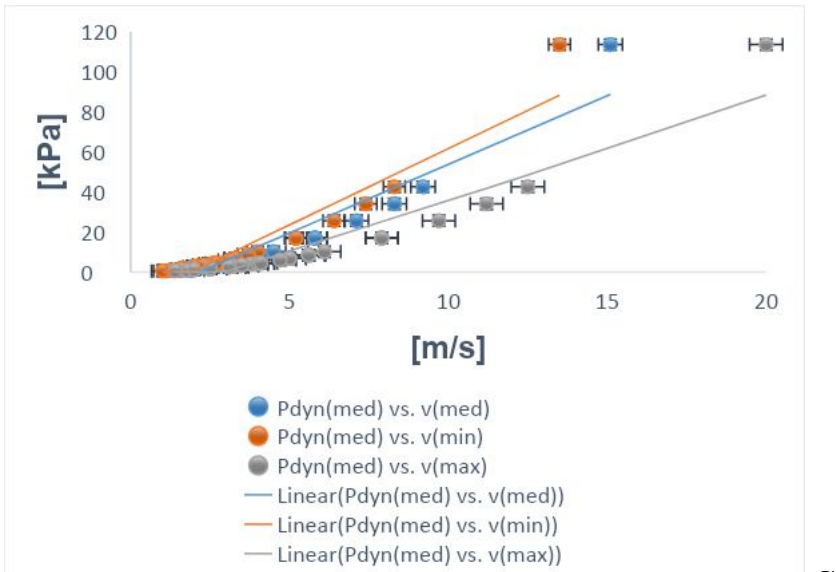
1018 where $a > 0$ depends on clast properties, and its square has dimension of pressure. On the other hand,
 1019 it is not straightforward to constrain local flow velocities with unique values of flow densities, mostly
 1020 because small variations of velocity correspond to large variations of density, and this is particularly
 1021 valid for volcaniclastic mass flows (Carling, 2013; Jenkins et al., 2015; Roche, 2015; Martí et al.,
 1022 2019; Guzman et al., 2020; Thouret et al., 2022).



A



B



C

1025

1026 Fig. A1. [Local dynamic pressures and velocities for the syn- and post-eruptive Pollena lahars calculated with the reverse](#)
 1027 [engineering approach](#). A, dynamic pressure for the initially-fluidized and slightly expanded case vs. dynamic pressure for
 1028 the initially-fluidized and non-expanded (blue) and non-fluidized (orange) cases; B, velocity for the initially-fluidized
 1029 and slightly expanded case vs. velocity for the initially-fluidized and non-expanded (blue) and non-fluidized (orange)
 1030 cases; C, dynamic pressure for the initially-fluidized and slightly expanded case vs. velocity for the initially-fluidized and
 1031 slightly expanded (blue), vs. velocity for the initially-fluidized and non-expanded (orange), vs. velocity for the non-
 1032 fluidized (grey) cases.

1033

1034 At some locations in the study area, we found lahar deposits against meter-scale manufacturing
 1035 obstacles (Di Vito et al., 2009). The peculiarity is that the deposits in proximity of the obstacles are
 1036 thicker than the correlated ones in the free field, but never reach the top of the obstacles themselves.
 1037 This means that the lahars were not much expanded, so unable to overcome the obstacles as stratified
 1038 flows would have done (cf. Spence et al., 2004; Gurioli et al., 2005; Doronzo, 2013; Breard et al.,
 1039 2015). With this field evidence, we can assume that local flow height, H , was similar to deposit
 1040 thickness against the obstacle, h_o , as follows

$$1041 H \approx h_o \quad (A6)$$

1042 In order to estimate flow density using Eq. 2, we focus on particle volumetric concentration. For well-

1043 sorted deposits, such concentration can be defined with an average value over flow height as follows
1044 (modified after Doronzo and Dellino, 2013; see also Eq. 30 in de' Michieli Vitturi et al., [submitted this](#)
1045 [issue](#))

$$1046 C = \frac{h_f}{H} \quad (A7)$$

1047 where h_f is deposit thickness in the free field. Substituting Eq. 6 into Eq. 7 gives

$$1048 C \approx \frac{h_f}{h_o} \quad (A8)$$

1049 In particular, h_f refers to those lahar deposits relatively close to the obstacles, but which were not
1050 affected by them during emplacement, i.e. close but not so much. We assessed that correlation taking
1051 into account the stratigraphic and sedimentological characteristics of the lahar deposits, and the fact
1052 that Eq. 7 performs better with layers emplaced after remobilization of primary pyroclastic fallout or
1053 dominantly ash flow deposits.

1054 Lastly, we macroscopically assessed erosion in the field, by characterizing the unconformities present
1055 both on the primary pyroclastic and lahar deposits. In particular, the syn-eruptive lahar deposits
1056 consist of more than one flow unit, so it is important to understand how the different flow pulses
1057 interacted with each other during emplacement. The main unconformities that are found in the field
1058 are referred to the partial absence of a flow unit, and the loss of lateral continuity despite some flat
1059 geometry of the deposits. On the other hand, at some locations we were not able to assess if erosion
1060 occurred or not due to multiple open issues: i) [eventual possible](#) absence of the primary pyroclastic
1061 deposits; ii) [eventual possible](#) exclusive presence of the post-eruptive lahar deposits; iii) impossibility
1062 to get to some outcropping deposit base and [eventual possible](#) unconformities.

1063

1064 **Appendix B. Paleo-temperature and paleo-direction determinations**

1065 The magnetic fabric of a deposit was investigated by measurements of the magnetic susceptibility
1066 and its anisotropy (AMS). AMS was measured with a Kappabridge KLY-3 (AGICO), and data were
1067 elaborated by the software Anisoft5 (AGICO). AMS depends on the type, concentration, and
1068 distribution of all the minerals within the specimen. It is geometrically described by a triaxial
1069 ellipsoid, whose axes coincide with the maximum (k_1), intermediate (k_2) and minimum (k_3)
1070 susceptibility directions. The magnetic fabric of a specimen is then described by the direction of the
1071 k_1 axis, the magnetic lineation (L) and that of the k_3 axis, which is parallel to the pole of the magnetic
1072 foliation plane (F). Besides, the modulus of the susceptibility axes provides some magnetic
1073 parameters useful to express the intensity of the anisotropy (P_j) and the oblate/prolate fabric
1074 occurrence (T) (Jelinek, 1981). Generally, sedimentary ~~vs.~~ pyroclastic deposits fabric, here
1075 considered as the proxy of the lahar fabric, is oblate with a horizontal to gently imbricated (less than
1076 20°) magnetic foliation. The magnetic lineation is normally clustered along the foliation plunge. In
1077 this case, both the F imbrication and the L direction can provide the local flow direction. Other times,
1078 L is orthogonal to the F plunge or F is statistically horizontal, and it is not possible to infer the flow
1079 direction.

1080 For T_{dep} estimation, pottery sherds were subjected to progressive thermal demagnetization (PTD),
1081 with heating steps of 40 °C, up to the Curie Temperature (T_C), using the Schonstedt furnace and the
1082 spinner magnetometer JR6 (AGICO). The rationale of the method has been described in detail in
1083 several papers (McClelland and Druitt, 1989; Bardot, 2000, Porreca, 2007; Paterson et al., 2010; Lesti
1084 et al., 2011), many of them dedicated to PDCs of the [Vesuvian-Vesuvius](#) area (Cioni et al., 2004; Di
1085 Vito et al., 2009; Giordano et al., 2018; Zanella et al., 2007; 2018; 2015). Typically, measurements
1086 are made on accidental lava lithics that were entrained during pyroclastic or lahar flows. In this case,
1087 we had the opportunity to estimate the T_{dep} by measuring ancient pottery artifacts. Briefly, pottery is
1088 characterized by a thermal remanent magnetization (TRM) acquired during its manufacture and its
1089 subsequent history of daily use. Whenever it is heated, part of its TRM, the one associated with
1090 blocking temperatures (T_b) below the heating one (T_h), is overwritten. Without alteration phenomena,

1091 the heating/cooling is a reversible process, except for the magnetic directions. The original TRM
1092 shows a random paleomagnetic direction, due to the transport during emplacement. Subsequent
1093 TRMs show directions parallel to the Earth's magnetic field during their cooling. This is clearly
1094 illustrated in the Zijderveld diagrams. The composition of the different magnetization components
1095 reveals thermal intervals characteristic of the heating history of the potsherd. Of course, this
1096 explanation is simplified, but the method is well-established and has been shown to work well with
1097 heated artifacts, such in the case of tiles and pottery embedded in the PDC deposits at Pompeii
1098 (Gurioli et al., 2005; Zanella et al., 2007), Afragola (Di Vito et al., 2009) and Santorini (Tema et al.,
1099 2015). In case of lahar, we expect low T_{dep} or cold deposits. This can be a major concern because of
1100 the difficulties to distinguish between the TRM secondary components, and the chemical (CRM) and
1101 viscous (VRM) remanent magnetization. The CRM may develop due to mineralogical changes during
1102 reheating (McClelland, 1996). Instead, VRM is typical of ferromagnetic grains with low T_b and often
1103 occurs in most rocks. Following Bardot and McClelland (2000) relationship for time intervals in the
1104 10^2 – 10^6 year range, $T_b = 75 + 15 \log$ (acquisition time in years), and using the Pollena eruption date
1105 (472 [ADCE](#)), we obtain a lower limit of the T_b around 123 °C. This means that this temperature helps
1106 us in discriminating between “hot” ($T_b > 120$ °C) or “cold” lahar ($T_b < 120$ °C).
1107 Finally, routine magnetic measurements on the lahar matrix were done on the lahar matrix to
1108 determine the Characteristic Remanent Magnetization (ChRM) by Thermal and Alternating Field
1109 demagnetizations. The direction of the Earth's Magnetic Field during the Pollena eruption is well-
1110 known (Zanella et al., 2008). If the sampled lahars were emplaced shortly after the eruption, both the
1111 secondary TRMs and the matrix of the lahars should show a remanent magnetization direction similar
1112 to the Pollena ones. ChRMs can also test if the two lahars ([Acerra at 12 km from Somma-Vesuvius](#),
1113 and [Nola at 10-15 km from Apennine source valleys](#)) are coeval.
1114

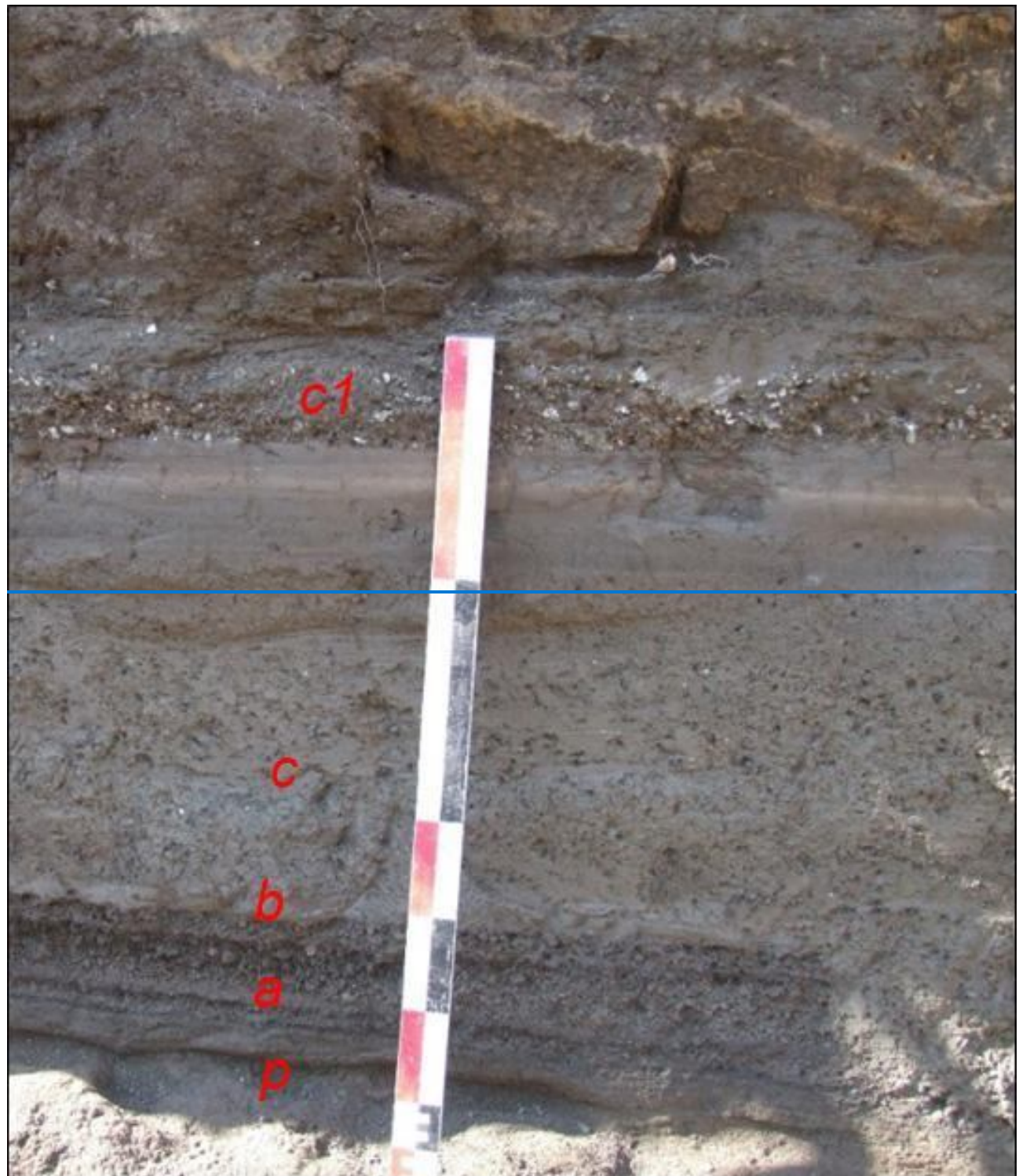
1115 **Appendix C. Description of the studied areas**

1116 *Area 1 – Nola*

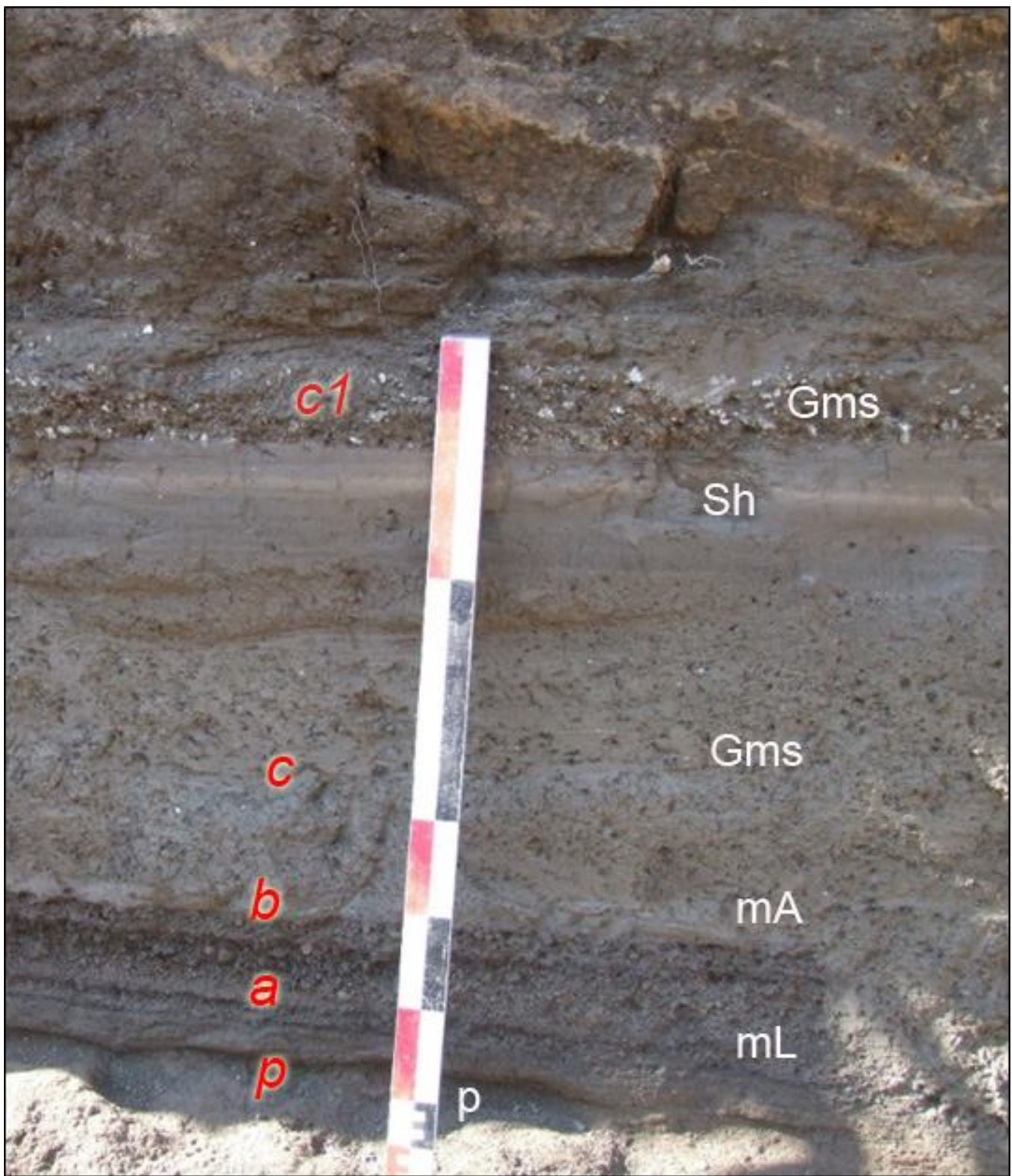
1117 In the area surrounding Nola ([10-15 km from Apennine source valleys](#)), it is possible to recognize
1118 the complete fallout sequence of the Pollena eruption (a in [Ffig. C1 and C2](#)), which usually covers
1119 ploughed soils (p in [Ffig C1](#)) and late Roman archaeological remains. The sequence is composed [by](#)
1120 [of](#) an alternation of coarse pumice and thin ash fallout layers. Its top is always made of a [cohesive](#)
1121 [fine](#) ash bed related to the phreatomagmatic phase of the eruption (b in [Ffig. C1 and C2](#)), with a
1122 thickness ranging from 1 to 14 cm due to erosion. They are almost always overlain by lahar deposits
1123 composed of several flow units (c in [Ffig. C1 and C2](#)) with a large thickness variability due to
1124 channeling and presence of barriers and [edifices](#)[buildings](#). They sometimes include blocks, tiles, and
1125 other archaeological remains.

1126 In Fig. C1, above the primary deposit, there is an example of a well-exposed sequence composed [by](#)
1127 [of](#) at least five units (c in [Ffig. C1](#)). The first one is a massive and matrix-supported deposit composed
1128 [by](#)[of](#) fine and not vesiculated ash (lithofacies Gms), with fragments of greenish to blackish scoriae
1129 and minor fragments of pumices, lavas and limestones. The fragments are cm-sized and are both
1130 angular and rounded. The second flow unit is similar to the one below, but is darker and contains less
1131 coarse fragments. Its matrix is composed [by](#)[of](#) an alternation of fine to medium ash [layers](#). It follows
1132 a plane-parallel sequence of well-sorted fine sand and silt layers characterized by the lithofacies fM.
1133 A massive deposit follows upward, it is progressively humified and contains abundant reworked and
1134 rounded pumice [clasts](#) from the Avellino eruption. The top humified surface is almost always eroded
1135 by anthropogenic activity and is generally ploughed (p1 in Fig. C2), [whose surface](#). [It](#) is overlain by
1136 the primary deposits of the [1631](#) eruption [of 1631](#) (d in Fig. C2). It is few cm thick and is composed
1137 [by](#)[of](#) a basal layer of dark coarse ash (small pumice fragments), overlain by a [very cohesive and](#)
1138 massive ash bed, containing abundant accretionary lapilli. The following deposit thickens in the
1139 [plowing](#)[ploughing](#) furrows and depressions, and is composed [by](#)[of](#) massive fine-ash beds,
1140 vesiculated and cohesive, and is interpreted as a lahar deposit (lithofacies mM) (e in Fig. C2). This

1141 deposit (e in Fig. C3) overlies the foundations of Palazzo Orsini (blocks in Fig. C3), now seat of the
1142 Court of Nola and built in the second half of the XV century (Fig. C3). The top is always eroded by
1143 the modern anthropogenic activity, and locally by deposits of recent eruptions of Vesuvius (e.g., 1822,
1144 1906).



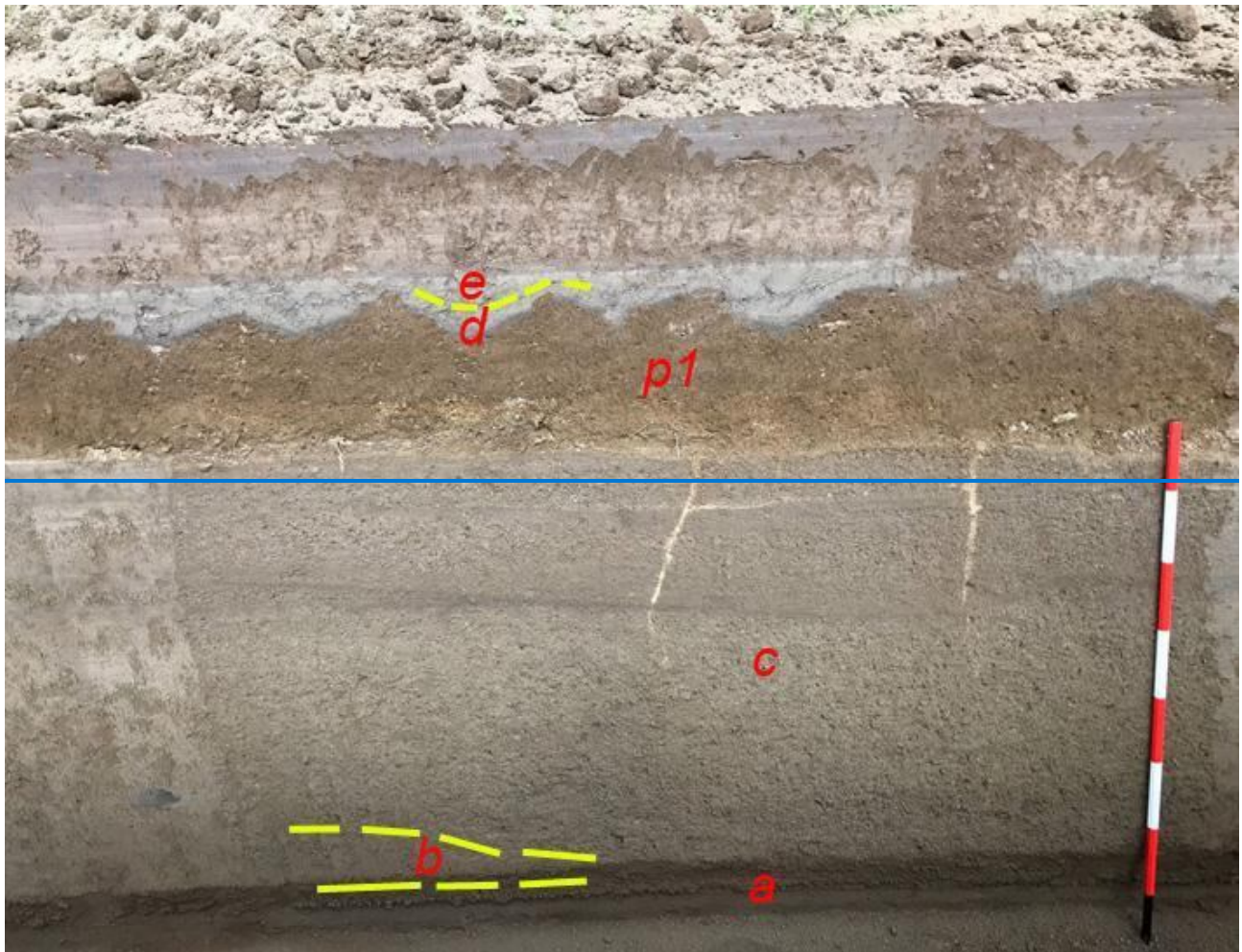
1145



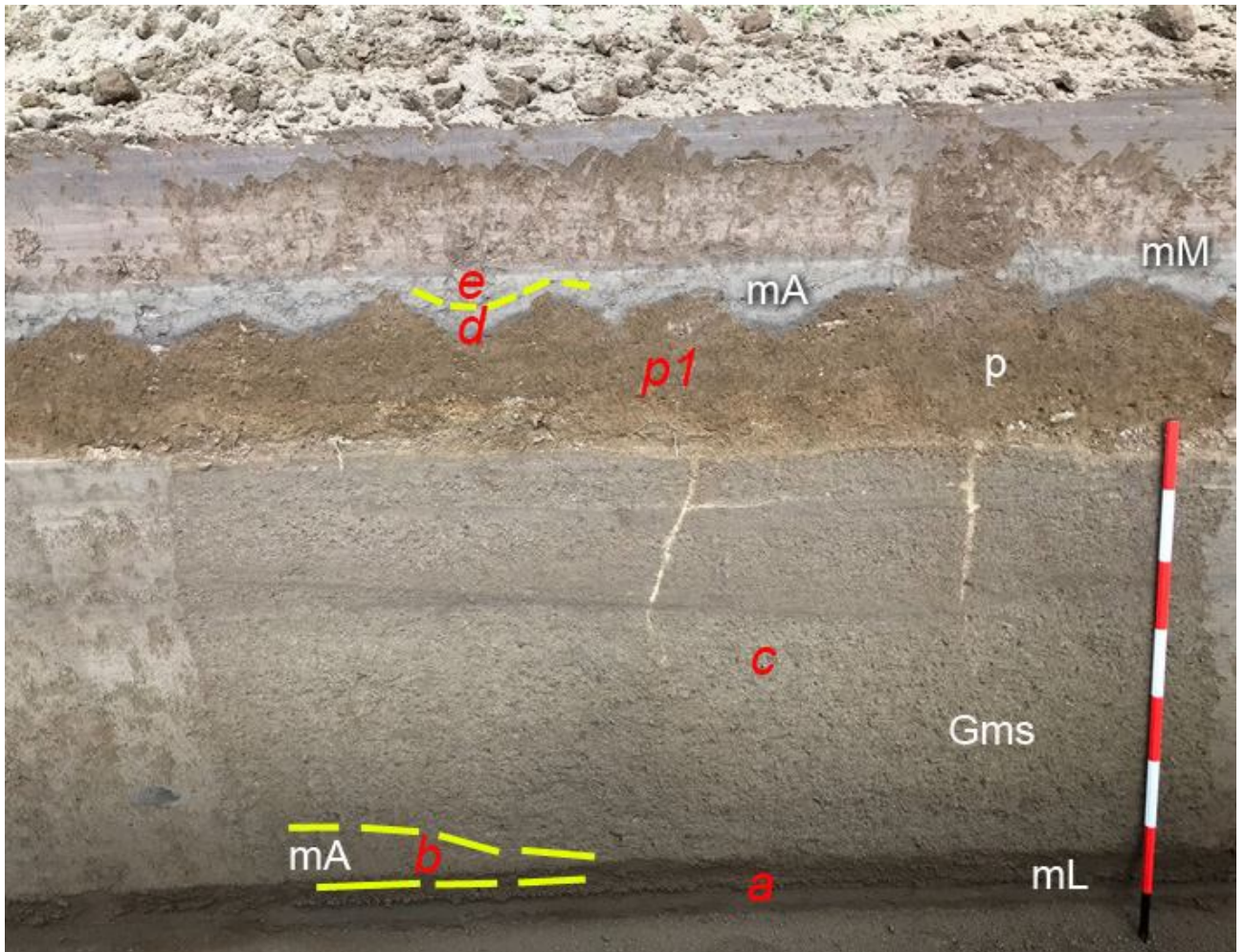
1146

1147 Fig. C1. Nola ([10-15 km from Apennine source valleys](#)), Pollena fallout deposits overlain by at least five lahar units. [In](#)
1148 [particular: p = paleosol; a = alternation of coarse and fine fallout sequence of the Pollena eruption; b = final ash fallout](#)
1149 [of the eruption; c = sequence of syn-eruptive lahars; c1 = post-eruptive lahar containing white pumice fragments of the](#)
1150 [Pomice di Avellino eruption. For the description of lithofacies see Tab. 2.](#)

1151



1152



1154 Fig. C2. Nola, Pollena lahar deposits overlain by a cultivated paleosol₁ and by the 1631 ash fallout and lahars. In
1155 particular: a = alternation of coarse and fine fallout sequence of the Pollena eruption; b = final ash fallout of the eruption,
1156 partially eroded; c = sequence of three lahar units; p1 = ploughed paleosol; d = 1631 ash fallout deposit mantling the
1157 undulated paleosol; e = lahar deposit composed of a massive ash layer. For the description of lithofacies see Tab. 2.

1158



1159



1160

1161

1162

1163

1164

1165

1166

1167

Fig. C3. Palazzo Orsini, Nola (1631 fallout and lahars). [In particular: d = 1631 ash fallout deposit overlying the foundations of the building \(in the inset\); e = syn-eruptive lahar deposit. For the description of lithofacies see Tab. 2.](#)

1168 is well visible in the Amphitheater Laterizio, which was completely filled by the primary and
1169 secondary deposits, and the same in Cimitile, where in the archaeological site of the Early Christian
1170 basilicas the present ground level is about two meters higher than the one before the eruption. It is
1171 worth noting that in Cimitile the flows were able to carry limestone blocks of 50 cm in diameter,
1172 likely along the main flow direction of the lahars (Fig. C4).



1173



1174

1175 Fig. C4. Cimitile-S. sequence of three m-thick syn-eruptive lahar units with the evidencess of transport of calcareous block
 1176 (up to 50 cm). The largest are in the lower unit. The base of the lahar sequence and the underlying fallout deposit of the
 1177 Pollena eruption are not visible in the photo. For the description of lithofacies see Tab. 2.

1178

1179 *Area 2 – Acerra-Afragola*

1180 The Acerra and Afragola territories (about 12 km from Somma-Vesuvius) are located north and north-
 1181 west of Vesuvius, and are almost flat areas crossed by the Clanis river. Both the coarse fallout deposits
 1182 of the Pollena and 1631 eruptions are absent in this area. Here, only a thin, centimetric ash bed
 1183 overlies the Late Roman paleosoil. This fine ash bed, which we correlate with the final
 1184 phreatomagmatic phases of the Pollena eruption, is homogeneous, cohesive and mantles the ground
 1185 without any significant lateral variation. The overlying deposit is characterized by high thickness
 1186 variations, it is generally massive and contains vesicles from circular to flattened and coated by fine
 1187 ash. It has a matrix-supported texture and is composed of fine to very fine, very cohesive ash, and
 1188 contains scattered and more or less abundant pumice and lithic fragments (lithofacies mM) and

1189 remains of vegetation (Barone et al., 2023). From one to three depositional units have been
1190 recognized, marked by unconformities, and differences in grain-size or color. The uppermost unit
1191 always contains white pumice fragments of the Avellino eruption. Very common are drying out
1192 structures and water escape structures, which are vertical structures (Fig. C5)-looking like fractures
1193 a few cm large, filled by finer material transported by the escaping water, formed soon after the
1194 emplacement of the sequence of the syn-eruptive lahars (Fig. C5). The maximum thickness recorded
1195 in this area is about 90 cm.



1196
1197 Fig. C5. Acerra (12 km from Somma-Vesuvius). Lahar deposit (unit 2) in Acerra overlaying a cultivated paleosoil (unit
1198 3). The index finger indicates a water escape structure crossing the sequence of lahars. For the description of lithofacies
1199 see Tab. 2.

1200

1201 The top is almost always horizontal due to the erosion related to the modern anthropogenic activity,
1202 and only in a few exposures it is capped by a paleosol, with traces of human presence of the Medieval
1203 times and of the deposits of the 1631 eruption as well. The base of this latter deposit is a cm-thick
1204 fine-ash bed with an internal plane-parallel layering emplaced by fallout. It underlies a massive
1205 deposit with high thickness variations (max 20 cm) at the outcrop scale. It is composed by fine
1206 ash, cohesive and vesiculated and contains scattered small pumice fragments (lithofacies mM). The
1207 pumice fragments are vesicular, dark gray to blackish, highly porphyritic with leucite, pyroxene and
1208 feldspar crystals. The stratigraphic position and lithology confirm their attribution to the 1631 primary
1209 and secondary (lahars) deposits.

1210

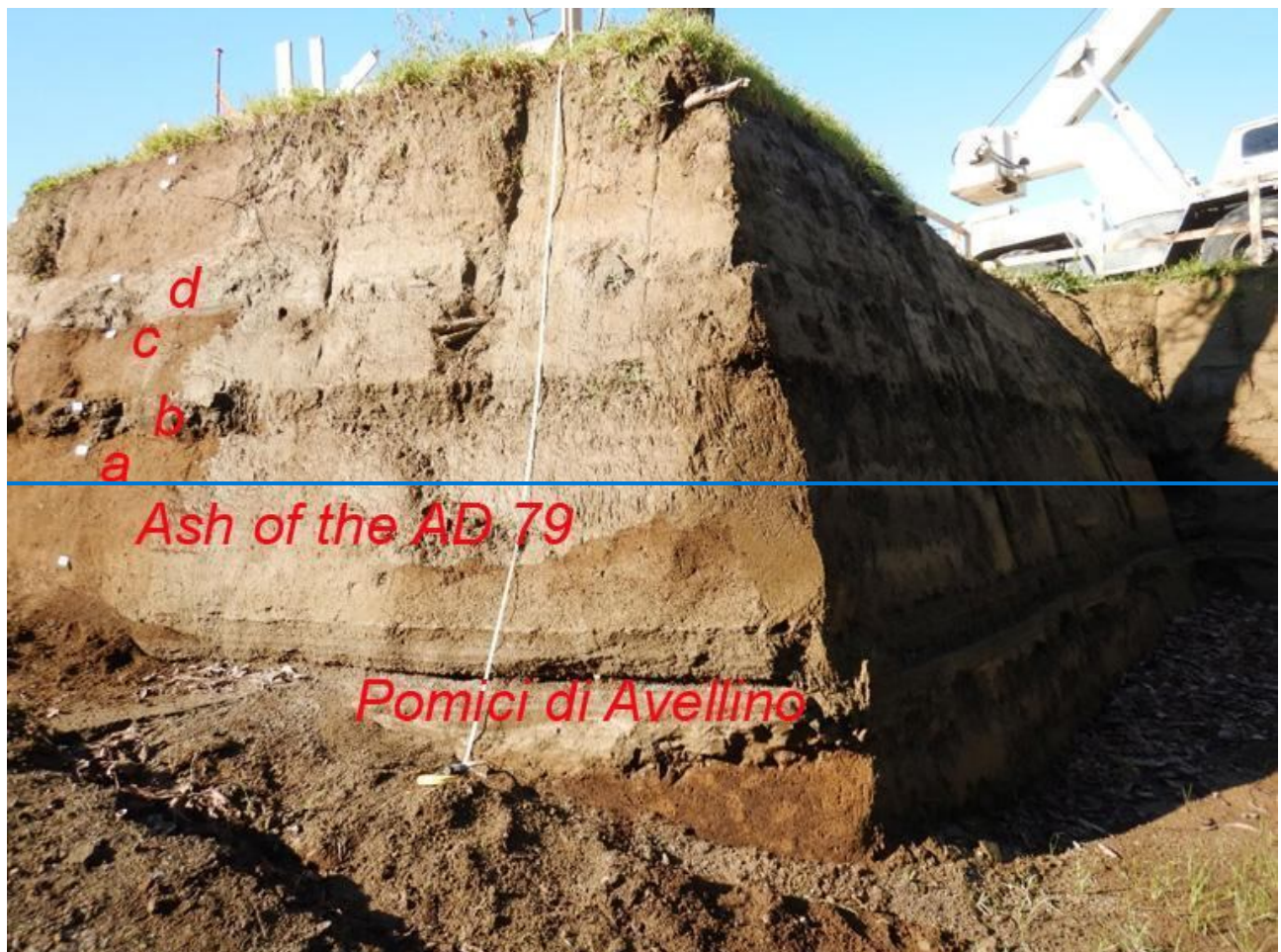
1211 *Area 3 – Pomigliano-Marigliano*

1212 This area is located along the northern outer part of the Vesuvius apron (Santacroce et al., 2003). The
1213 studied sequences start from the paleosol developed on top of the ash deposits of the AD 79
1214 eruption. The paleosol is mature and contains pottery fragments till the II century AD. Its top is
1215 undulated with traces of ploughing spaced about 50 cm (a in Fig. C6). Representative sequences of
1216 the area include a basal ash layer with a thickness ranging from 1 to 4 cm (b in Fig. C7), thickening
1217 in the depressions, cohesive and locally vesiculated. It is here interpreted as co-ignimbritic ash
1218 emplaced by fallout during the phreatomagmatic final phases of the Pollena eruption. Upwardly, the
1219 sequence includes several lahar units from massive to slightly stratified, composed by fine and
1220 very cohesive ash, and containing scattered greenish pumice fragments (lithofacies mM) (b1 in Fig.
1221 C7). Locally this deposit, also in the case of multiple units, is cut by vertical drying cracks. The
1222 sequence is overlain by a 25-30 cm thick mature paleosol, containing cultivation traces and majolica
1223 fragments (c in Figs. C6 and C7).

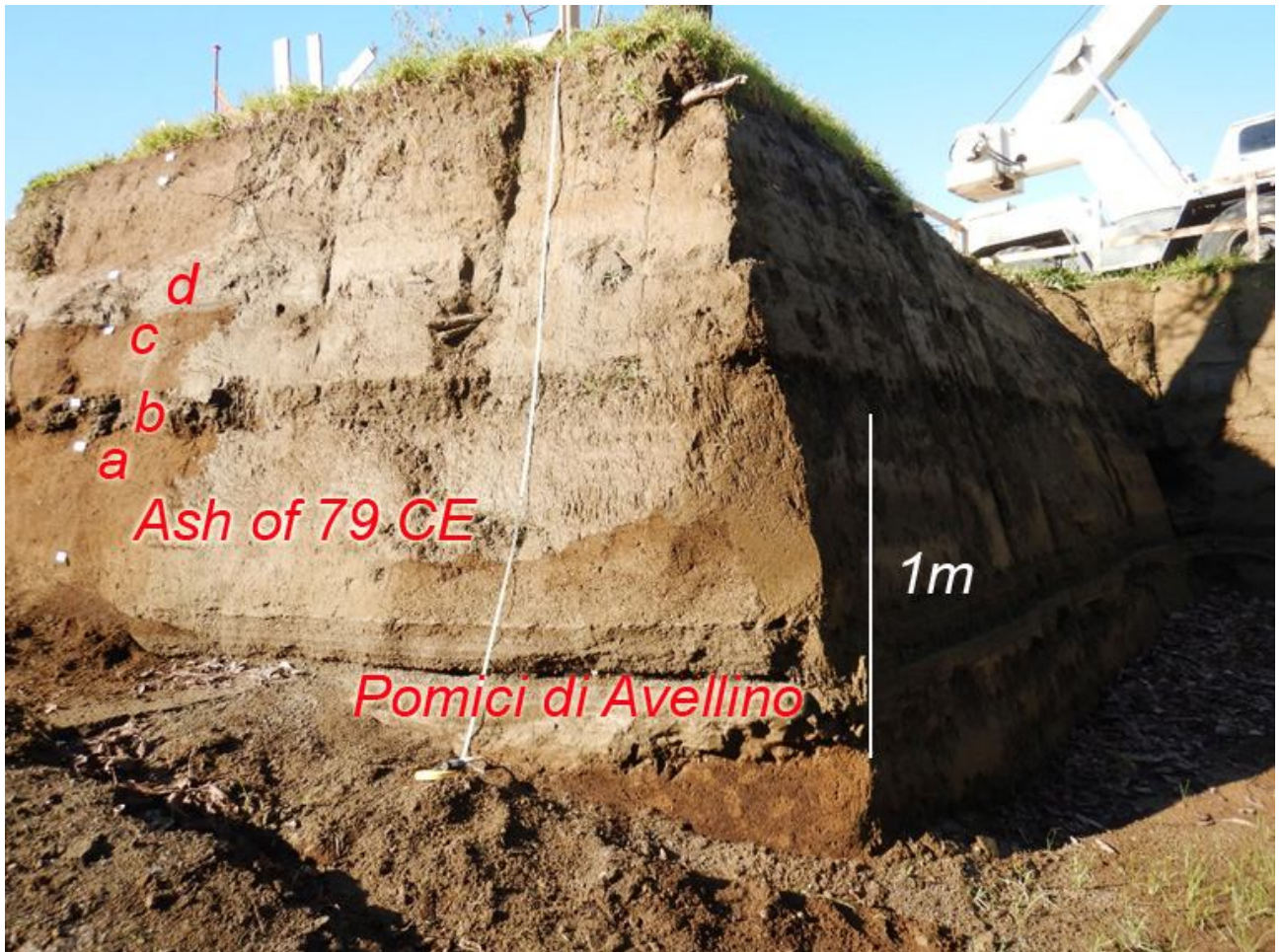
1224 The top of this paleosol is undulated and covered by the primary deposit of the 1631 eruption (d in
1225 Fig. C7). This latter is represented by a discontinuous medium-to-fine ash layer, slightly laminated
1226 for contrasting grain-size, up to 5 cm thick, with a gray to violet color, and containing dark pumice

1227 fragments and loose crystals of leucite, pyroxene and biotite (Fig. C7). Its thickness variation is due
1228 both to slight internal variations (thickening in correspondence of depressions) and erosion by the
1229 following lahars. These latter are composed of one to three flow units (d1 in Fig. C7), with a
1230 cumulative total thickness varying from 10 to 45 cm. They are composed of massive fine and very
1231 cohesive ash, and contain rare scattered dark pumice fragments similar to those of the 1631 eruption
1232 (lithofacies mM). These sequences are overlain by recent, cultivated soil. Locally, thin ash beds of
1233 the recent Vesuvius activity (like 1822, 1906) overlie the 1631 deposits.

1234



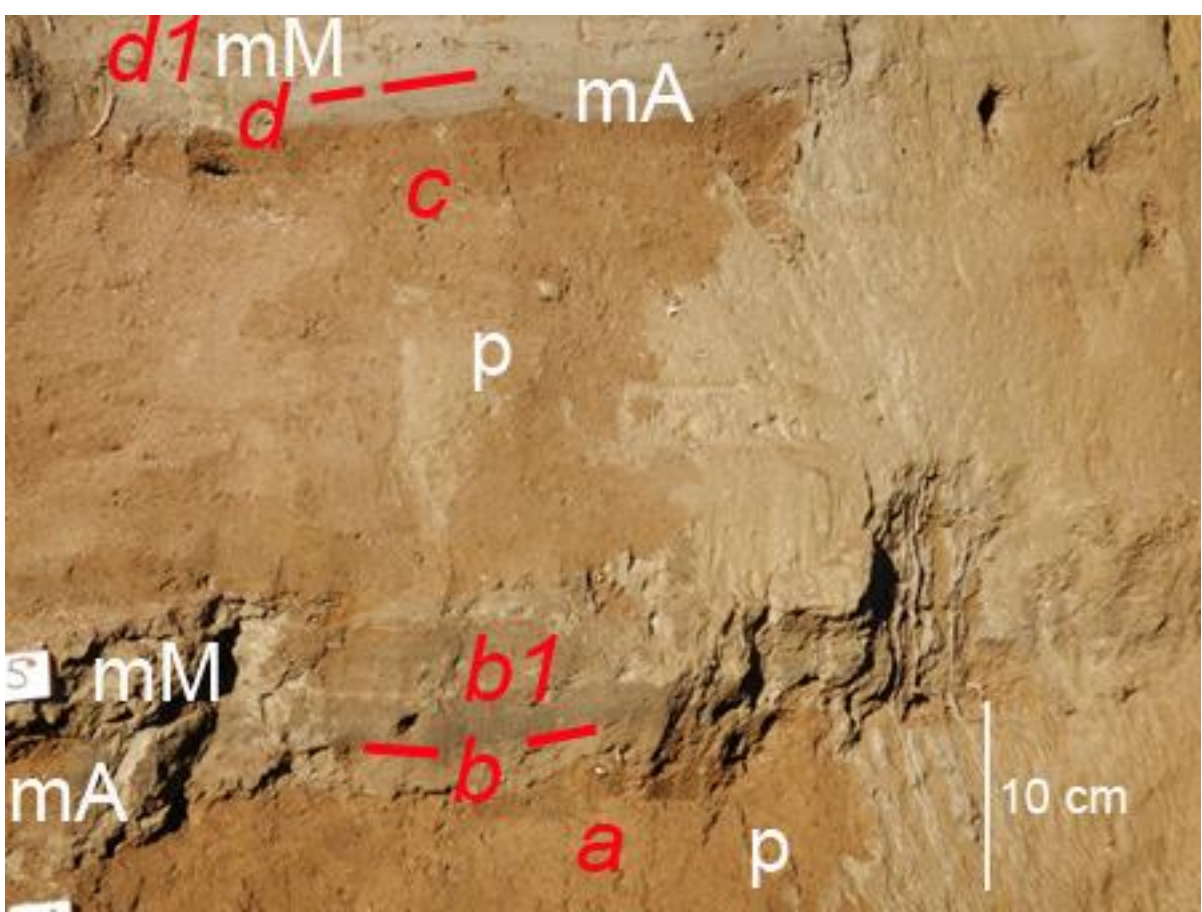
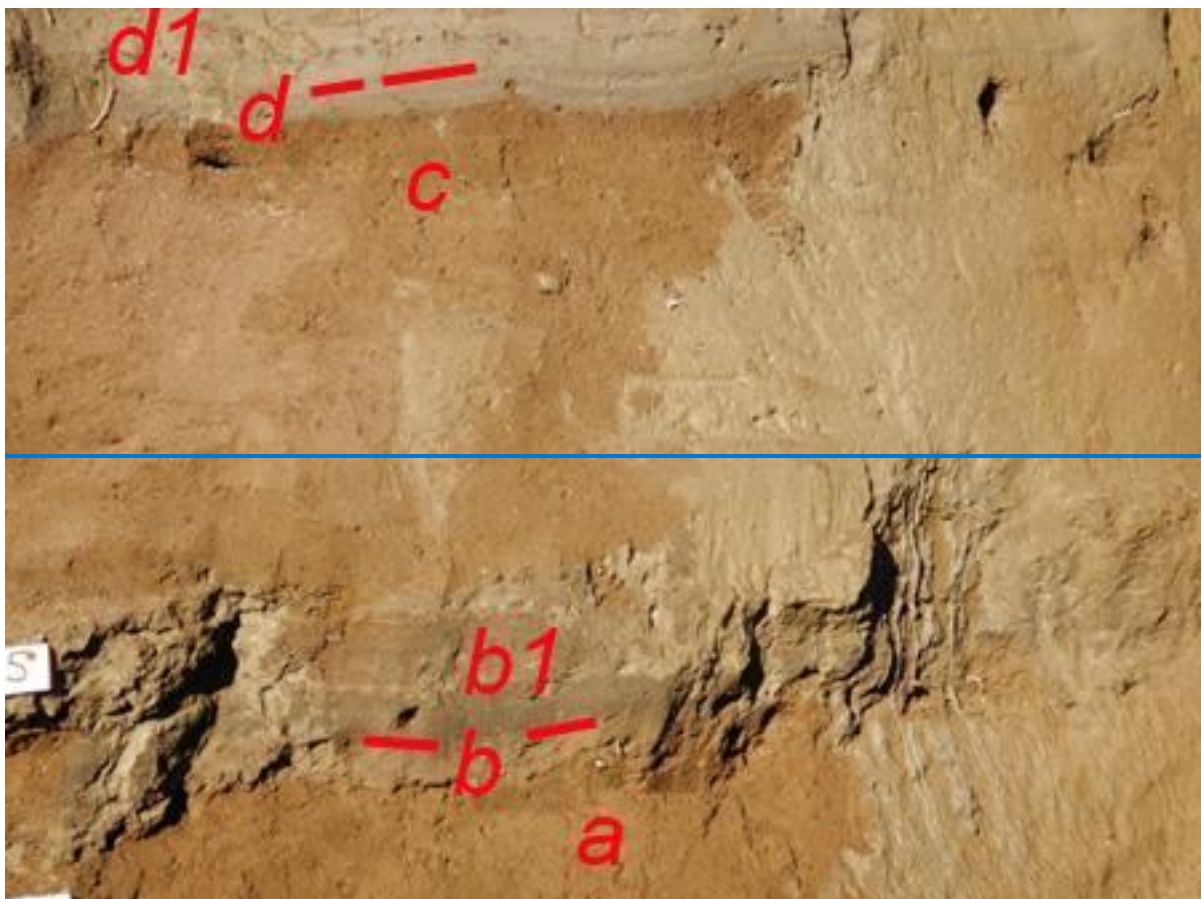
1235



1236

1237 Fig. C6. Pomigliano [locality](#). [S](#) sequence of deposits including bottom to top: Bronze Age paleosoil, Pomici di Avellino
1238 (unit EU 5 of Di Vito et al., 2009), paleosoil developed on top of Pomici di Avellino and buried by the Pollena eruption
1239 deposits. In the central part, fine ash deposits of the 79 CE eruption are visible. The top of the paleosoil is undulated and
1240 ploughed. [In particular: a = paleosol of Roman Age; a,b = primary and secondary deposits of the Pollena eruption; c =](#)
1241 [paleosoil between Pollena and 1631 deposits; d = 1631 primary and secondary deposits.](#) [Further details in Fig. C7.](#)

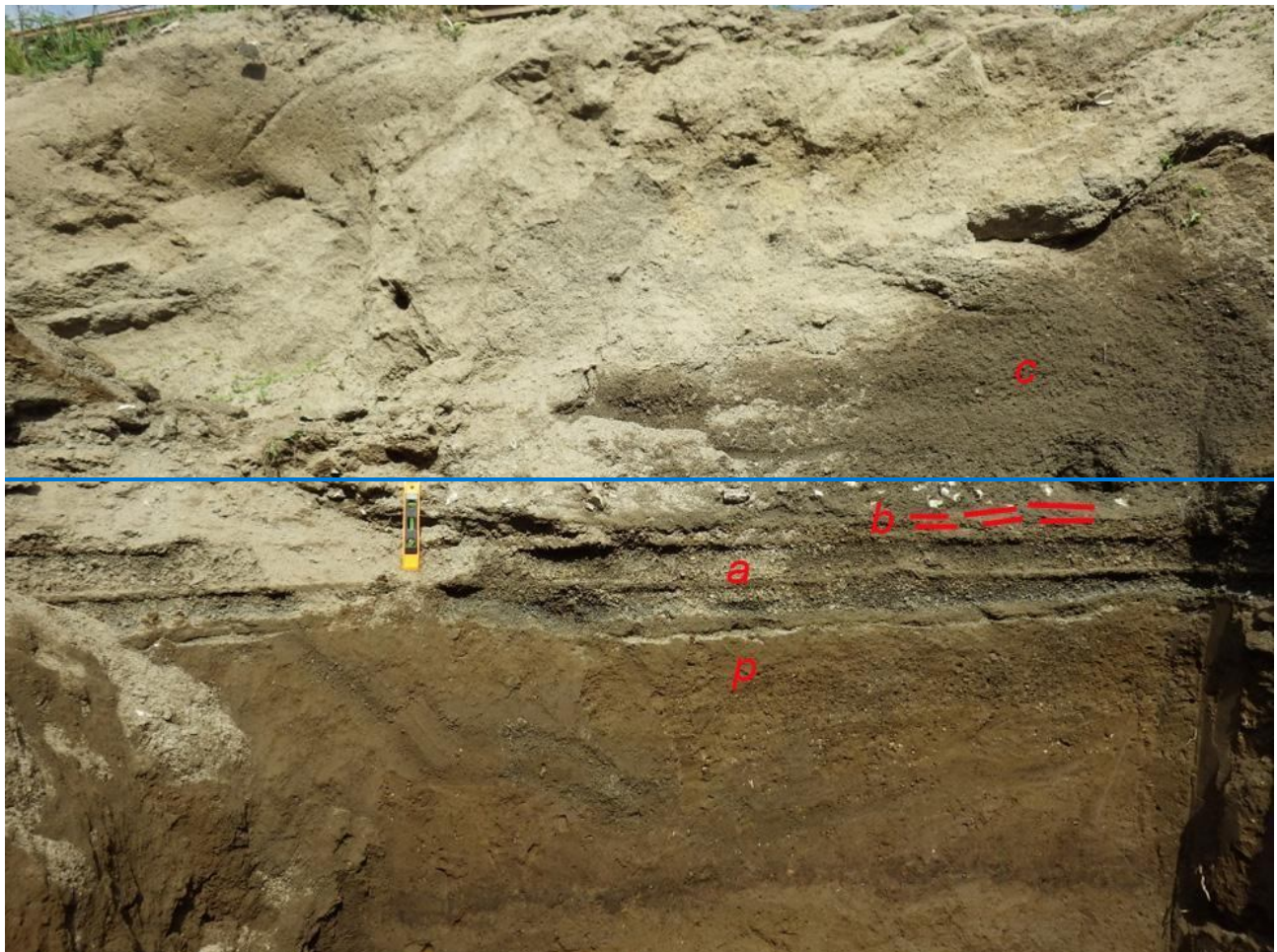
1242

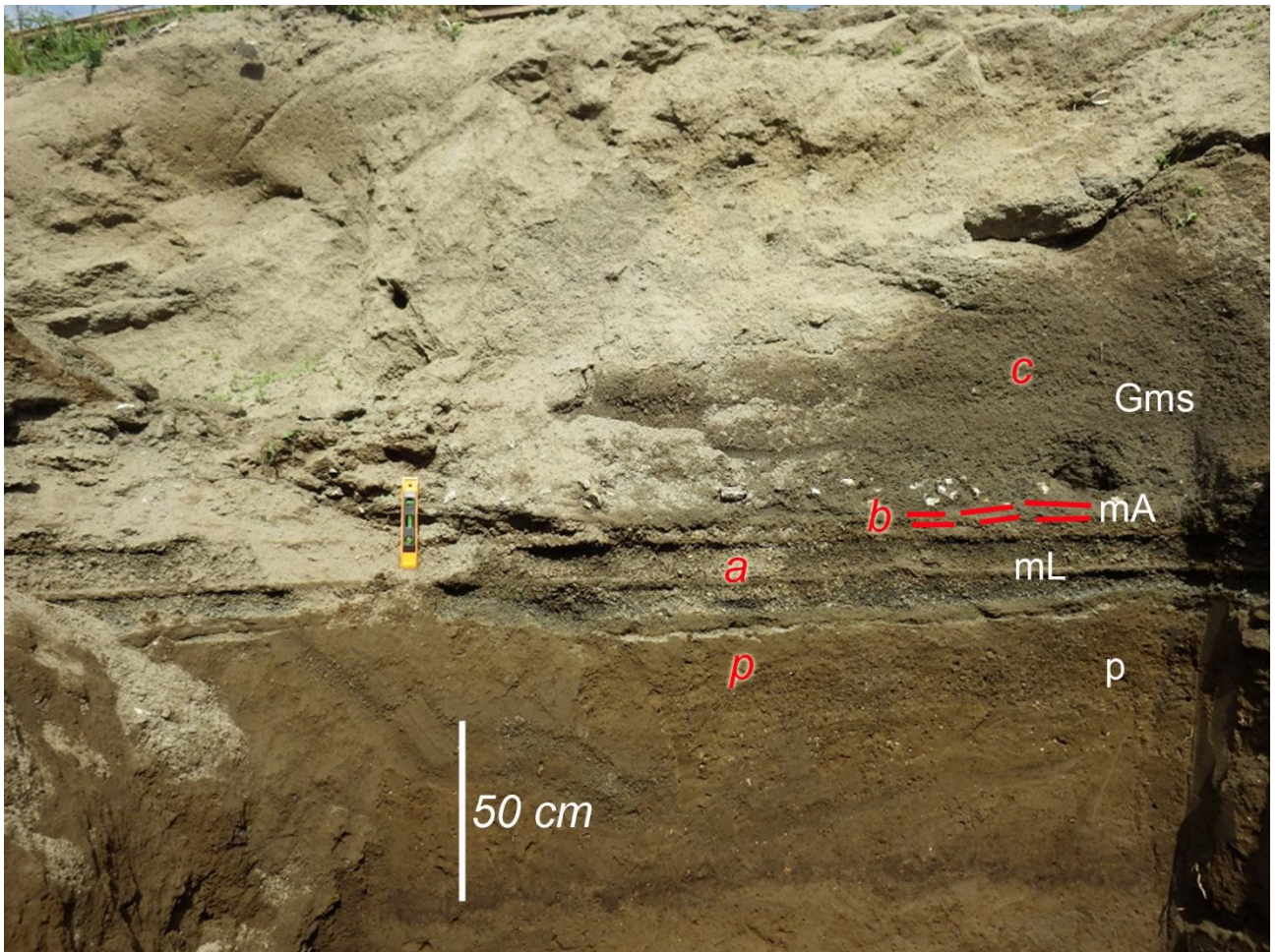


1245 Fig. C7. Pomigliano, particular of the Fig. C6: a paleosol containing potteries of the II Cent. AD; b ash deposit
1246 of the Pollena eruption; b1 syn-eruptive lahar of the Pollena eruption; c paleosol between Pollena and 1631; d
1247 primary deposits of the 1631 eruption; overlain by syn-eruptive lahar (d1). For the description of lithofacies see Tab. 2.
1248

1249 *Area 4 – Avella-Baiano Valley*

1250 We have analyzed several sequences along the *Avella-Baiano Valley*, both exposed and excavated
1251 for the present work. Here the sequences of primary deposits are often affected by deep erosion, in
1252 fact, in some places the Pollena primary deposits are completely lacking and only the syn-eruptive
1253 lahar deposits are present on top of the late Roman paleosol. Where preserved, the paleosol has often
1254 an undulated surface due to cultivation (ploughing and hoeing). The Pollena eruption sequence
1255 consists of an alternation of coarse pumice and fine ash layers emplaced by fallout (a in Fig. C8). It
1256 is up to 50 cm thick and ends with a cohesive yellowish ash layer (b in Fig. C8), overlain by the lahar
1257 deposits, generally composed by of 2-3 flow units (c in Fig. C8). The total thickness of the lahars is
1258 largely variable with maxima at the base of the slopes where it can reach 2-3 m. In some excavations
1259 we did not reach the base of the deposit, deeper than 3.5 m. In Fig. C8, it is possible to observe a
1260 complete sequence of the Pollena deposits of Pollena overlying a late Roman paleosol. The sequence
1261 includes the fallout layers and thick lahar deposits. These latter are always massive, matrix-supported,
1262 and contain abundant scattered pumice and lithic fragments (lithofacies Gms). In some cases, the
1263 lower part contains several limestone fragments up to 10 cm in diameter. The described deposit has
1264 been also found in the Roman Amphitheatre of Avella, where it has a variable thickness (order of
1265 decimetric). Here, it has been almost all excavated and only remnants are presently exposed.
1266 Generally, the upper part of the sequences is composed by of an alternation of plane-parallel to cross-
1267 layered sands and gravels, with abundant rounded limestone fragments, emplaced by several alluvial
1268 episodes (post-eruptive) (lithofacies Sh-Ss). In these post-eruptive deposits, it is not uncommon to
1269 find terracotta fragments from the Imperial Roman age.



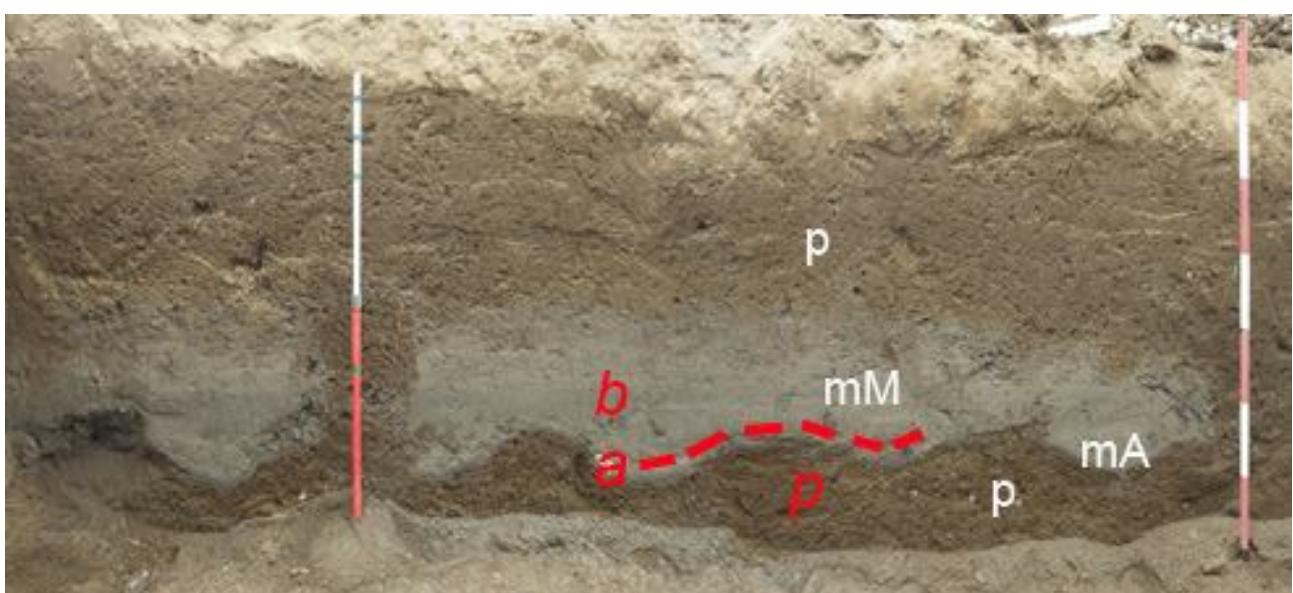
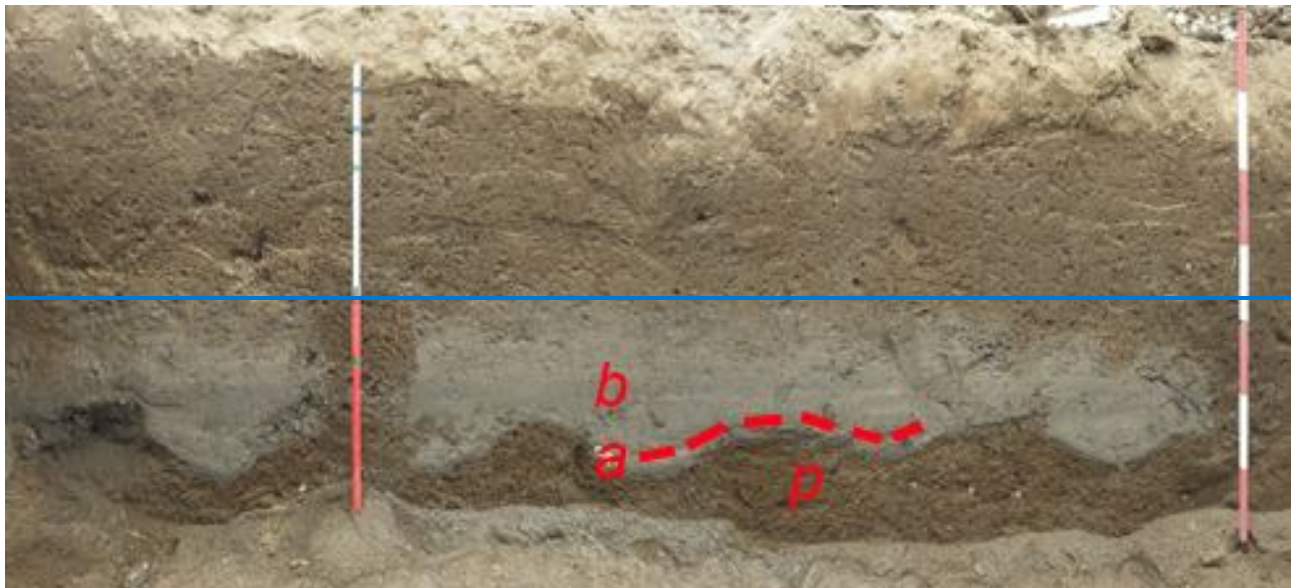


1271

1272 Fig. C8. Avella-Baiano Valley [Avella valley](#). [T](#)he Pollena primary deposit (a,b) lies on a ploughed soil (p) and ~~is~~ is
1273 covered by at least three flow units of lahars [\(c\)](#). [For the description of lithofacies see Tab. 2.](#)

1274

1275 The Pollena primary and secondary sequences are overlain by a mature paleosol with frequent
1276 evidence of cultivation (ploughing, p in Fig. C9) and locally by the 1631 eruption deposits. The
1277 primary deposit related to the 1631 eruption is not always present. It is up to 2 cm (a in Fig. C9) thick
1278 ash layer, gray-violet in color deposited by fallout deposit and overlaying a ploughed paleosol (p in
1279 Fig. C9). It is overlain by lahar deposits (b in Fig. C9) composed [by of](#) several units and characterized
1280 by contrasting grain-sizes. The deposits are composed of medium ash, are massive and matrix-
1281 supported, and contain abundant scattered mm- to cm-sized pumice fragments (all with the same
1282 lithology of the primary deposits) and sometimes vegetal remain traces (lithofacies Gms).



1285 Fig. C9. Avella-Baiano Valley [Avella valley](#),¹² particular of the 1631 primary (a) and secondary deposits (b, syn-eruptive
1286 lahars) in a trench at Ciccianno locality. [For the description of lithofacies see Tab. 2.](#)

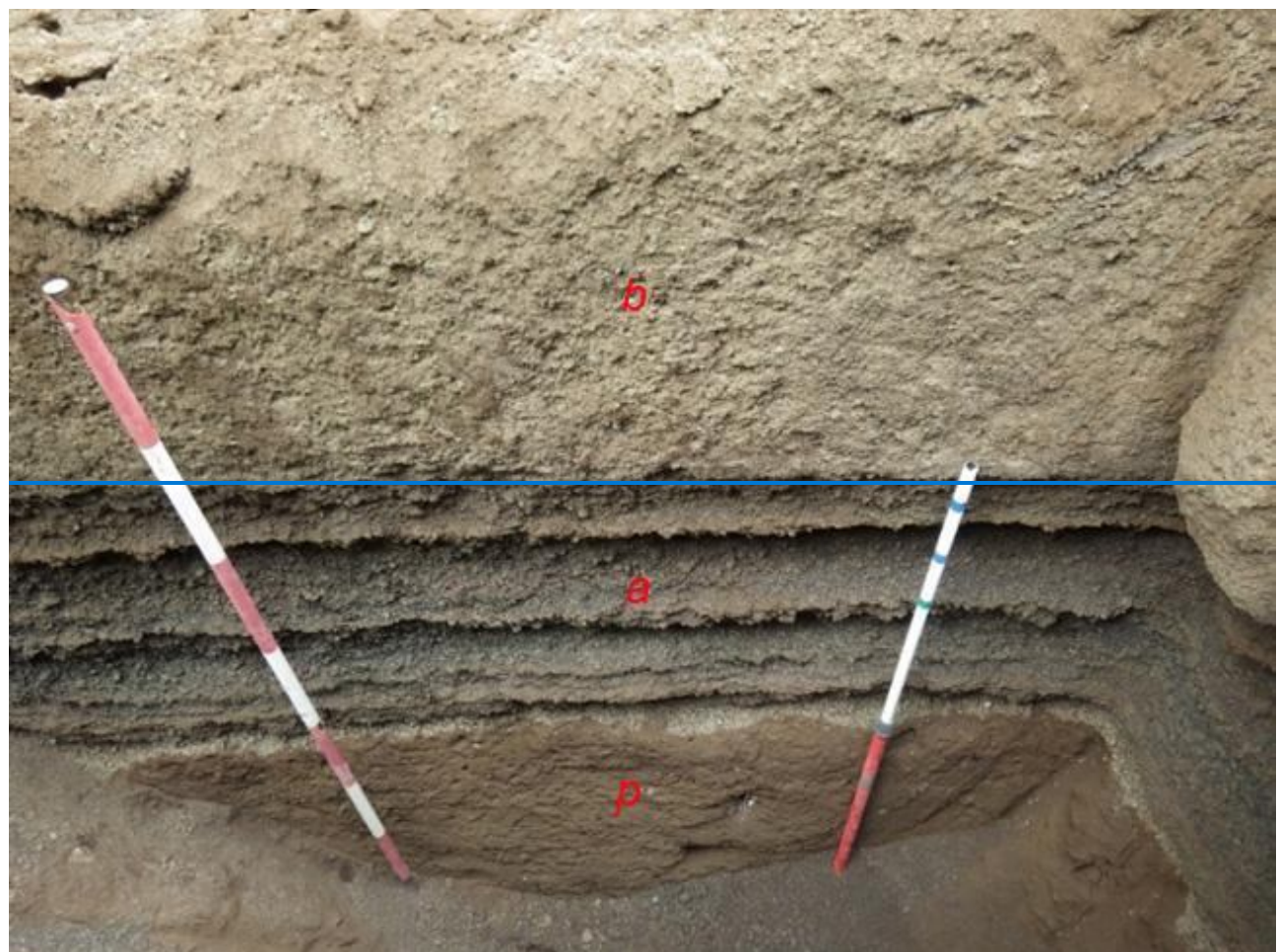
1287

1288 *Area 5 – Lauro Valley [Vallo di Lauro](#)*

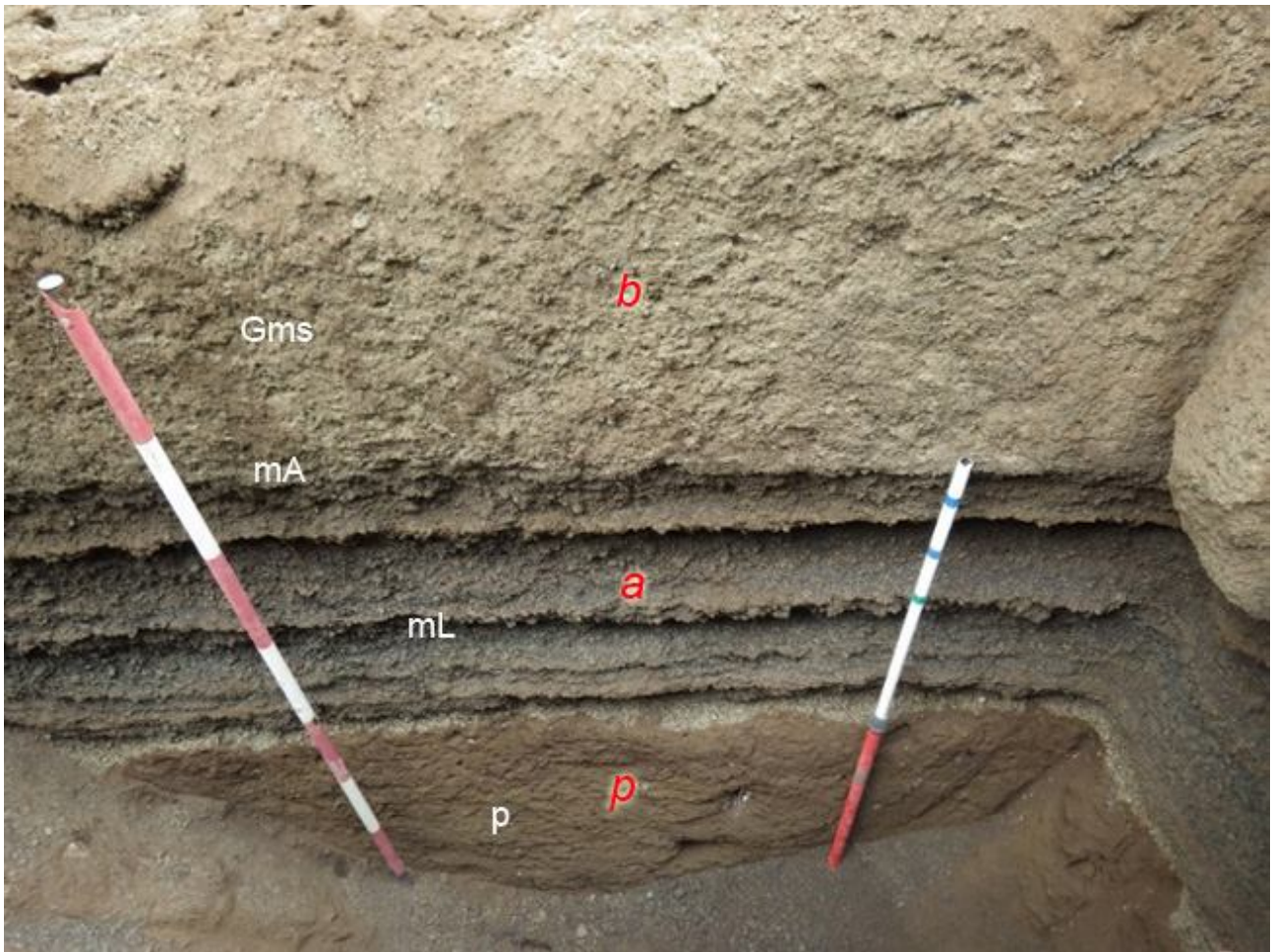
1289 Lauro Valley [Vallo di Lauro](#) has characteristics similar to the Avella-Baiano Valley [Avella valley](#), but
1290 the primary deposits of Pollena and 1631 eruptions are thicker (Figs. 5 and 6) and coarser. In this
1291 valley,¹² also the sequences are locally deeply eroded. In fact, the deposits of the Pollena eruption
1292 (normally 50-70 cm thick) (Fig. C10) are sometimes missing. They overlie a mature paleosoil with
1293 abundant traces of cultivation. Overall, the characteristics of the deposits are very similar to the ones

1294 of the Nola area ([10-15 km from Apennine source valleys](#)). The overlying lahar deposits are always
1295 massive, matrix-supported, and composed of fine and very cohesive ash with abundant scattered
1296 pumices and lithic fragments (similar in lithology to those of the primary deposits) (lithofacies Gms).
1297 These deposits have a high variable thickness, with a measured maximum ~~up to~~ 2 m, but sometimes
1298 reduced by erosion. In some trenches the base of the sequences was deeper than the investigated depth
1299 (>3.5 m).

1300



1301



1302

1303 Fig. C10. Lauro valley, Pago del Lauro ValleyValloVallo di Lauro, in particular: a = sSequence of the Pollena fallout
 1304 deposits (a) overlain by syn-eruptive lahars (b); p = At the base the late Roman paleosoil at the base (p). For the
 1305 description of lithofacies see Tab. 2.

1306

1307 It is possible to evaluate the effects of the lahars on building in the Roman Villa di Lauro, at Taurano,
 1308 where a 70 cm thick fallout is overlain, without paleosoil, by syn-eruptive lahars which engulfed and
 1309 transported pieces of walls, bricks and potteries. The lahar deposits are matrix supported and
 1310 composed by of fine to coarse ash and contain abundant pumice lapilli (all similar to the Pollena
 1311 fallout deposits). They are massive, cohesive and have a thickness up to about 1 m, thickening in
 1312 depressions and near barriers (Fig. C11).

1313 The sequence related to the eruption of 1631 is not always present, but it is possible to find its primary
 1314 deposit, composed by of a basal layer of stratified fine and medium thin ash beds, and minor dark

1315 pumice and lithic fragments overlain by a thin, very fine and cohesive accretionary lapilli-rich ash
1316 bed. The maximum measured thickness is 30 cm. The overlying lahar deposits are massive and
1317 matrix-supported, composed of fine to coarse ash and contain abundant pumice fragments of the
1318 primary deposit.



1319

1320 Fig. C11. Taurano (Villa Lauro), baulk showing a thick sequence of [the Pollena syn-eruptive](#) lahar units filling the Roman
1321 Villa. Some units engulf and transport pieces of walls and large blocks. [The fallout sequence is not exposed in the Villa,](#)
1322 [likely due to the presence of a roof. The deposit below the damaged walls is composed of multiple lahar units represented](#)
1323 [by the Gms lithofacies \(see Tab. 2\).](#)

1324

1325 **Author contribution**

1326 MDV: conceptualization, investigation, methodology, writing - original draft preparation, writing -
1327 review & editing, funding acquisition; IR: data curation, investigation, writing - original draft
1328 preparation; SdV: investigation, writing - original draft preparation, writing - review & editing; DMD:

1329 investigation, methodology, data curation, writing - original draft preparation, writing - review &
1330 editing; MB: data curation, methodology, writing - original draft preparation; MdMV: writing -
1331 review & editing; MR: conceptualization, writing - review & editing; LS: writing - review & editing;
1332 GZ: investigation, writing - review & editing; EZ: investigation, methodology, writing - original draft
1333 preparation; AC: conceptualization, writing - review & editing, funding acquisition.

1334

1335 **Acknowledgements**

1336 This work benefited of the agreement between Istituto Nazionale di Geofisica e Vulcanologia and the
1337 Italian Presidenza del Consiglio dei Ministri, Dipartimento della Protezione Civile (DPC),
1338 Convenzione INGV-DPC All. B2. The work was also supported by the INGV project Pianeta
1339 Dinamico—Working Earth (CUP 1466 D53J19000170001—“Fondo finalizzato al rilancio degli
1340 investimenti delle 1467 amministrazioni centrali dello Stato e allo sviluppo del Paese”, legge
1341 145/2018)—Task V3 (MDV). The paper does not necessarily represent DPC official opinion and
1342 policies. We thank very much Ulrich Kueppers, Lucia Capra, an anonymous reviewer and the editor
1343 Andrea Di Muro for their help in improving this manuscript in the revision process.

1344

1345 **References**

1346 Acocella V and Funiciello R (2006) Transverse systems along the extensional Tyrrhenian margin of
1347 Central Italy and their influence on volcanism. *Tectonics* 25,1-24.

1348 Arguden AT and Rodolfo KS (1990) Sedimentologic and dynamic differences between hot and cold
1349 laharic debris flows of Mayon Volcano, Philippines. *Geological Society of America Bulletin* 102,
1350 865-876.

1351 Bardot L (2000) Emplacement temperature determinations of proximal pyroclastic deposits on
1352 Santorini, Greece, and their implications. *Bulletin of Volcanology* 61, 450-467.

- 1353 Bardot L, McClelland E (2000) The reliability of emplacement temperature estimates using
1354 paleomagnetic methods: a case study from Santorini, Greece. *Geophysical Journal International* 143,
1355 39-51.
- 1356 Bartole R (1984) Tectonic Structure of the Latian-Campanian Shelf (Tyrrhenian Sea). *Bollettino di*
1357 *Oceanologia Teorica Applicata* 2, 197-230.
- 1358 Baumann V, Bonadonna C, Cuomo S, Moscariello M (2020) Modelling of erosion processes
1359 associated with rainfall-triggered lahars following the 2011 Cordon Caulle eruption (Chile). Journal
1360 of Volcanology and Geothermal Research 390, 106727.
- 1361 Bisson M, Pareschi MT, Zanchetta G, Sulpizio R, Santacroce R (2007) Volcaniclastic debris-flow
1362 occurrences in the Campania region (Southern Italy) and their relation to Holocene–Late Pleistocene
1363 pyroclastic fall deposits: implications for large-scale hazard mapping. *Bulletin of Volcanology* 70,
1364 157-167.
- 1365 Bisson M, Spinetti C, Sulpizio R (2014) Volcaniclastic flow hazard zonation in the Sub-Appennine
1366 Vesuvian area using GIS and remote sensing. *Geosphere* 10, 1419-1431.
- 1367 Bisson M, Zanchetta G, Sulpizio R, Demi F (2013) A map for volcaniclastic debris flow hazards in
1368 Apennine areas surrounding the Vesuvius volcano (Italy). *Journal of Maps* 9, 230-238.
- 1369 Blott SJ and Pye K (2001) Gradistat: A Grain Size Distribution and Statistics Package for the Analysis
1370 of Unconsolidated Sediments. *Earth Surface Processes and Landforms* 26, 1237-1248.
- 1371 Braccini GC (1632) Dell'Incendio Fattosi nel Vesuvio a XVI di Dicembre MDCXXXI. Secondino
1372 Roncagliolo, 104 pp.
- 1373 Brancaccio L, Cinque A, Romano P, Rosskopf C, Russo F, Santangelo N, Santo A (1991)
1374 Geomorphology and neotectonic evolution of a sector of the Tyrrhenian flank of the Southern
1375 Apennines (Region of Naples, Italy). *Zeitschrift für Geomorphologie Supplement Bd.* 82, 47-58.

- 1376 Breard ECP, Lube G, Cronin SJ, Valentine GA (2015) Transport and deposition processes of the
1377 hydrothermal blast of the 6 August 2012 Te Maari eruption, Mt. Tongariro. *Bulletin of Volcanology*
1378 77, 100.
- 1379 [Breard ECP, Lube G \(2017\) Inside pyroclastic density currents – uncovering the enigmatic flow](#)
1380 [structure and transport behaviour in large-scale experiments. Earth and Planetary Science Letters 458,](#)
1381 [22-36.](#)
- 1382 Brocchini D, Principe C, Castradori D, Laurenzi MA, Gorla L (2001) Quaternary evolution of the
1383 southern sector of the Campanian Plain and early Somma-Vesuvius activity: insights from the Trecase
1384 1 well. *Mineralogy and Petrology* 73, 67-91.
- 1385 [Capra L, Sulpizio R, Marquez-Ramirez VH, Covello V, Doronzo DM, Arambula-Mendoza R, Cruz](#)
1386 [S \(2018\) The anatomy of a pyroclastic density current: the 10 July 2015 event at Volcan de Colima](#)
1387 [\(Mexico\). Bulletin of Volcanology](#) 80, 34.
- 1388 Carling PA (2013) Freshwater megaflood sedimentation: What can we learn about generic processes?
1389 *Earth-Science Reviews* 125, 87-113.
- 1390 Carrara E, Iacobucci F, Pinna E, Rapolla A (1973) Gravity and magnetic survey of the Campanian
1391 volcanic area, S. Italy. *Bollettino di Geofisica Teorica e Applicata* 15, 39-51.
- 1392 Cas RAF, Wright HMN, Folkes CB, Lesti C, Porreca M, Giordano G, Viramonte JG (2011) The flow
1393 dynamics of an extremely large volume pyroclastic flow, the 2.08-Ma Cerro Galán Ignimbrite, NW
1394 Argentina, and comparison with other flow types. *Bulletin of Volcanology* 73, 1583-1609.
- 1395 Cinque A and Robustelli G (2009) Alluvial and coastal hazards caused by long-range effects of
1396 Plinian eruptions: The case of the Lattari Mts. After the AD 79 eruption of Vesuvius. *Geological*
1397 *Society London Special Publications* 322, 155-171.

- 1398 [Cioni R, Santacroce R, Sbrana A \(1999\) Pyroclastic deposits as a guide for reconstructing the multi-](#)
- 1399 [stage evolution of the Somma-Vesuvius Caldera. Bulletin of Volcanology 60, 207-222.](#)
- 1400 Cioni R, Gurioli L, Lanza R, Zanella, E (2004) Temperatures of A.D. 79 pyroclastic density current
- 1401 deposits (Vesuvius, Italy). *Journal of Geophysical Research* 109, B02207.
- 1402 Costa JE (1997) Hydraulic modeling for lahar hazards at Cascades volcanoes. *Environmental*
- 1403 *Engineering Geoscience* 3, 21-30.
- 1404 D'Argenio B, Pescatore TS, Scandone P (1973) Schema geologico dell'Appennino meridionale
- 1405 (Campania e Lucania). In: *Moderne vedute sulla geologia dell'Appennino. Convegno (Roma, 16-18*
- 1406 *Febbraio 1972). Accademia Nazionale dei Lincei, Problemi Attuali di Scienza e Cultura, Quaderni*
- 1407 183, 49-72.
- 1408 [De Falco M, Forte G, Marino E, Massaro L, Santo A \(2023\) UAV and field survey observations on](#)
- 1409 [the November 26th 2022 Celario flowslide, Ischia Island \(Southern Italy\). Journal of Maps 19,](#)
- 1410 [2261484.](#)
- 1411 de' Michieli Vitturi M, Costa A, Di Vito MA, Sandri L, Doronzo DM ([submittedthis issue](#)). Lahar
- 1412 events in the last 2,000 years from Vesuvius eruptions. Part 2: Formulation and validation of a
- 1413 computational model based on a shallow layer approach.
- 1414 De Simone GF, Perrotta A, Scarpati C (2011) L'eruzione del 472 d.C. ed il suo impatto su alcuni siti
- 1415 alle falde del Vesuvio. *Rivista Studi Pompeiani* 22, 61.71.
- 1416 De Vivo B, Rolandi G, Gans PB, Calvert A, Bohrson WA, Spera FJ, Belkin HE (2001) New
- 1417 constraints on the pyroclastic eruptive history of the Campanian volcanic Plain (Italy). *Mineralogy*
- 1418 and *Petrology* 73, 47-65.
- 1419 Di Crescenzo G and Santo A (2005) Nuovo contributo sul ruolo svolto dai livelli pomicei nelle aree
- 1420 di distacco delle frane di colata rapida dei massicci carbonatici campani. *Convegno Nazionale La*

- 1421 mitigazione del rischio da colate di fango a Sarno e negli altri Comuni colpiti dagli eventi del maggio
1422 1998. Napoli, 2 e 3 maggio 2005 - Sarno 4 e 5 maggio 2005.
- 1423 Di Vito MA, Castaldo N, de Vita S, Bishop J, Vecchio G (2013) Human colonization and volcanic
1424 activity in the eastern Campania Plain (Italy) between the Eneolithic and Late Roman periods.
1425 Quaternary International 303, 132-141
- 1426 Di Vito M.A., Calcaterra D., Petrosino P., Zanchetta G., De Vita S., Marotta E., Cesarano M. , De
1427 Simone A., Sansivero F., Rucco I. (2019) Landslides, volcanism and volcano-tectonics: the fragility
1428 of the Neapolitan territory. Geol. F. Trips Maps, Volume 11 (1.1)/2019.
1429 <https://doi.org/10.3301/GFT.2019.01> - pp 1-53.
- 1430 Di Vito MA, Sulpizio R., Zanchetta G (1998). I depositi ghiaiosi della valle dei torrenti Clanio e
1431 Acqualonga (Campania centro-orientale): significato stratigrafico e ricostruzione paleoambientale. Il
1432 Quaternario Italian Journal of Quaternary Sciences 11, 273-286.
- 1433 Di Vito MA, Talamo P, de Vita S, Rucco I, Zanchetta G, Cesarano M (2019) Dynamics and effects
1434 of the Vesuvius Pomice di Avellino Plinian eruption and related phenomena on the Bronze Age
1435 landscape of Campania region (Southern Italy). Quaternary International 499, 231-244.
- 1436 Di Vito M, Zanella E, Gurioli L, Lanza R, Sulpizio R, Bishop J, Tema E, Boenzi G, Laforgia E (2009)
1437 The Afragola settlement near Vesuvius, Italy: The destruction and abandonment of a Bronze Age
1438 village revealed by archeology, volcanology and rock-magnetism. Earth and Planetary Science
1439 Letters 277, 408-421.
- 1440 Doronzo DM (2012) Two new end members of pyroclastic density currents: Forced-convection
1441 dominated and inertia-dominated. Journal of Volcanology and Geothermal Research 219-220, 87-91.
- 1442 Doronzo DM, Martí J, Sulpizio R, Dellino P (2012) Aerodynamics of stratovolcanoes during
1443 multiphase processes. Journal of Geophysical Research 117, B01207.

- 1444 Doronzo DM, Dellino P (2013) Hydraulics of subaqueous ash flows as deduced from their deposits:
1445 2. Water entrainment, sedimentation, and deposition, with implications on pyroclastic density current
1446 deposit emplacement. *Journal of Volcanology and Geothermal Research* 258, 176-186.
- 1447 Doronzo DM (2013) Aeromechanic analysis of pyroclastic density currents past a building. *Bulletin*
1448 *of Volcanology* 75, 684.
- 1449 Duller RA, Mountney NP, Russell AJ, Cassidy NC (2008) Architectural analysis of a volcaniclastic
1450 jökulhlaup deposit, southern Iceland: sedimentary evidence for supercritical flow. *Sedimentology* 55,
1451 939-964.
- 1452 Faccenna C, Funiciello R, Bruni A, Mattei M, Sagnotti L (1994) Evolution of a transfer related basin:
1453 the Ardea basin (Latium, Central Italy). *Basin Resources* 5, 1-11.
- 1454 Fedi M and Rapolla A (1987) The Campanian Volcanic Area: analysis of the magnetic and
1455 gravimetric anomalies. *Bollettino della Società Geologica Italiana* 106, 793-805.
- 1456 Finetti I and Morelli C (1974) Esplorazione di sismica a riflessione nei Golfi di Napoli e Pozzuoli.
1457 *Bollettino di Geofisica Teorica e Applicata* 16, 62-63.
- 1458 Fiorillo F and Wilson RC (2004) Rainfall induced debris flows in pyroclastic deposits, Campania
1459 (southern Italy). *Engineering Geology* 75, 263-289.
- 1460 Giordano G, Zanella E, Trolese M, Baffioni C, Vona A, Caricchi C, De Benedetti AA, Corrado S,
1461 Romano C, Sulpizio R, Geshi N (2018) Thermal interactions of the AD79 Vesuvius pyroclastic
1462 density currents and their deposits at Villa dei Papiri (Herculaneum archaeological site, Italy). *Earth*
1463 and Planetary Science Letters 490, 180-192.
- 1464 Girolami L, Roche O, Druitt T, Corpelli T (2010) Velocity fields and depositional processes in
1465 laboratory ash flows, with implications for the dynamics of dense pyroclastic flows. *Bulletin of*
1466 *Volcanology* 72, 747-759.

- 1467 Gurioli L, Pareschi MT, Zanella E, Lanza R, Deluca E, Bisson M (2005) Interaction of pyroclastic
1468 density currents with human settlements: Evidence from ancient Pompeii. *Geology* 33, 441-444.
- 1469 Gurioli L, Sulpizio R, Cioni R, Sbrana A, Santacroce R, Luperini W, Andronico D (2010) Pyroclastic
1470 flow hazard assessment at Somma-Vesuvius based on the geological record. *Bulletin of Volcanology*
1471 72, 1021-1038.
- 1472 Guzman S, Doronzo DM, Martí J, Seggiaro R (2020). Characteristics and emplacement mechanisms
1473 of the Coranzulí ignimbrites (Central Andes). *Sedimentary Geology* 405, 105699.
- 1474 Ippolito F, Ortolani F, Russo M (1973) Struttura marginale tirrenica dell'Appennino campano:
1475 reinterpretazioni di dati di antiche ricerche di idrocarburi. *Memorie della Società Geologica Italiana*
1476 12, 227–250.
- 1477 Iverson RM, Denlinger RP, LaHusen RG, Logan M, (2000) Two-phase debris-flow across 3-D
1478 terrain: Model predictions, *in* Wieczorek GF and Naeser ND, eds., *Debris-Flow Hazard Mitigation,*
1479 *Mechanics, Prediction, and Assessment*: Taipei, Taiwan, 16-18 August 2000: Rotterdam, Balkema,
1480 521-529.
- 1481 Jenkins SF, Phillips JC, Price R, Feloy K, Baxter PJ, Sri Hadmoko D, de Bélizal E (2015) Developing
1482 building-damage scales for lahars: application to Merapi volcano Indonesia. *Bulletin of Volcanology*
1483 77, 1-17.
- 1484 Lesti C, Porreca M, Giordano G, Mattei M, Cas R, Wright H, Viramonte J (2011) High temperature
1485 emplacement of the Cerro Galán and Toconquis Group ignimbrites (Puna plateau, NW Argentina)
1486 determined by TRM analyses. *Bulletin of Volcanology* 73, 1535-1565.
- 1487 Lowe DR, Williams SN, Leigh H, Connort CB, Gemmell JB, Stoiber RE (1986) Lahars initiated by
1488 the 13 November 1985 eruption of Nevado del Ruiz, Colombia. *Nature* 324, 51-53.

- 1489 Lowe DR (1988) Suspended-load fallout rate as an independent variable in the analysis of current
1490 structures. *Sedimentology* 35, 765–776.
- 1491 Lube G, Cronin S, Manville V, Procter J, Cole S, Freundt A (2012) Energy growth in laharic mass
1492 flows. *Geology* 40, 475-478.
- 1493 Macedonio G and Pareschi MT (1992) Numerical simulation of some lahars from Mount St. Helens.
1494 *Journal of Volcanology and Geothermal Research* 54, 65-80.
- 1495 Manville V, Nemeth K, Kano K (2009) Source to sink: A review of three decades of progress in the
1496 understanding of volcaniclastic processes, deposits, and hazards. *Sedimentary Geology* 220, 136-161.
- 1497 Mariani M and Prato R (1988) I bacini neogenici costieri del margine tirrenico: approccio sismico-
1498 stratigrafico. *Memorie della Società Geologica Italiana* 41, 519-531.
- 1499 Marotta E., Berrino G., de Vita S., Di Vito M.A., Camacho A.G., 2022. Structural setting of the Ischia
1500 resurgent caldera (Southern Tyrrhenian Sea, Italy) by integrated 3D gravity inversion and geological
1501 models. In: Marotta, E., D'Auria, L., Zaniboni, F. and Nave, R. (eds) *Volcanic Island: from Hazard*
1502 *Assessment to Risk Mitigation*. Geological Society, London, Special Publications, 519.
- 1503 Martí J, Doronzo DM, Pedrazzi D, Colombo F (2019) Topographical controls on small-volume
1504 pyroclastic flows. *Sedimentology* 66, 2297-2317.
- 1505 McClelland E, Druitt TH (1989) Paleomagnetic estimates of emplacement temperatures of
1506 pyroclastic deposits on Santorini, Greece. *Bulletin of Volcanology* 51, 16-27.
- 1507 McClelland E (1996) Theory of CRM acquired by grain growth, and its implications for TRM
1508 discrimination and paleointensity determination in igneous rocks. *Geophysical Journal International*
1509 126, 271-280.
- 1510 Newhall CG and Punongbayan R (Eds.) (1996) *Fire and mud: eruptions and lahars of Mount*
1511 *Pinatubo, Philippines*. Quezon City: Philippine Institute of Volcanology and Seismology, 1126 pp.

- 1512 Orsi G, de Vita S, Di Vito MA (1996) The restless, resurgent Campi Flegrei Nested Caldera Italy.:
1513 constraints on its evolution and configuration. *Journal of Volcanology and Geothermal Research* 74,
1514 179-214.
- 1515 Pareschi MT, Favalli M, Giannini F, Sulpizio R, Zanchetta G, Santacroce R (2000) May 5, 1998,
1516 Debris flows in circumvesuvian areas (Southern Italy), insights for hazard assessment. *Geology* 28,
1517 639-642.
- 1518 Pareschi MT, Santacroce R, Sulpizio R, Zanchetta G (2002) The volcaniclastic mass flow hazard
1519 related to the remobilization of fallout deposits in southern Campania, Italy. Explosive volcanism in
1520 subduction zones, Mount Pelée, Martinique, 12-16 May 2002, abstract volume.
- 1521 Patacca E and Scandone P (2007) Geology of the Southern Apennines. *Bollettino della Società
1522 Geologica Italiana* Special Issue 7, 75-119.
- 1523 Paterson, GA, Muxwhorty AR, Roberts AP, MacNiocaill C (2010). Paleomagnetic determination of
1524 emplacement temperatures of pyroclastic deposits: un under-utilized tool. *Bulletin of Volcanology*,
1525 72, 309-330.
- 1526 Peccerillo A (2003) Plio-Quaternary magmatism in Italy. *Episodes* 26, 222-226.
- 1527 Perrotta A, Scarpati C, Luongo G, Aoyagi M (2006) Burial of Emperor Augustus' villa at Somma
1528 Vesuviana (Italy) by post-79 AD Vesuvius eruptions and reworked (lahars and stream flow) deposits.
1529 *Journal of Volcanology and Geothermal Research* 158, 445-466.
- 1530 Pierson TC (1985) Initiation and flow behavior of the 1980 Pine Creek and Muddy River lahars, Mt.
1531 St. Helens, Washington. *Geological Society of America Bulletin* 96, 1056-1069.
- 1532 Piochi M, Pappalardo L, ~~Dea~~ Astis G (2004) Geo-chemical and isotopical variations within the
1533 Campanian Comagmatic Province: implications on magma source composition, *Annals of
1534 Geophysics* 47, 1485-1499.

- 1535 Pittari A, Cas RAF, Monaghan JJ, Martí J (2007) Instantaneous dynamic pressure effects on the
1536 behaviour of lithic boulders in pyroclastic flows: the Abrigo Ignimbrite, Tenerife, Canary Island.
1537 Bulletin of Volcanology 69, 265-279.
- 1538 Porreca M, Mattei M, Mac Niocaill C, Giordano G, McClelland E, Funiciello R (2007) Paleomagnetic
1539 evidence for low-temperature emplacement of the phreatomagmatic Peperino Albano ignimbrite
1540 (Colli Albani volcano, Central Italy). Bulletin of Volcanology 70, 877-893.
- 1541 Roche O (2012) Depositional processes and gas pore pressure in pyroclastic flows: an experimental
1542 perspective. Bulletin of Volcanology 74, 1807-1820.
- 1543 Roche O, Niño Y, Mangeney A, Brand B, Pollock N, Valentine GA (2013) Dynamic pore-pressure
1544 variations induce substrate erosion by pyroclastic flows. Geology 41, 1107-1110.
- 1545 Roche O (2015) Nature and velocity of pyroclastic density currents inferred from models of
1546 entrainment of substrate lithic clasts. Earth and Planetary Science Letters 418, 115-125.
- 1547 Rodolfo KS (2000) The hazard from lahars and jökulhlaups. In: Encyclopedia of Volcanoes:
1548 Academic Press, Philadelphia, 973-995.
- 1549 Rodolfo KS and Arguden AT (1991) Rain-lahar generation and sediment-delivery systems at Mayon
1550 Volcano, Philippines: Sedimentation in Volcanic Settings, SEPM Special Publication 45, 71-87.
- 1551 Rodríguez-Sedano LA, Sarocchi D, Caballero L, Borselli L, Ortiz-Rodríguez AJ, Cerca-Ruiz MF,
1552 Moreno-Chávez G, Franco Ramos O (2022) Post-eruptive lahars related to the 1913 eruption in La
1553 Lumbre Ravine, Volcán de Colima, Mexico: The influence of ravine morphometry on flow dynamics.
1554 Journal of Volcanology and Geothermal Research 421, 107423.
- 1555 Rolandi G, Barrella AM, Borrelli A (1993) The 1631 eruption of Vesuvius. Journal of Volcanology
1556 and Geothermal Research 58, 183-201.

- 1557 Rolandi G, Munno R, Postiglione I (2004) The A.D. 472 eruption of the Somma volcano. *Journal of*
1558 *Volcanology and Geothermal Research* 129, 291-319.
- 1559 Rosi M, Principe C, Vecci R (1993) The 1631 Vesuvius eruption. A reconstruction based on historical
1560 and stratigraphical data. *Journal of Volcanology and Geothermal Research* 58, 151-182.
- 1561 Rosi M and Santacroce R (1983) The A.D. 472 “Pollena” eruption: volcanological and petrological
1562 data for this poorly-known, Plinian-type event at Vesuvius. *Journal of Volcanology and Geothermal*
1563 *Research* 17, 249-271.
- 1564 Russell AJ, Knudsen O (1999) An ice-contact rhythmite (turbidite) succession deposited during the
1565 November 1996 catastrophic outburst flood (jökulhlaup), Skeidarárjökull, Iceland. *Sedimentary*
1566 *Geology* 127, 1-10.
- 1567 Sandri L, de' Michieli Vitturi M, Costa A, Di Vito MA, Rucco I, Doronzo DM, Bisson M, Gianardi
1568 R, de Vita S, Sulpizio R, ([submitted this issue](#)) Lahar events in the last 2,000 years from Vesuvius
1569 eruptions. Part 3: Hazard assessment over the Campanian Plain.
- 1570 Santacroce R, Cioni R, Marianelli P, Sbrana A, Sulpizio R, Zanchetta G, Donahue DJ, Joron JL
1571 (2008) Age and whole rock-glass compositions of proximal pyroclastics from the major explosive
1572 eruptions of Somma-Vesuvius: A review as a tool for distal tephrostratigraphy. *Journal of*
1573 *Volcanology and Geothermal Research* 177, 1-18.
- 1574 Santacroce R., Sbrana A., Andronico D., Cioni R., Di Vito M., Marianelli P., Sulpizio R., Zanchetta
1575 G., Arrighi S., Benvenuti E., Gurioli L., Leoni F.M., Luperini W., 2003. *Carta Geologica del Vesuvio*
1576 in scala 1:15.000, Santacroce R., Sbrana A., eds. *Cartografia derivata dai rilievi geologici in scala*
1577 1:10.000 *Regione Campania e dai rilievi in scala 1:25.000 del Progetto CARG., S.E.L.C.A., Firenze.*
- 1578 Santangelo N, Romano P, Ascione A, Russo Ermolli E (2017) Quaternary evolution of the Southern
1579 Apennines coastal plains: A review. *Geologica Carpathica* 68, 43-56.

- 1580 Scott KM (1989) Magnitude and frequency of lahars and lahar-runout flows in the Toutle-Cowlitz
1581 River System. U. S. Geological Survey Professional Paper 1447-B, 1–33.
- 1582 Scott KM, Vallance JW, Pringle PT (1995) Sedimentology, behavior, and hazard of debris flows at
1583 Mount Rainer, Washington. U. S. Geological Survey Professional Paper 1547, 1-56.
- 1584 Scott KM, Macías JL, Naranjo JA, Rodriguez S, McGeehin JP (2001) Catastrophic debris flows
1585 transformed from landslide in volcanic terrains: mobility, hazard assessment and mitigation
1586 strategies. US Geol Surv Prof Pap. 1630, 1-59.
- 1587 Sheridan MF, Bonnard C, Carrero C, Siebe C, Strauch W, Navarro M, Calero JC, Trujillo NB (1999)
1588 Report of the 30 October 1998 rock fall/avalanche and breakout flow of Casita Volcano, Nicaragua,
1589 triggered by Hurricane Mitch. Landslide News 12, 2-4.
- 1590 Siebe C, Schaaf P, Urrutia-Fucugauchi J (1999) Mammoth bones embedded in a late Pleistocene lahar
1591 from Popocatépetl volcano, near Tocuila, central Mexico. Geological Society of America Bulletin
1592 111, 1550-1567.
- 1593 [Smith G, Williams R, Rowley PJ, Parsons DR \(2018\) Investigation of variable aeration of](#)
1594 [monodisperse mixtures: implications for pyroclastic density currents. Bulletin of Volcanology 80, 67.](#)
- 1595 Spence RJS, Zuccaro G, Petrazzuoli S, Baxter PJ (2004) Resistance of buildings to pyroclastic flows:
1596 analytical and experimental studies and their application to Vesuvius. Natural Hazards Review 5, 48-
1597 59.
- 1598 [Stanzione M, Di Vito MA, Aurino P, Lumaga MRB \(2023\) Sacred plant impressions from Somma-](#)
1599 [Vesuvius volcanic ash deposits: A medicinal garden in Late Antique Acerra \(Naples, Campania,](#)
1600 [Italy\)? Journal of Archaeological Science: Reports 47, 103802.](#)

- 1601 Sulpizio R, Mele D, Dellino P, La Volpe L (2005) A complex, Subplinian-type eruption from low-
1602 viscosity, phonolitic to tephri-phonolitic magma: the AD 472 (Pollena) eruption of Somma-Vesuvius,
1603 Italy. *Bulletin of Volcanology* 67, 743-767.
- 1604 Sulpizio R, Zanchetta G, Demi F, Di Vito MA, Pareschi MT, Santacroce R (2006) The Holocene
1605 syneruptive volcaniclastic debris flows in the Vesuvian area: Geological data as a guide for hazard
1606 assessment. *Geological Society of America Special Paper* 402, 203-221.
- 1607 Sulpizio R, Dellino P, Doronzo DM, Sarocchi D (2014) Pyroclastic density currents: state of the art
1608 and perspectives. Journal of Volcanology and Geothermal Research 283, 36-65.
- 1609 Tema E, Zanella E, Pavón-Carrasco FJ, Kondopoulo D, Pavlides S (2015) Palaeomagnetic analysis
1610 on pottery as indicator for the pyroclastic flows deposit temperature: New data and statistical
1611 interpretation from the Minoan eruption of Santorini, Greece. *Geophysical International Journal* 203,
1612 33-47.
- 1613 Thouret JC, Arapa E, Charbonnier S, Guerrero A, Kelfoun K, Cordoba G, Rodriguez D, Santoni O
1614 (2022) Modeling tephra fall and sediment-water flows to assess their impact on a vulnerable building
1615 stock in the City of Arequipa, Peru. *Frontiers in Earth Science* 10, 865989.
- 1616 Toyos G, Gunasekera R, Zanchetta G, Oppenheimer C, Sulpizio R, Favalli M, Pareschi MT (2008)
1617 GIS-assisted modelling for debris flow hazard assessment based on the events of May 1998 in the
1618 area of Sarno, Southern Italy: II. Velocity and dynamic pressure. *Earth Surface Processes and*
1619 *Landforms* 33, 1693-1708.
- 1620 Vallance JW and Iverson R (2015) Lahars and their deposits. In: Sigurdsson, H., Houghton, B.F.,
1621 McNutt, S.R., Rymer, H., Stix, J. (Eds.), *Encyclopedia of Volcanoes*. Academic Press, London, 649-
1622 664.

- 1623 Vallance JW and Scott KM (1997) The Osceola mudflow from Mount Rainier: Sedimentology and
1624 hazards implications of a huge clay-rich debris flow. Geological Society of America Bulletin 109,
1625 143-163.
- 1626 Vitale S and Ciarcia S (2018) Tectono-stratigraphic setting of the Campania region (southern Italy),
1627 Journal of Maps 14, 9-21.
- 1628 Voight B (1990) The 1985 Nevado del Ruiz volcano catastrophe: anatomy and retrospection. Journal
1629 of Volcanology and Geothermal Research 42, 151-188.
- 1630 Waitt RB Jr, TC Pierson TC, MacLeod NS, Janda RJ, Voight B, Holcomb RT (1983) Eruption-
1631 triggered avalanche, flood, and lahar at Mount St. Helens - Effects of winter snowpack. Science 221,
1632 1394-1397.
- 1633 Walsh B, Coviello V, Capra L, Procter J, Marquez-Ramirez V (2020) Insights into the internal
1634 dynamics of natural lahars from analysis of 3-component broadband seismic signals at Volcan de
1635 Colima, Mexico.
- 1636 Whipple KX, Hancock GS, Anderson RS (2000) River incision into bedrock: Mechanics and relative
1637 efficacy of plucking, abrasion, and cavitation. Geological Society of America Bulletin 112, 490-503.
- 1638 White S, García-Ruiz JM, Martí-Bono C, Valero B, Errea MP, Gómez-Villar A (1997) The 1996
1639 Biescas campsite disaster in the Central Spanish Pyrenees and its spatial and temporal context.
1640 Hydrological Processes 11, 1797-1812.
- 1641 Zanchetta G, Sulpizio R, Pareschi MT, Leoni FM, Santacroce R (2004a) Characteristics of May 5-6,
1642 1998 volcaniclastic debris flows in the Sarno area (Campania, southern Italy): relationships to
1643 structural damage and hazard zonation. Journal of Volcanology and Geothermal Research 133, 377-
1644 393.

- 1645 Zanchetta G, Sulpizio R, Di Vito MA (2004b). The role of volcanic activity and climate in alluvial
1646 fan growth at volcanic areas: an example from southern Campania (Italy). *Sedimentary Geology* 168,
1647 249-280.
- 1648 ~~Zanchetta G, Sulpizio R, Pareschi MT, Leoni FM, Santacroce R (2004a) Characteristics of May 5-6,~~
1649 ~~1998~~ ~~volcaniclastic debris flows in the Sarno area (Campania, southern Italy): relationships to~~
1650 ~~structural damage and hazard zonation. Journal of Volcanology and Geothermal Research~~ 133, 377-
1651 ~~393.~~
- 1652 Zanella E, Gurioli L, Pareschi MT, Lanza R (2007). Influences of urban fabric on pyroclastic density
1653 currents at Pompeii (Italy): 2. Temperature of the deposits and hazard implications. *Journal of*
1654 *Geophysical Research* 112, B05214.
- 1655 Zanella E, Gurioli L, Lanza R, Sulpizio R, Bontempi M (2008). Deposition temperature of the AD
1656 472 Pollena pyroclastic density current deposits, Somma-Vesuvius, Italy. *Bulletin of Volcanology*
1657 70, 1237-1248.
- 1658 Zanella E, Sulpizio R, Gurioli L, Lanza R (2015). Temperatures of the pyroclastic density currents
1659 deposits emplaced in the last 22 kyr at Somma-Vesuvius (Italy). *Geological Society, London, Special*
1660 *Publication, The Use of Palaeomagnetism and Rock Magnetism to Understand Volcanic Processes*
1661 396.
- 1662 Zaragoza G, Caballero-Garcia L, Capra L, Nieto-Torres A (2020) Lahares secundarios en el volcan
1663 Popocatepetl: El lahar Nexpayantla del 4 de febrero, 2010. Revista Mexicana de Ciencias Geologicas
1664 37, 121-134.
- 1665 Zuccaro G, De Gregorio D (2013) Time and space dependency in impact damage evaluation of a sub-
1666 Plinian eruption at Mount Vesuvius. *Natural Hazards* 68, 1399-1423.